Flood Risk Management and Adaptation Under Sea-Level Rise Uncertainty

Catastrophe and Climate

DECEMBER | 2022

Flood Risk Management and Adaptation Under Sea-Level Rise Uncertainty

AUTHORS Chi Truong, PhD
Department of Actuarial Studies and Business Analytics, Macquarie University

Han Li, PhD, AIAA
Centre for Actuarial Studies
The University of Melbourne

Stefan Trueck, PhD
Department of Actuarial Studies and Business Analytics, Macquarie University

Matteo Malavasi, PhD
Department of Actuarial Studies and Business Analytics, Macquarie University

SPONSOR Catastrophe and Climate Strategic Research Program Steering Committee

CONTENTS

Flood Risk Management and Adaptation Under Sea-Level Rise Uncertainty

Executive Summary

Assessing climate risk and its potential impacts on our cities and economies is of fundamental importance. Extreme weather events, such as hurricanes, floods, and storm surges can lead to cause catastrophic damages. In urban settings, and particularly in coastal regions, factoring in climate uncertainty when identifying and assessing optimal adaptation policies, has become essential to increase resilience to storm surge risk.

Our study presents a comprehensive approach of real option analysis to climate adaptation policies aiming to mitigate flood risk. Our framework focuses on pricing catastrophic risk in coastal regions, allowing for economic growth and uncertainty in the mean sea level rise. The framework also provides insights into the optimal investment timing, both for single investment projects and for optimal adaptation pathways, when multiple projects are feasible.

We showcase our proposed methodology with three case studies based in New York City, Copenhagen, and South-East Queensland. We use the block maxima approach from extreme value theory combined with the generalized additive model for location scale and shape framework, to model the behavior of extreme sea level events using climate indices as covariates. We then combine the estimation results with the proposed real option framework in the three case studies, evaluating both hard and soft climate adaptation policies.

1: Introduction

Catastrophes such as hurricanes, floods, and storm surges have caused significant damages in coastal regions. Hurricane Katrina in 2005 claimed more than 1800 lives and a total damage cost of $108 billion (Wang et al., 2015), while the total costs of recent hurricanes Harvey and Irma also exceeded $100 billion. More recently, Hurricane Ian in 2022 claimed more than 131 lives and costs more than $50 billion (NOAA, 2022). These catastrophes have increased the debt under the National Flood Insurance Program (NFIP) in the US to nearly $20 billion and have raised serious concerns about the sustainability of the program (Musulin, 2017). In the presence of growth in physical asset values and population in coastal areas, the frequency and severity of losses from catastrophic events can be expected to increase further with the impact of climate change (IPCC, 2007). Optimal planning for adaptation to these emerging risks is therefore paramount for coastal regions. It is particularly important for those regions with considerable wealth and concentration of exposure such as New York, New Orleans, and South Florida.

Adaptation options for reducing flood and storm surge risk in coastal areas include hard protection measures and soft measures. Hard protection measures such as dikes or sea walls aim to protect the region up to the designed flood height. Soft measures include building codes that require buildings to be elevated to a certain height, dry flood-proofing measures that seal the buildings to prevent water from entering into the buildings, and wet flood-proofing measures that move valuable assets to a higher level. Soft measures also include land use policy that converts the most vulnerable housing areas to parkland.

Previous studies on adaptation to catastrophic risk typically use the net present value (NPV) rule to guide adaptation (see, e.g., Brouwer and van Ek, 2004; Michael, 2007; Kirshen et al., 2008; Aerts et al., 2014; Smajgl et al., 2015; Han et al., 2020). While the NPV rule is simple and easy to use, it is not an optimal rule for adaptation investment since it ignores the value of flexibility and the uncertainty of climate change. Real options theory, on the other hand, takes into account the value of flexibility, when the costs, benefits, and value of investment are uncertain. However, there are very few studies that apply real options to evaluate flood risk mitigation projects (see, e.g., Gersonius et al., 2013; Kim et al., 2017). To the best of our knowledge, none of these studies has allowed to consider the impact of climate change on storm surges. In addition, no study has used real options to determine the optimal pathways that allow for more flexibility to reduce flood risk for coastal regions.

In this report, we examine optimal adaptation pathways to increase the resilience of coastal regions to flood and storm surge risk. The proposed modeling framework allows us to examine the timing of investment, when both hard protection measures and soft measures are available. It also enables us to take into account the economic growth in loss exposure and the uncertain impacts of climate change. The project aims to:

- Develop a new modeling framework for pricing catastrophic risk in coastal regions, taking into account the impact of economic growth, the seasonal impact of tides, uncertainty about the mean sea-level rise, and the stochastic volatility of storm surges.

- Develop a real options framework that can determine flexible adaptation pathways, *i.e.,* the optimal time to invest into single investment projects, and optimal pathways for adaptation, when multiple adaptation measures are available.

- Calculate appropriate insurance premiums for flood risk without adaptation, as well as when the optimal adaptation pathway is followed.

- Apply the proposed models to three coastal regions, namely New York, Copenhagen, and South East Queensland (Australia).

The report documents the results of the project and is organized as follows. In the next section, we provide a review of the literature related to the work conducted in this report. In Section 3, we investigate the empirical behavior of sea levels in the studied regions. We then provide the methodology for optimal adaptation strategies in Section 4 and conduct the corresponding empirical work for the three case studies in Section 5. The distributions of insurance premiums are examined in Section 6 and the report is concluded in Section 7.

2: Literature review

Due to scarcity of data on catastrophes, the impact of climate change on sea levels and on the frequency and severity of catastrophic storms is not well understood until recently (Jongman et al., 2015; Winsemius et al., 2016; Tanoue et al., 2016; Letzing and Berkley, 2021). The improvement in imagery and monitoring technology has helped to provide more complete information. In a recent study, Tellman et al. (2021) use daily satellite imagery to estimate flood extent and population exposure for 913 large flood events in the world over the period 2000-2018. Tellman et al. (2021) provide a global database (available online via website: http://global-flood-database.cloudtostreet.info/) that includes information about the number of flood events per country, the cumulative exposed population to flood risk, the time evolution of the flooded areas and the exposed population over the period 2000-2018. Based on this more accurate database, Tellman et al. (2021) and Letzing and Berkley (2021) report that the proportion of people living in areas of severe flood risk is underestimated by a factor of 10 in previous studies.

Upon comparing the proportion of the observed flood-exposed population in 2015 to that in 2000 for each country, Tellman et al. (2021) find that the proportion of the population exposed to floods has increased in 70 out of 119 countries across all continents, which is much higher than 22 or 55 countries previously reported in the literature. The more accurate data set is then used to examine the accuracy of flood models. A model (GLOFRIS) whose flood exposure estimates have high correlation (0.89) with the flood exposure observations in the data set is then used to provide forecast for 2030. Tellman et al. (2021) identify 57 countries where exposure is predicted to grow (IPCC, 2007). The upward trends in population and property values in risk-prone regions, combined with the impact of climate change, will cause the frequency and severity of catastrophe losses to continue to grow (IPCC, 2007). Optimal adaptation strategies will play important roles in the coming years to cope with the increasing global catastrophic risk (Dixit and Pindyck, 1994; Wang et al., 2019).

Optimal adaptation strategies require sound financial analysis of climate adaptation infrastructures and adequate measurement of the involved key variables. A number of studies have used the NPV rule to determine whether to proceed with a catastrophic risk adaptation project (see, e.g., West et al., 2001; Brouwer and van Ek, 2004; Michael, 2007; Kirshen et al., 2008; Symes et al., 2009; Aerts et al., 2014). For a given project, the NPV is obtained by aggregating the present value of net benefits offered by the project. If the NPV is positive, the project is invested, otherwise, it is ignored. Climate adaptation projects may also be compared based on their NPVs to select the one with the highest NPV.

2.1 DETERMINISTIC DYNAMIC INVESTMENT MODEL

As a rule, NPV has many advantages: it is simple, easy to use, and easy to communicate. However, NPV has been shown not to be an optimal investment rule when there is the possibility of deferral, mitigation, and adaptation. Truong and Trück (2016) show that when catastrophic risk increases over time, deferring investment to a future time may actually increase the value of investment; in these cases, a dynamic deterministic model is preferred to the NPV rule.

Figure 1

BENEFIT OF DYNAMIC MODEL

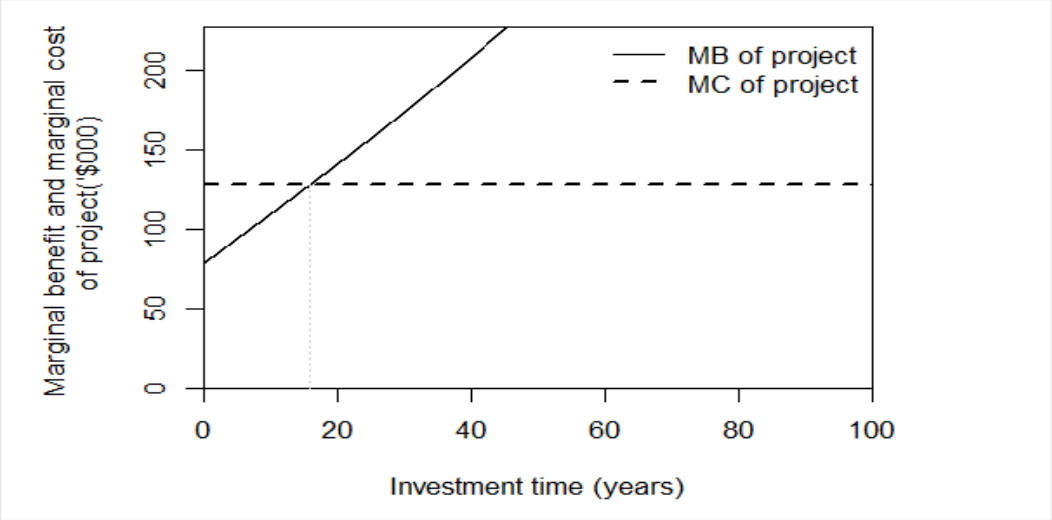

(a) Marginal analysis

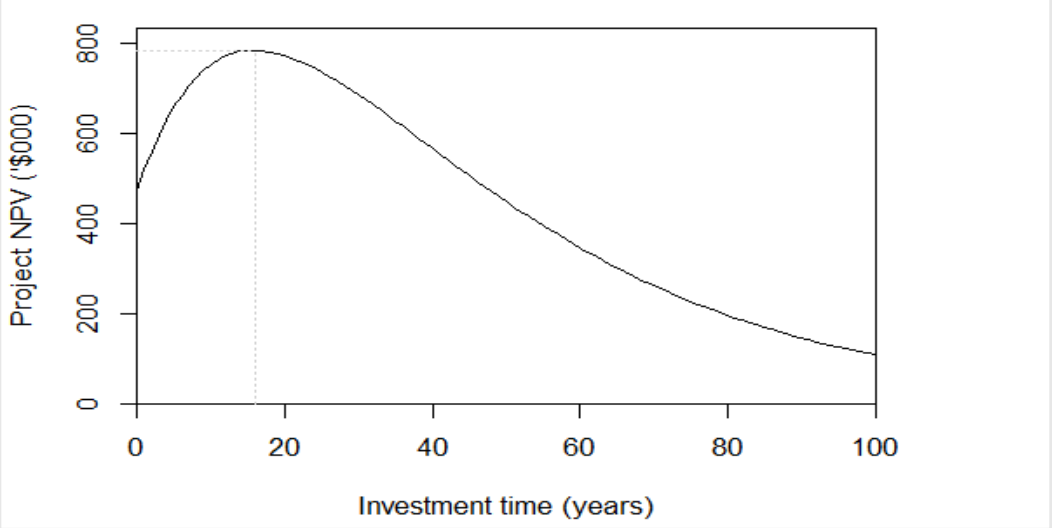

(b) NPV decision rule

This figure illustrates the dynamic marginal analysis (a) and the NPV decision rule (b). Applying a simple NPV rule (invest when NPV > 0 at t = 0) would lead to immediate investment without allowing for deferring the decision to invest. However, later investment could lead to a superior performance as illustrated in panel (b). Source: Truong and Trück (2016).

Figure 1 illustrates the benefit of using a dynamic investment model rather than the NPV rule. Panel (a) shows the marginal benefit compared to the marginal cost of deferring investment by one more year. On the one hand, deferring investment will defer the use of investment cost and generate the

interest revenue associated with that cost. On the other hand, the benefit of the project in terms of reduced catastrophic risk will be foregone. As shown in panel (a), at the initial time, deferring the investment by one year will generate a higher benefit compared to the cost and it is optimal to do so. Deferring the investment decision continues to be optimal until the annual benefit of the project is equal to the annual interest revenue. As a result, although the NPV of the project may be positive at the current time, deferring investment to a future time may lead to an even higher NPV, as shown in panel (b). Dynamic deterministic models have also been used for flood and storm surge risk (see, e.g., Wang and De Neufville, 2005; Zhu et al., 2007; Tsvetanov and Shah, 2013; Eijgenraam et al., 2016).

In deterministic studies, the impact of uncertainty is not considered, and the investment decision is based on the current information and forecasts, myopically disregarding the possibility of changes in the underlying conditions. Since the decision to invest in a climate adaptation project shares many similarities with the decision to exercise an American call option, such as irreversibility of the investment, unstable cash flow, and flexible investment timing, many authors have identified the problem under the umbrella of decision making under uncertainty, with adaptation pathways and real option theory being the main proposed frameworks (see, e.g., Dixit and Pindyck, 1994; Kim et al., 2017; Haasnoot et al., 2013; Ranger et al., 2013; Woodward et al., 2011, 2014; Kim and Kim, 2018; Kim et al., 2019).

2.2 ADAPTATION PATHWAYS

The value of flexibility in decision making under climate change uncertainty has been recognized in "adaptation pathways" studies. Adaptation pathways provide insights into the sequencing of actions over time, aiming to construct flexible strategies that can then be adapted as new information is revealed, or when the conditions are changed (see, e.g., Haasnoot et al., 2013; Ranger et al., 2013; Kim et al., 2019). To deal with uncertainty about the future, the possibility to spread, expand, or even abandon an investment over time should be considered (Dobes, 2010; Haasnoot et al., 2013; Nicholls et al., 2014).

The map in Figure 2 shows an example of the decision-making process in the adaptation pathways framework. The map compares alternative climate adaptation strategies achieving the same goal in 100 years' time. As shown in the figure, thanks to its flexibility, adaptation pathways can deal with multiple tipping points during the lifespan of climate adaptation projects. The map can also be used by decision makers to select which actions can be undertaken in the short run and to plan ahead in order to implement a specific project if future conditions change. Adaptation pathways have been successfully applied to complex contexts, involving, among other features, conflicting incentives and distributed decision makers impacted by uncertainty, such as biodiversity, natural resource management, and coastal development (see, among others, Downing, 2012; Haasnoot et al., 2012, 2013; Wise et al., 2014; Fazey et al., 2016). Despite its relative success, the adaptation pathways framework has typically been applied in a qualitative way only, while the selected adaptation actions can also be strongly subjective.

Figure 2

EXAMPLE OF ADAPTATION PATHWAYS MAP

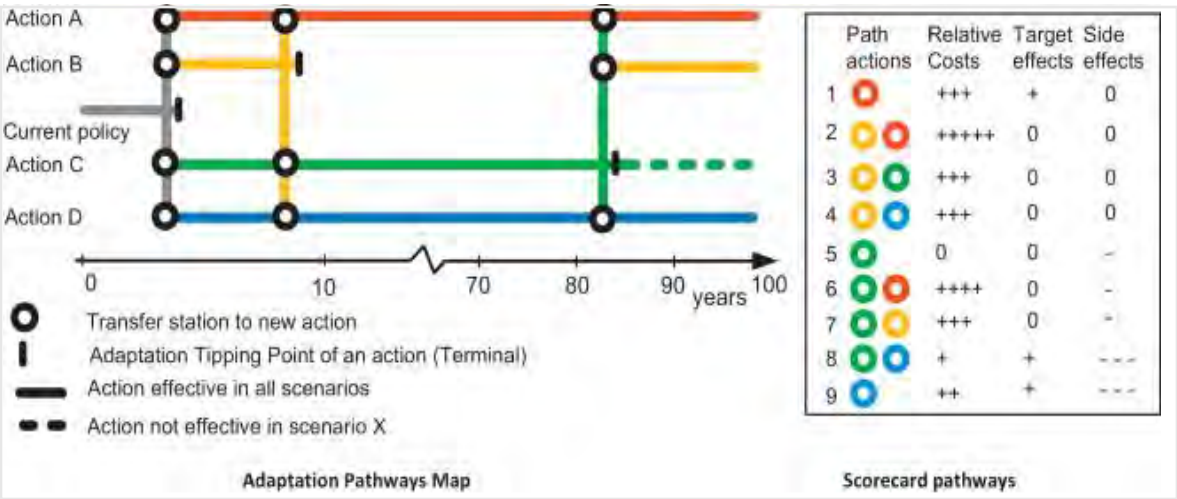

This figure shows an example of an adaptation pathways map (on the left) and scorecard (on the right) for four possible actions with nine possible pathways. The current policy (gray) misses the target after 4 years. Actions A (red) and D (blue) will succeed in achieving the goal in 100 years, under all climate scenarios. Action B reaches a tipping point in about 5 years, shifting to one of the other strategies will be needed. Action C requires a shift to either Action A, B, or D if scenario X occurs after 80 years. Source Haasnoot et al. (2013).

2.3 REAL OPTIONS WITH UNCERTAINTY

Real option analysis shares many appealing aspects with adaptation pathways, providing at the same time the ability to estimate the value of flexibility, and reducing the relative cost of adaptation (see, Dobes, 2010; Woodward et al., 2011, 2014; Wreford et al., 2020). Commonly used methods to determine the value of real options include binomial tree, Monte Carlo simulation, and finite difference methods. Binomial/decision tree and Monte Carlo simulation pricing frameworks have been applied to flood disaster prevention mechanisms on both river estuaries (see, among others, Woodward et al., 2011, 2014; Kind et al., 2018; Ryu et al., 2018) and coastal protection from sea level rise (see, e.g., Kontogianni et al., 2014; Brown et al., 2018).

Figure 3 illustrates the use of a decision tree to evaluate the optimal time to provide flood defense for electricity substations in the UK (Brown et al., 2018). The authors first calculate hazard ratings and estimate flood depth for electricity substations as shown in panel a). The flood hazard is then used to evaluate the benefit of providing flood defense over time. Panel b) shows the real option evaluation of the climate adaptation project, which suggests that the investment in the flood defense should be deferred until 2090.

Figure 3

EXAMPLE OF REAL OPTION ANALYSIS

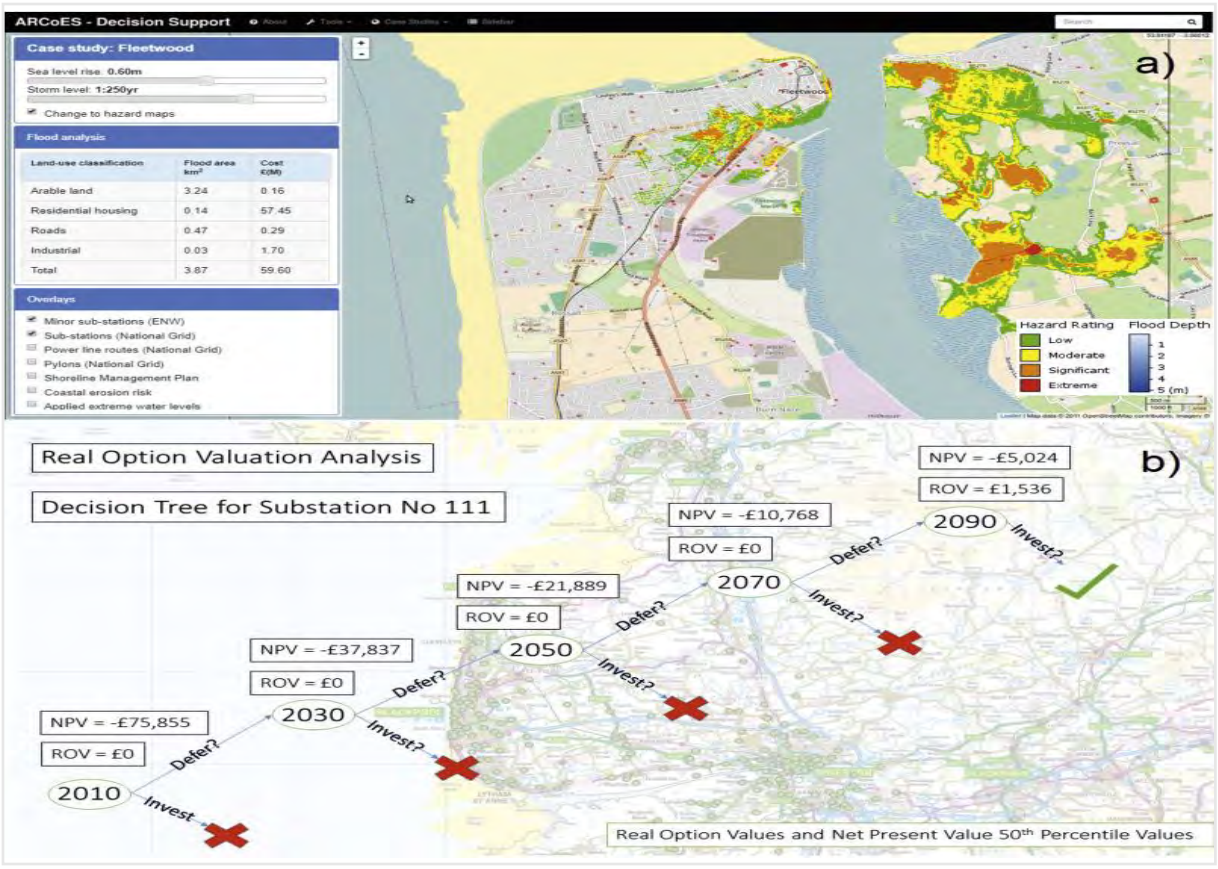

This figures shows an example of real option analysis assessing the vulnerability of the electricity grid to coastal hazards, in Fleetwood, Northwest England. Panel a) shows hazard ratings, estimated flood depth, and locations of the already in place electricity substations (red dots). Panel b) shows the decision tree for the construction of a flood defense for an electricity substation. The NPV and real option value at each step are estimated based on the hazardous ratings and estimated flood depth of panel a). Real option analysis suggests that for this particular case, construction of the climate adaptation project should go ahead in 2090. Source Brown et al. (2018).

Park et al. (2014) and Chan et al. (2016) apply a similar framework to drainage projects and defensive strategies against catastrophic rainstorms, while Oh et al. (2018) extended the framework to include a climate-driven economic evaluation. These studies show that allowing for more flexible investment options can increase the value of the project. As pointed out by Park et al. (2014) and Kim and Kim (2018), the value of flexible investment can be great and significant even for projects that do not pass the NPV rule ($NPV > 0$) at the current time.

Binomial/decision trees are approximation methods which assume a finite number of steps that can be taken by the change in a random variable. A more realistic method is to use Brownian motion to model uncertainty (see Regan et al., 2017; Schiel et al., 2019; Ginbo et al., 2021). Gersonius et al. (2011) provide a real option analysis based on a Brownian motion for coastal defense adaptation

evaluation. They find that real option analysis is more suitable in decision making concerning flood risk and coastal management than the classic NPV rule. In Gersonius et al. (2013), the change in rainfall intensity is modeled to follow a geometric Brownian motion, and therefore the variance of rainfall intensity increases over time. This is consistent with the intuition that the forecast of future rainfall becomes more uncertain as the forecast horizon increases. The optimal investment timing for coastal flood adaptation given the sea-level rise has been analyzed also in Kim et al. (2019). Their findings suggest that real option analysis in climate change adaptation studies needs two critical components: a model that allows the monetized benefit of the adaptation measure to depend on the climatic variables that cause the sea-level rise, and an observation mechanism to determine the critical value triggering the adaptation at the optimal investment timing.

2.4 LIMITATIONS OF PREVIOUS STUDIES

Although existing studies provide a good introduction to real options thinking in catastrophic risk mitigation, there are several shortcomings. First, the drift rate of the underlying process plays an important part in the investment evaluation. Nevertheless, the literature on climate adaptation does not provide a rigorous justification for how this parameter is selected. For example, Kim et al. (2017, 2019) set it at the risk-free rate. This assumption leads to the conclusion that exercising the option early is never optimal, implying that in a finite horizon setting, investment always happens in the final period (Dixit and Pindyck, 1994).

Second, although population and wealth may have important impact on catastrophic losses and may be the primary reason for risk mitigation, most studies do not consider the impact of loss exposure growth on adaptation strategies.

Third, catastrophic losses are often found to follow heavy tailed distributions (Embrechts et al., 1999). Typically, extreme value theory (EVT) is often used in catastrophic risk quantification, in insurance and actuarial science. Nonetheless, there exist only a few studies applying EVT to climate adaptation problems (see, e.g., Towler et al., 2010; Cheng et al., 2014; Ban et al., 2020).

Fourth, most papers that use real options on catastrophic mitigation assume a zero-market price for catastrophic risk, such as Truong et al. (2017). Since Froot (2001) shows that insurance premiums are usually high relative to the expected catastrophic losses and Garmaise and Moskowitz (2009) show that the inefficiency of catastrophic risk insurance market is magnified in the credit markets, where banks hesitate to extend credit to finance real estate in high-risk areas. It is thus important to develop a model that can allow for positive premiums for catastrophic risks.

Finally, some assumptions in real option models are too simple to be realistic: for example, Gersonius et al. (2011) assume that for each 15-year interval, sea-level rise can only take one of two values.

In this project, we address these issues by introducing a real options model to determine the optimal adaptation strategy for flood risk. We make use of the EVT to quantify flood risk and allow for climate change as well as loss exposure growth in future years. We analyze the impact of different adaptation measures on reducing flood risk and show how the investment value and the optimal investment time can be determined. The real options model is then extended to find the optimal

pathways to invest in multiple projects, as well as the optimal investment strategy for a project that can be invested in several stages.

3: Empirical behavior of extreme sea level

3.1 RELEVANT CLIMATE INDICES

Sea-surface temperature and atmospheric pressure have important impacts on the occurrence of storms and other extreme events. Indices have been constructed based on these climate variables to predict climate related extreme events. We examine climate indices relevant to our case studies and later on use them to predict extreme sea levels.

North Atlantic Oscillation Index

The North Atlantic Oscillation (NAO) index measures the difference in the atmospheric pressure at the sea level between two locations in the North Atlantic: a low figure near Iceland, and a high figure near the Azores Islands. When the index is positive and large, the difference in the pressure between the two regions results in a stronger Atlantic jet stream and a northward shift of the storm track. Positive phases of the NAO are often associated with higher air pressure, fewer cold-air outbreaks, and decreased storminess in eastern North America and Southern Europe. In contrast, increased storminess and precipitation, and warmer-than-average temperatures will be observed in Northern Europe (Dahlman, 2009).

The NAO is one of the major contributors to the precipitation patterns of North America and therefore is affecting the extreme sea-level event magnitude (Menéndez and Woodworth, 2010; Lobeto et al., 2018). Moreover, recent papers have linked positive and negative phases of the NAO to the sea level in North America via the so-called "inverted barometer" effect, where high atmospheric pressure pushes the sea levels down, and raises them when air pressure plummets (Piecuch and Ponte, 2015).

Niño 3.4

Niño 3.4 is one of the indices tracking the sea-level temperature in the tropical Pacific Area, and it is one of the most commonly used indices in defining El Niño or La Niña events (Trenberth and Stepaniak, 2001). Niño 3.4 represents the average equatorial sea-surface temperature across the Pacific from the date line to the South America coast (5°S to 5°N latitude and 170°W to 120°W longitude).

Scandinavian Pattern

The Scandinavian Pattern (SCAND) is a climate index derived from the monthly-mean 700mb height anomalies[1] over the extratropical Northern Hemisphere. Positive phases of the SCAND correspond to below-normal atmospheric pressures in Southern Europe, and above-normal atmospheric pressures in Northern Europe (Bueh and Nakamura, 2007). It is one of the major drivers of the European climate being associated with increasing occurrences of extreme rainfall events in the United Kingdom and Northern Europe, as well as extreme sea-surface temperature in the North Atlantic (see, Blackburn and Hoskins, 2001; Walter et al., 2001).

[1] A 700mb height is the height of the location where the atmospheric pressure is 700mb. A height anomaly is the difference between the height observed at a given time and its long run average.

Indian Ocean Dipole

The Indian Ocean Dipole (IOD) is a coupled ocean-atmosphere phenomena, thought to be linked with El Niño Southern Oscillation. It measures the difference in sea-surface temperature between the western dipole (10°S to 10°N latitude and 50°E to 70°E longitude) and the eastern dipole (10°S to 0° latitude and 90°E to 108°E longitude). It is one of the major contributors to the Australian climate variability, where positive phases are associated with El Niño and negative events with La Niña, therefore affecting the probability of extreme rainfall events.

Antarctic Oscillation

The Antarctic Oscillation (AAO) measures atmospheric pressure difference between polar and subpolar regions in the southern hemisphere. Positive phases increase the chances of extreme rainfalls in south-eastern Australia, and it is usually positively correlated with La Niña type of events (Thompson et al., 2011).

Southern Oscillation Index

The Southern Oscillation Index (SOI) measures the strength of the Walker Circulation, and it is calculated using the difference in atmospheric pressures between Tahiti and Darwin[2]. Sustained positive phases are associated with stronger Pacific winds and higher sea-surface temperature in Northern Australia, which increases the probability of wetter-than-normal rainfalls in Eastern and Northern Australia.

3.2 DATA COLLECTION

Data for the empirical studies in this project are collected from various sources. For sea-level data, we use hourly data available from the archives of the University of Hawaii Sea Level Center (http://uhslc.soest.hawaii.edu). These data have been used in many previous studies, see *e.g.,* Menéndez and Woodworth (2010).

For New York City and Copenhagen case studies, sea-level data are dated back to 1930 and 1890, respectively. However, since data on climate indices are available only from 1950, we use sea-level data that start from 1950. In addition, for Copenhagen, the tidal gauge was relocated to Gothenborg in 2013 and the available time series data ends in 2012. Data at the new tide gauge have not been quality checked as for other stations. We therefore use the current data available and provide a robustness check that makes use of the data at the new gauge station. For the Southeast of Queensland in Australia, the time series starts from 1984.

For other climate indices, we use the NAO and the Niño 3.4 indices for the US, and the SCAND for Europe. For Australia, we use the AAO, the IOD and the SOI. These indices are collected from different sources. AAO is available from the British Antarctic Survey (http//www.nerc-bas.ac.uk/icd/gjma/sam.html), IOD and SOI are available from the Bureau of Meteorology, Australia (http://www.bom.gov.au/) and the rest of the indices are available from the National Oceanic and Atmospheric Administration (http://www.cpc.ncep.noaa.gov).

[2] More details available at http://www.bom.gov.au/climate/glossary/soi.shtml

3.3 DATA VISUALIZATION

3.3.1 MAXIMUM SEA LEVEL AND TIDES

Figure 4 shows the monthly maximum sea level (red) and the monthly maximum tide (blue) observed at the three stations: New York (panel [a]), Copenhagen (panel [b]), and Brisbane (panel [c]). Tide is estimated using the *UTide* package by Codiga (2011) and the most recent four years of data. The plot of maximum sea level in New York (panel [a]) reflects some extreme hurricane events, especially Hurricane Sandy that occurs in 2012. The time series of both water level and tide in Copenhagen (panel [b]) reach lower levels and exhibit less extreme events, both in frequency and magnitude, compared to the New York City (NYC) site. Finally, for panel (c), it can be seen that tide has considerable variation relative to the sea level at the Brisbane site. In addition, for sea-level observations, we do not observe the very extreme outliers as in the case of New York City.

Figure 4

MAXIMUM SEA LEVEL AND MAXIMUM TIDE AT THE THREE STATIONS

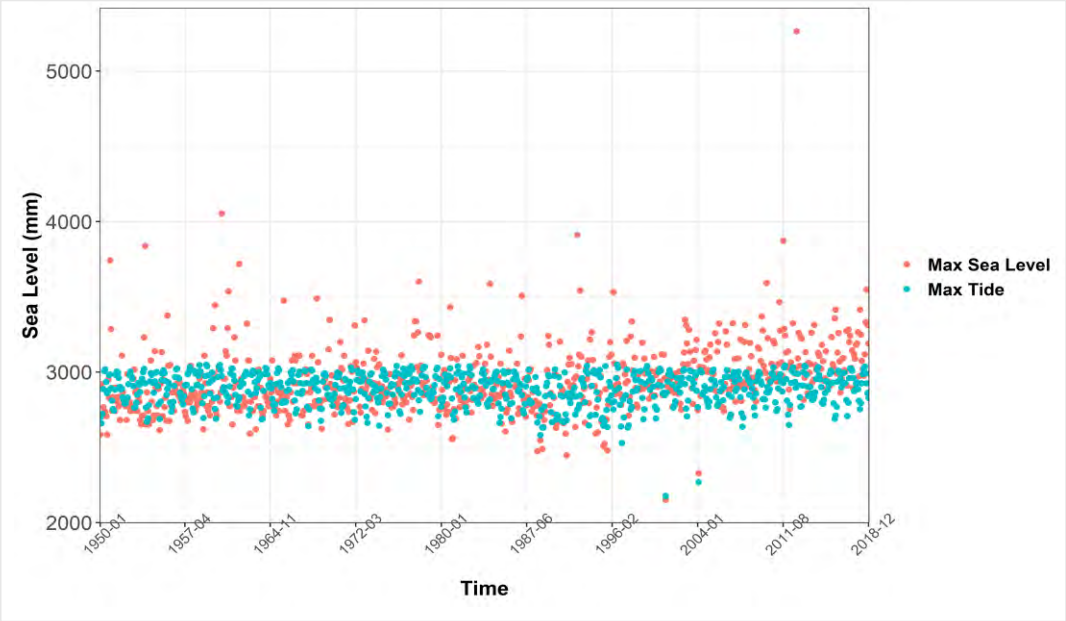

(a) Maximum sea level at New York Station (red) and the maximum estimated tide (blue).

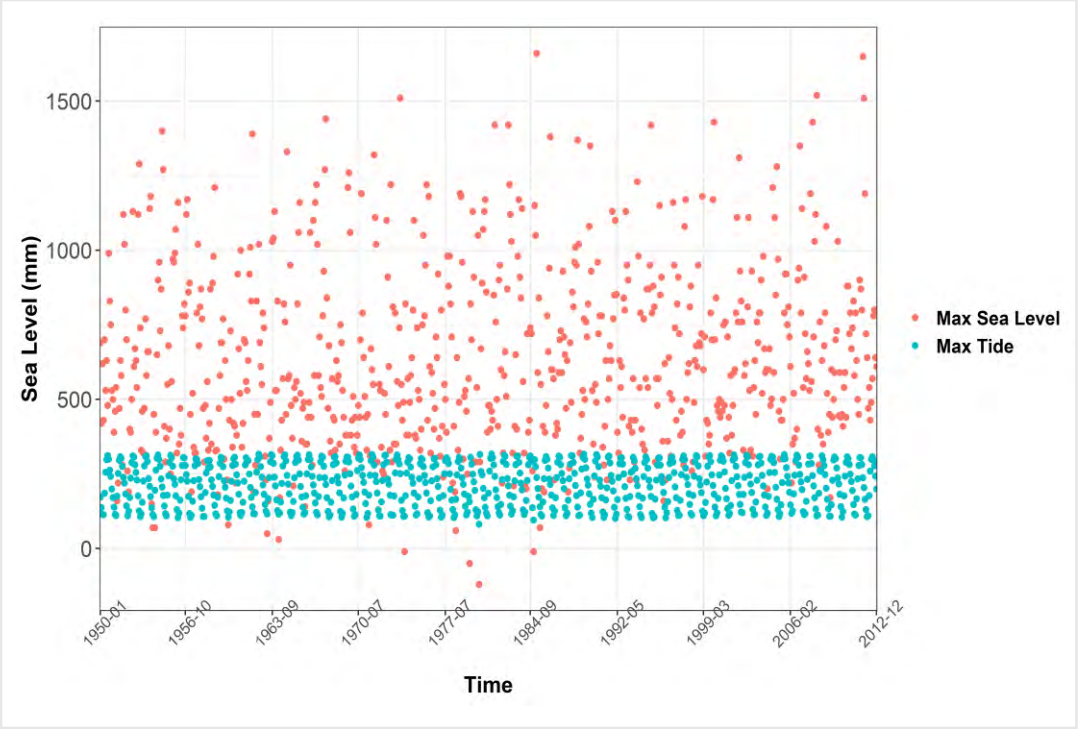

(b) Maximum sea level at Copenhagen Station (red) and the maximum estimated tide (blue).

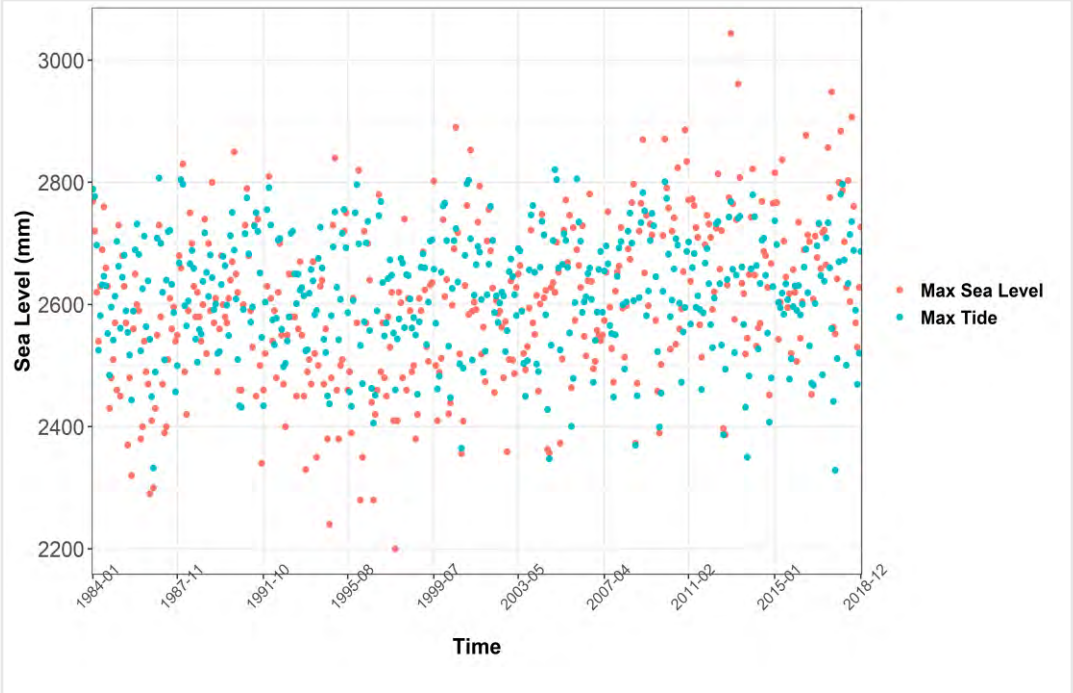

(c) Maximum sea level at Brisbane station (red) and the maximum estimated tide (blue).

3.3.2 CLIMATE INDICES

Figure 5 shows the time series of the NAO index and Niño 3.4 from 1950 to 2018. There seems to be little correlation between the two indices (the linear correlation coefficient estimate is equal to 0.012).

Figure 5

NORTH ATLANTIC OSCILLATOR INDEX AND NIÑO 3.4 FROM 1950 TO 2018

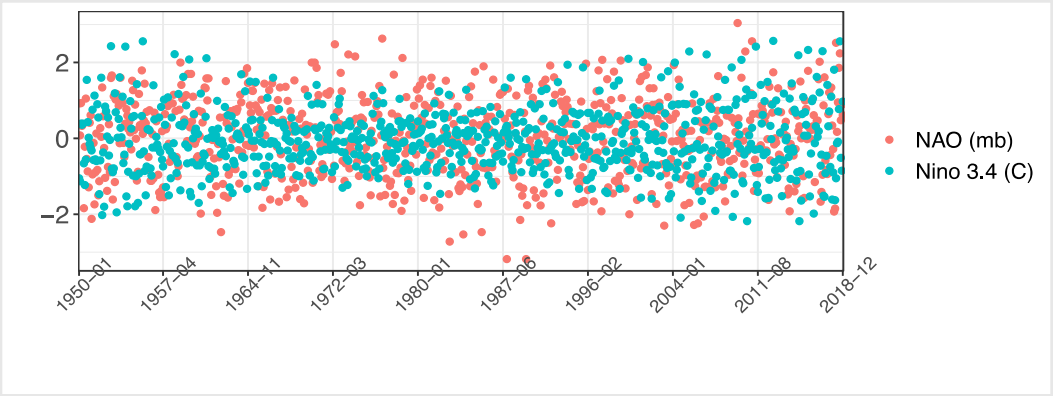

Figure 6 shows scatter plots of the sea levels (without tide) at the New York City site, against the value of the climate indices NAO (linear correlation coefficient of 0.032) and Niño 3.4 (linear correlation coefficient of 0.013). The blue line is a linear regression line using Ordinarily Least Squares (OLS). Overall, the impact of the considered climate indices on the sea level seems to be relatively small.

Figure 6

WATER LEVEL IN NYC VS CLIMATE INDICES

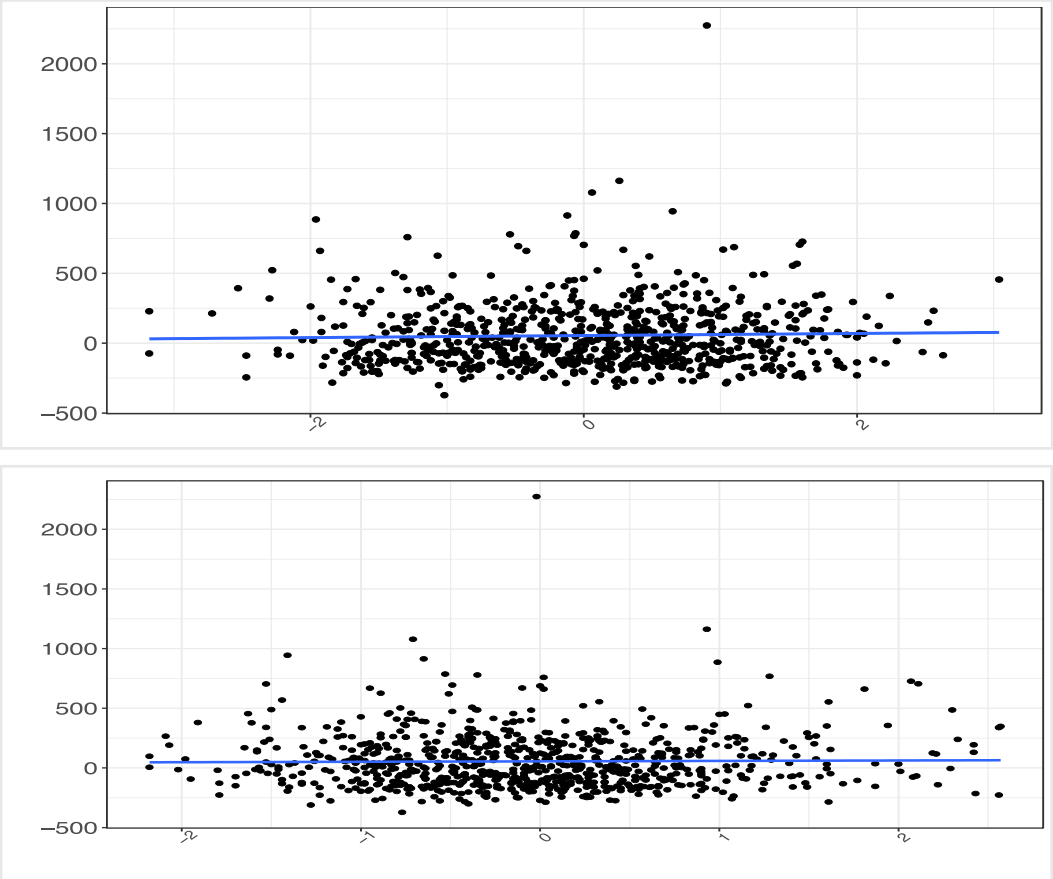

This figure shows water level without tide at New York site, plotted against the NAO (up) and Niño 3.4 (bottom).

The climate index relevant to Copenhagen is the SCAND index. As shown in Figure 7, the SCAND index is far from deterministic. The observations seem to be clustered with extreme values tending to be observed together, where subsequent values largely deviating from the average are typically observed in subsequent time periods.

Figure 7

SCANDINAVIAN PATTERN INDEX TIME SERIES FROM 1950 TO 2013

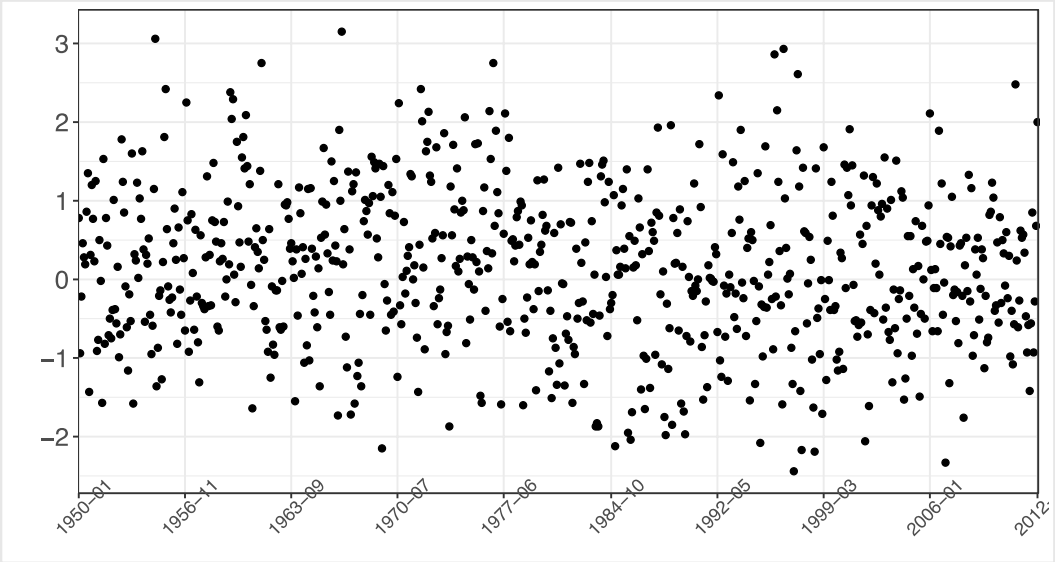

Figure 8 shows the scatter plots of the water levels at Copenhagen site without tide against the SCAND index. The blue line shows the fitting of a regression line using OLS. The linear correlation coefficient between the two variables is -0.33 (statistically significant at the 1% level). It seems that there is a relatively strong linear relationship between the two variables.

Figure 8

WATER LEVEL IN COPENHAGEN VS SCAND

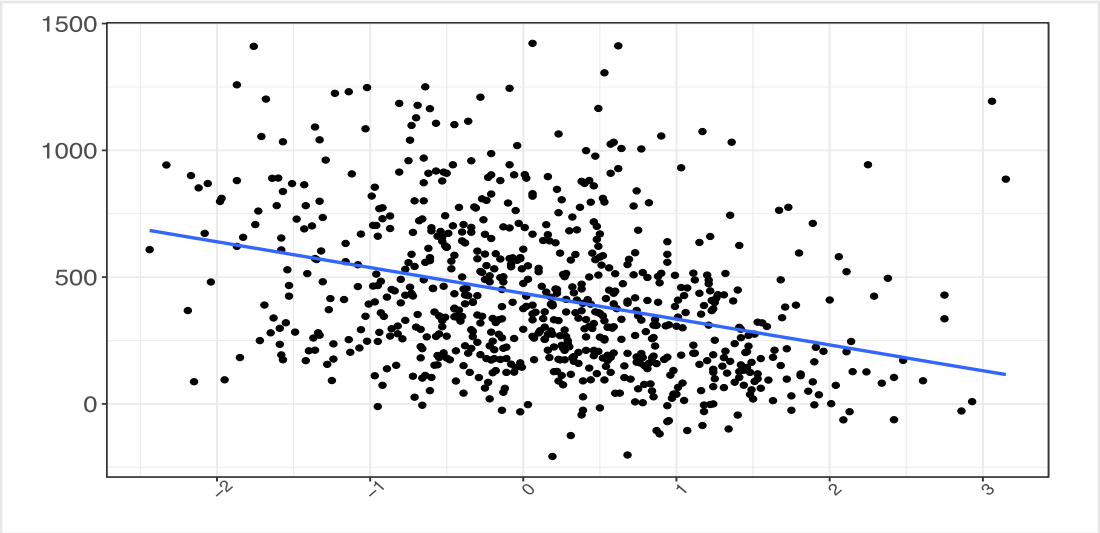

This figure shows the water level without tide, plotted against the SCAND.

Finally, for Brisbane, we examine three climate indices: AAO, IOD, and SOI. Their time series from 1984 to 2018 are depicted in Figure 9. AAO and IOD are positively correlated with a correlation coefficient of 0.003 and the coefficient is not statistically significant at the 5% significance level. In contrast, AAO and SOI are positively correlated with a correlation coefficient of 0.112 that is statistically significant at 5%. IOD and SOI are negatively correlated, with a correlation coefficient of -0.22 which is statistically significant at 1%.

Figure 9

ANTARTIC OSCILLATION, INDIAN OCEAN DIPOLE AND SOUTHERN OSCILLATION TIME SERIES FROM 1984 TO 2018

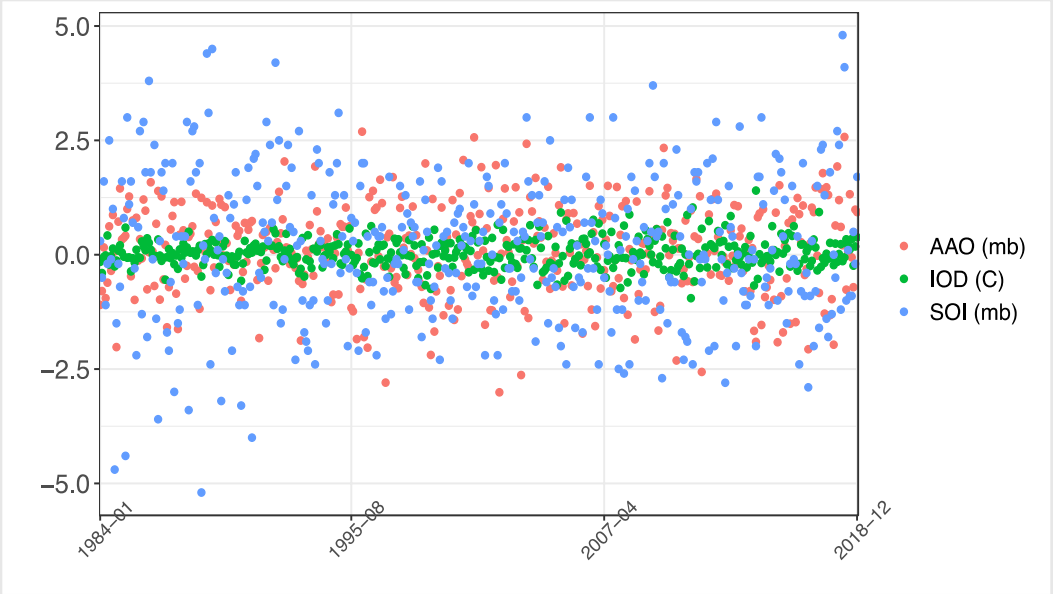

Antarctic Oscillation (AAO), Indian Ocean Dipole (IOD) and Southern Oscillation Index (SOI) time series from 1984 to 2018.

Figure 10 shows the scatter plots of sea levels without tide against the value of the climate indices IOD (linear correlation coefficient of 0.012), AAO (linear correlation coefficient of 0.009), and SOI (linear correlation coefficient of -0.04). The blue line corresponds to the regression line using OLS. The impact of the climate indices, if any, seems to be small.

Figure 10

WATER LEVEL IN SOUTH EAST QUEENSLAND VS CLIMATE INDICES

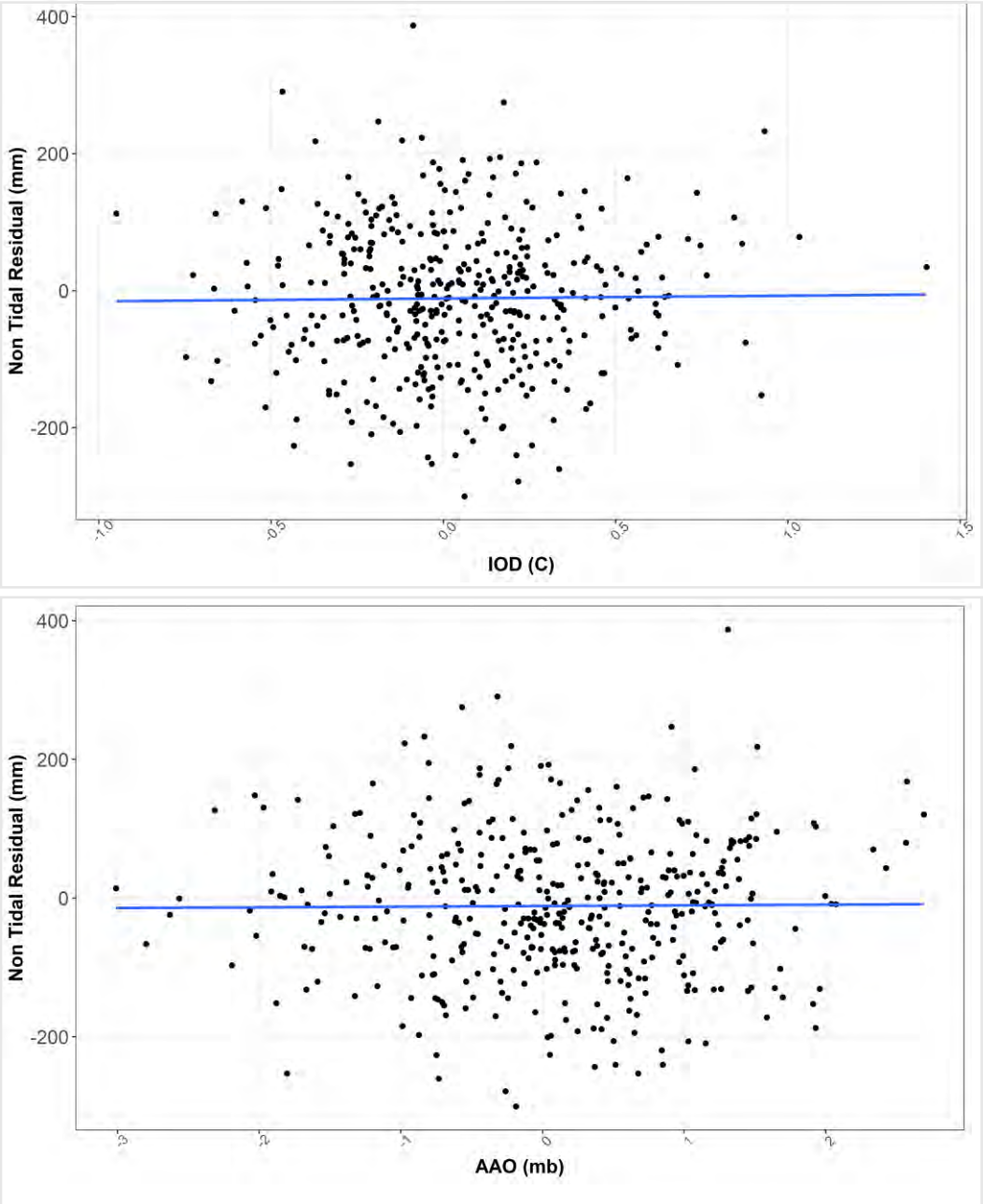

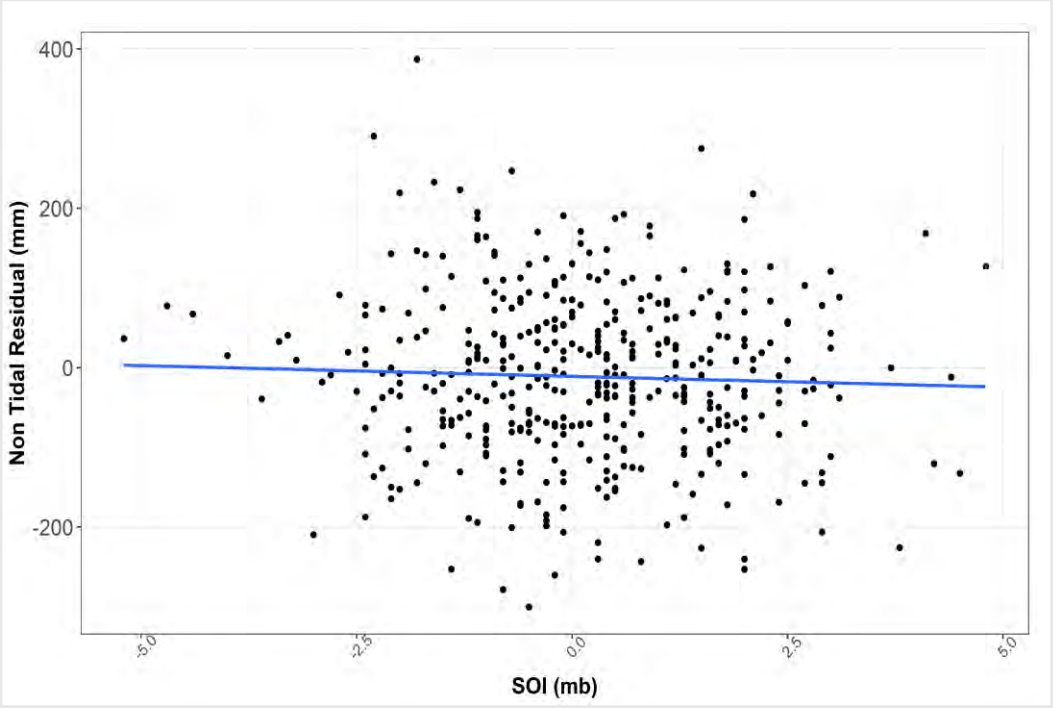

This figure shows water level without tide, plotted against the IOD (top), AAO (center), and SOI (bottom).

3.4 ESTIMATION METHOD

There are two approaches that are commonly used in modeling extreme sea level events: block maxima (BM) and the peaks over threshold (POT) approach. POT uses extreme sea level events with magnitude exceeding an adequately selected threshold in order to draw inference on the probability distribution of the sea level. Recent application of the POT on hydrology related problems can be found in, e.g., Roth et al. (2012, 2014); Silva et al. (2014, 2016); Prosdocimi et al. (2015); Razmi et al. (2017). BM models extreme sea level events by looking at the maximum values over a given time period (block). Typically, one may consider yearly or monthly maxima. One of the main advantages of BM over POT is that, relying on monthly maxima, BM requires fewer numbers of observations to estimate the underlying probability distribution (Menéndez and Woodworth, 2010; Lobeto et al., 2018; Salas et al., 2018). Among the many probability distributions used to model BM, the Generalized Extreme Value (GEV) distribution has become extremely popular in hydrology.

To allow for non-stationarity in extreme water levels, we model sea level monthly maxima to follow a time dependent GEV distribution:

$$H(S_t; a(t), b(t), \xi) = e^{-\left[1+\xi\frac{S_t-a(t)}{b(t)}\right]} \text{ with } 1+\xi\frac{S_t-a(t)}{b(t)} > 0. \quad (1)$$

with $1+\xi\frac{S_t-a(t)}{b(t)} > 0$.

Before estimating the GEV distribution, we follow the literature, see e.g., Menéndez and Woodworth (2010), to exclude the tide component from the water level. The residuals (in hourly frequency) are used to calculate the monthly maxima observations. These monthly maxima are then used in a maximum likelihood estimation (MLE) framework to fit the GEV distribution.

3.4.1 MAXIMUM LIKELIHOOD ESTIMATION FRAMEWORK

There are several ways to estimate time-dependent probability distributions using MLE. An R package called "extRemes" is designed specifically for extreme values distributions. Alternatively, there is a Generalized Additive Models for Location Scale and Shape (GAMLSS) framework that can be used for various distributions. Here, we adopt the more general GAMLSS introduced by Rigby and Stasinopoulos (2001, 2005). The log-likelihood function of the time-dependent GEV in Equation 1 is:

$$l(S; a(X,t), b(X,t), \xi) = \sum_{t=1}^{T} \log\big(h(S_t; a(X,t), b(X,t), \xi)\big),$$

where $h(\cdot; a(X,t), b(X,t), \xi)$ is the probability density function of a GEV random variable, S_t is monthly maximum non-tidal residual at time t, $a(X,t), b(X,t), \xi$ are the location, scale, and shape parameter respectively, and X is the set of problem specific covariates. The estimation routine also requires the specification of the so-called link functions. In this study, we employ a linear link function for the location parameter $a(X,t)$ and a log link function for the scale parameter $b(X,t)$:

$$a(X,t) = f_a(X,t)$$
$$\log(b(X,t)) = f_b(X,t),$$

while the shape parameter ξ is assumed to be constant due to the difficulty in obtaining a reliable estimate in the nonstationary case. The log link helps to ensure that the scale parameter is positive.

3.4.2 SELECTION OF COVARIATES

Given the monthly structure of the maximum sea levels, it is important to allow for the presence of seasonality in both location and scale parameters. Typically, seasonality is addressed via harmonic functions. Following Menéndez and Woodworth (2010), we consider annual and semiannual cycles:

$$f_{a,1}(X,t) = a_0 + \sum_{i=1}^{2} \beta_{2i-1}\, cos(i\omega t) + \beta_{2i} sin(i\omega t)$$
$$f_{b,1}(X,t) = b_0 + \sum_{i=1}^{2} \alpha_{2i-1}\, cos(i\omega t) + \alpha_{2i} sin(i\omega t)$$

where $\omega = 2\pi/12$. Astronomical modulations, such as the nodal cycle (18.6 years) or the interannual perigean influence (4.4 years) can affect the risk of extreme sea level events (Pugh, 1987). To take this into account, Menéndez and Woodworth (2010) consider two additional harmonic functions for each cycle:

$$f_{a,2}(X,t) = a_1(t) + \beta_{1,nodal} cos(\omega t/T_{nodal}) + \beta_{2,nodal} sin(\omega t/T_{nodal})$$
$$f_{b,2}(X,t) = b_1(t) + \alpha_{1,nodal} cos(\omega t/T_{nodal}) + \alpha_{2,nodal} sin(\omega t/T_{nodal})$$
$$f_{a,2}(X,t) = a_1(t) + \beta_{1,perigean} cos(\omega t/T_{perigean}) + \beta_{2,perigean} sin(\omega t/T_{perigean})$$
$$f_{b,2}(X,t) = b_1(t) + \alpha_{1,perigean} cos(\omega t/T_{perigean}) + \alpha_{2,perigean} sin(\omega t/T_{perigean})$$

To account for a long-term variability, a linear trend can also be included (Lobeto et al., 2018):

$$f_{a,3}(X,t) = f_{a,2}(X,t) + \beta_t t$$
$$f_{b,3}(X,t) = f_{b,2}(X,t) + \beta_t t$$

The magnitude of extreme sea level events may also depend on the natural climatic variability, adding an extra layer of randomness into the modeling (Kiem et al., 2003; Park et al., 2011). Therefore, large atmospheric mechanisms and oscillations are included as covariates as well. For each location, relevant climate indices are included as covariates for both location and scale according to the following equations:

$$f_a(X,t) = f_{a,3}(X,t) + \beta_{cl} Clim$$
$$f_b(X,t) = f_{b,3}(X,t) + \beta_{cl} Clim$$

Following Menéndez and Woodworth (2010) and Lobeto et al. (2018), variables are selected in three steps. In the first step, the seasonality structures in $f_{a,1}$ and $f_{b,1}$ are identified using the forward selection principle. For each covariate, a likelihood ratio test is performed with the following hypotheses: $H_0: \beta = 0$ vs $H_1: \beta \neq 0$. The covariate is included only if the null hypothesis is rejected. After variable selection is completed for the seasonality component, the perigean and nodal cycle effects are examined. In the next step, the impact of the long-term trend is investigated in $f_{a,3}$ and $f_{b,3}$. Once the time dependence has been selected according to its statistical significance, we then consider the climate indices. For completeness, we also consider the impact of interaction variables, and the non-linearity in the covariates.

3.5 ESTIMATION RESULTS

3.5.1 NEW YORK CITY

Estimation results for New York City are summarized in Table 1. The monthly maximum non-tidal residuals exhibit a high degree of seasonality, both in location and scale parameters. In contrast, the long-term trend affects only the location parameter and is not statistically significant for the scale parameter. We find that individual climate indices have low explanatory power as their coefficients are not statistically significant, although they have the correct signs. The positive coefficient of the NAO confirms the presence of the inverse barometer effect since positive values of the index correspond to low levels of atmospheric pressure on site. The negative coefficient for Niño 3.4 indicates that La Niña type of events negatively affect the location parameter.

In addition, we find a significant and positive joint effect of atmospheric pressures and equatorial sea-surface temperature. The joint effect means that below-normal atmospheric pressure in the North Atlantic and El Niño events have the potential to significantly increase the magnitude of extreme sea level events. Given the unit of measurement, even 1mb of atmospheric pressure per

degree of temperature can increase the surge level of 15 centimeters, on average. Overall, for New York City, the mean sea levels have been rising while the variability only follows seasonal patterns. These results agree with previous studies (Menéndez and Woodworth, 2010; Lobeto et al., 2018; Hieronymus and Kalén, 2020; Muis et al., 2018).

Table 1

COEFFICIENT ESTIMATES FOR NYC

Covariate	Name	Unit	Location	Scale(log-scale)
Constant	Base Level	mm	969.00	5.22
t	Long Term Trend	mm/month	3.79***	-
$\cos(2\pi t/12)$	Seasonal Component	mm/month	33.15***	-
$\sin(2\pi t/12)$	Seasonal Component	mm/month	29.42***	-0.04
$\sin(4\pi t/12)$	Seasonal Component	mm/month	-	0.08
$\cos(2\pi t/12 \times 18.6)$	Nodal Component	mm/month	16.77	-0.07**
$\cos(2\pi t/12 \times 4.4)$	Perigean Component	mm/month	-19.33**	0.07**
$Clim_{NAO,t}$	NAO	mm/millibar	4.14	0.002
$Clim_{Niño,t}$	Niño 3.4	mm/$^{\circ}C$	-8.08	0.01
$Clim_{NAO,t} \times Clim_{Niño,t}$	NAO/Niño interaction	mm/($^{\circ}C$millibar)	15.68**	-0.012

This table shows coefficient estimates for location parameter $a(t)$ and scale parameter $b(t)$ for the model, obtained using the procedure in Menéndez and Woodworth (2010). Significance levels are reported following the standard convention, i.e., $*$ corresponds to 10%, $**$ corresponds to 5%, and $***$ corresponds to 1%.

The estimation results are further visualized in Figure 11, which shows the values of the fitted GEV parameters and the predicted mean for the analyzed dataset. It is apparent that both the location parameter and the mean of the corresponding distribution exhibit an increasing trend coupled with a high degree of seasonality, while the scale parameter only shows seasonal dependence.

Figure 11

FITTED VALUES FOR THE LOCATION, AND SCALE PARAMETER AND THE CORRESPONDING DISTRIBUTIONAL MEAN VALUE, FOR THE GEV MODEL IN NEW YORK CITY

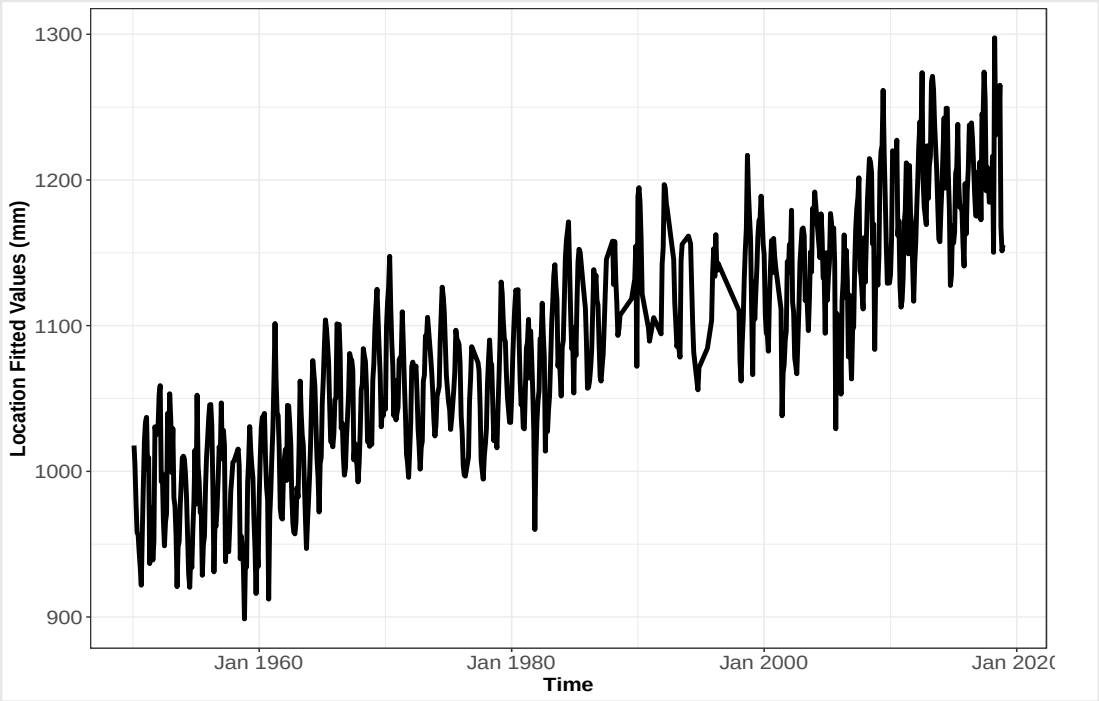

(a) Fitted location values for the New York Station

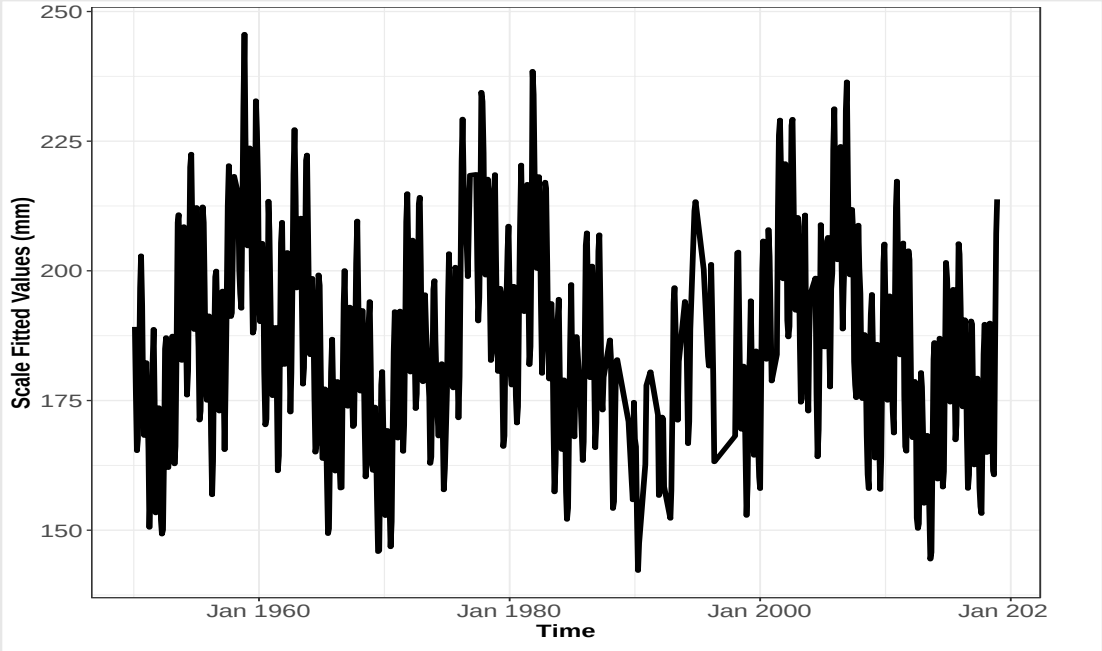

(b) Fitted scale value for the New York Station

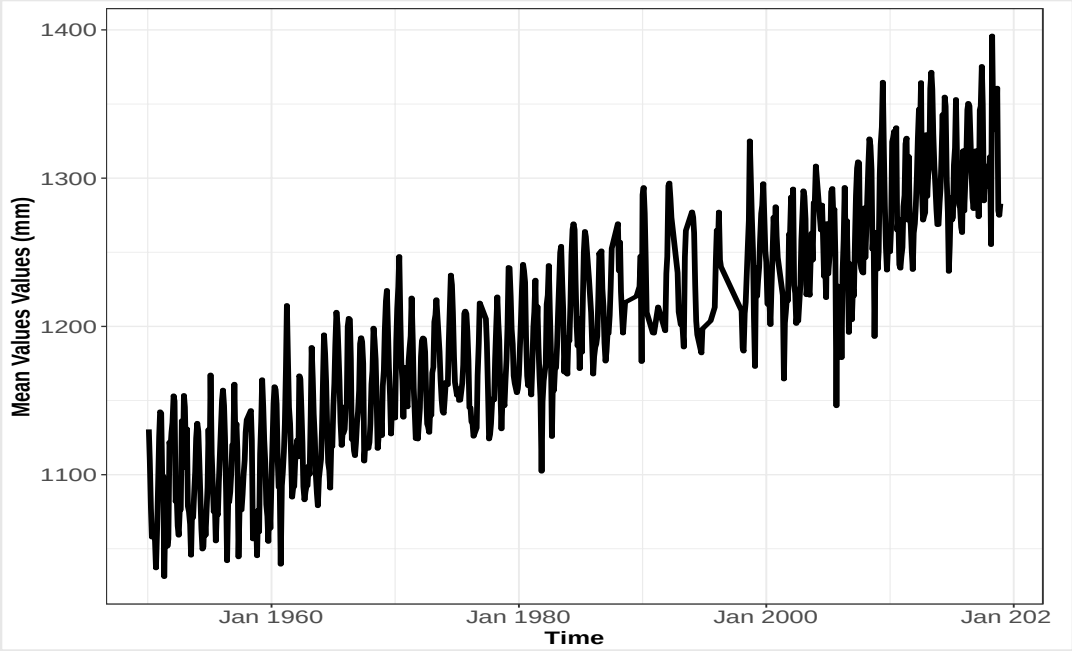

(c) Mean values for the New York Station

To illustrate how atmospheric phenomena affect the probability distribution of monthly maximum non-tidal residual, Figure 12 depicts the probability density functions corresponding to three scenarios: a low value of the climate index (5% quantile), the median value, and a high value of the climate index (95% quantile). The plots in Figure 12 show how extreme variation in climate indices are then reflected in the shape of the probability distribution. If a variation in the climate index determines a shift to the right, then an increase in the magnitude of maximum sea water level can be expected. If a variation in the climate index makes the distribution "wider," then an increase in the volatility of sea water level has to be expected. As can be seen, the change in the distribution is small when NAO and Niño 3.4 are considered alone, while a shift to the right can be observed in the case where both climate indices are included. This exercise shows the benefit of using the GAMLSS approach, which allows to directly evaluate the impact of covariates on the distribution.

Figure 12

IMPACT OF CLIMATE INDICES ON THE PROBABILITY DISTRIBUTION OF MAXIMUM NON-TIDAL RESIDUAL

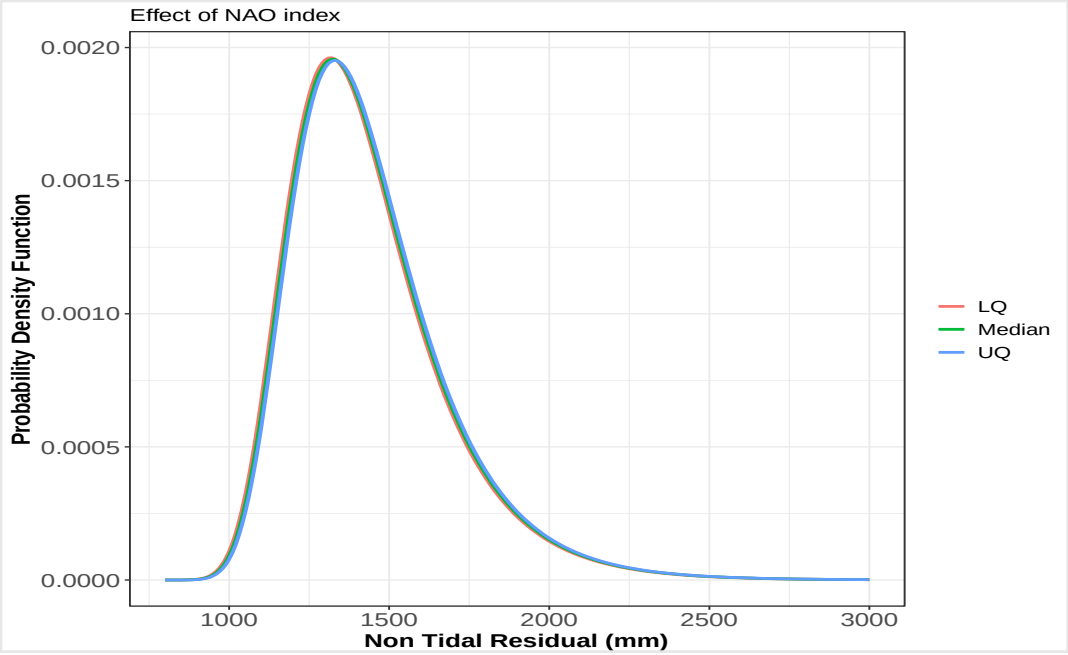

(a) Effects of variation in the NAO on the probability density function.

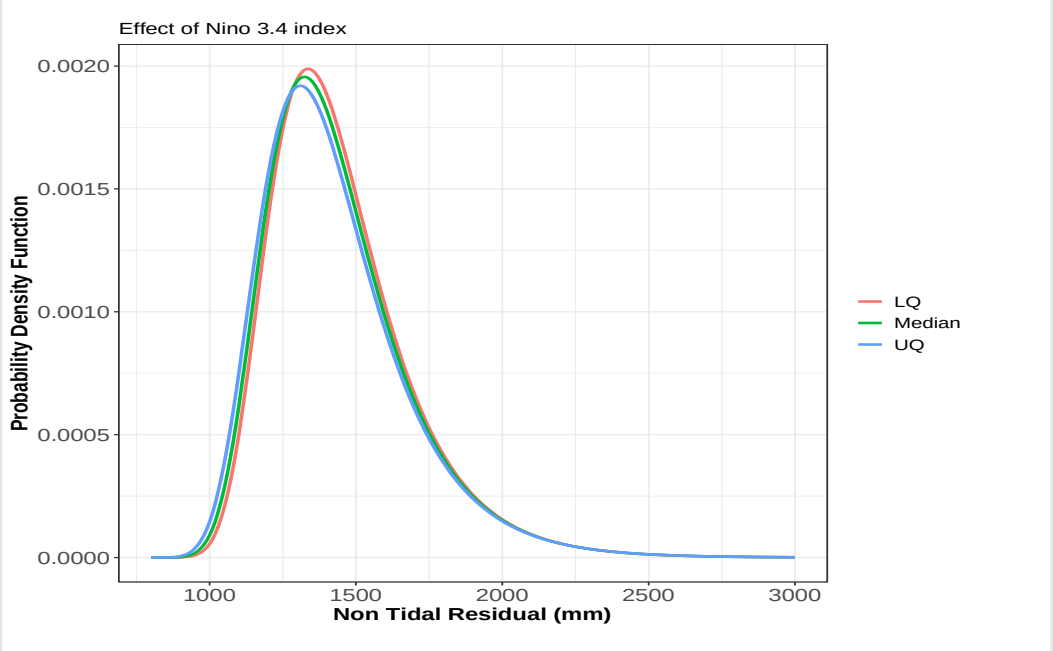

(b) Effects of variation in the Niño 3.4 on the probability density function.

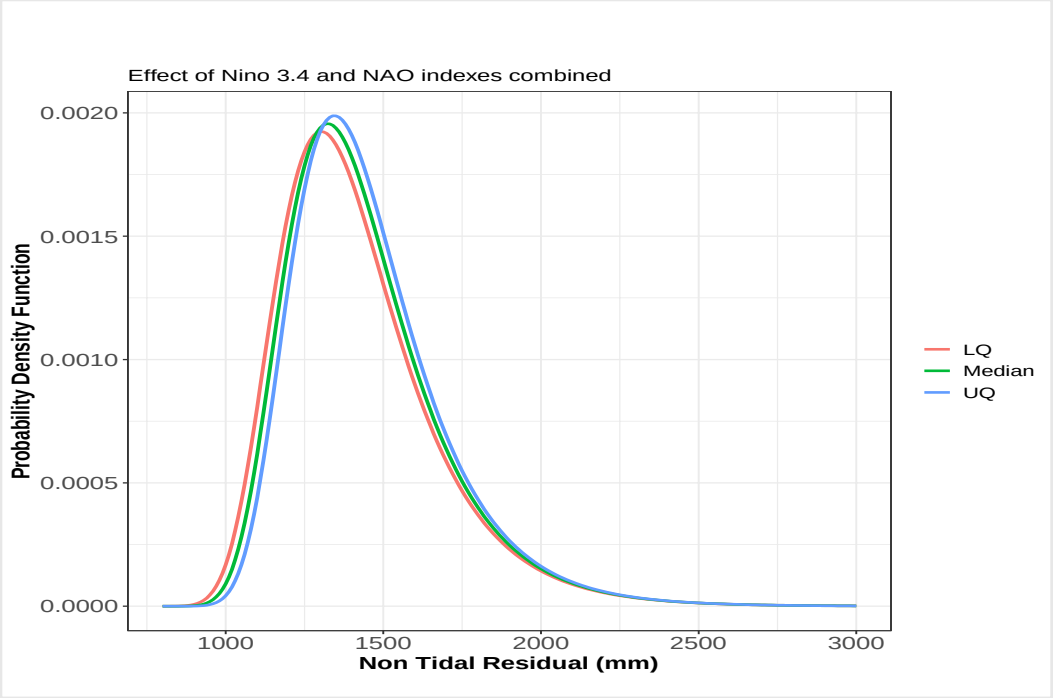

(c) Combined effect of NAO and Niño 3.4 on the probability density function.

As a goodness of fit test, Figure 13 compares the QQ plots of a stationary GEV models and the GEV model in Table 1. It is apparent that including covariates into the model allows to achieve a better fit.

Figure 13

QQ PLOTS OF STATIONARY AND NON-STATIONARY MODELS IN NYC

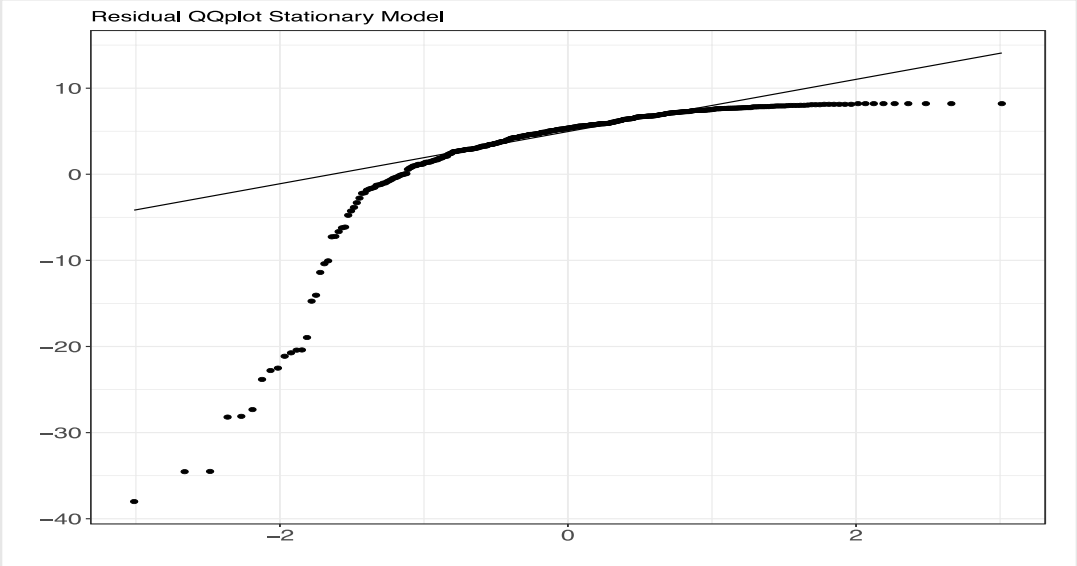

(a) QQplots of the model residual without covariates.

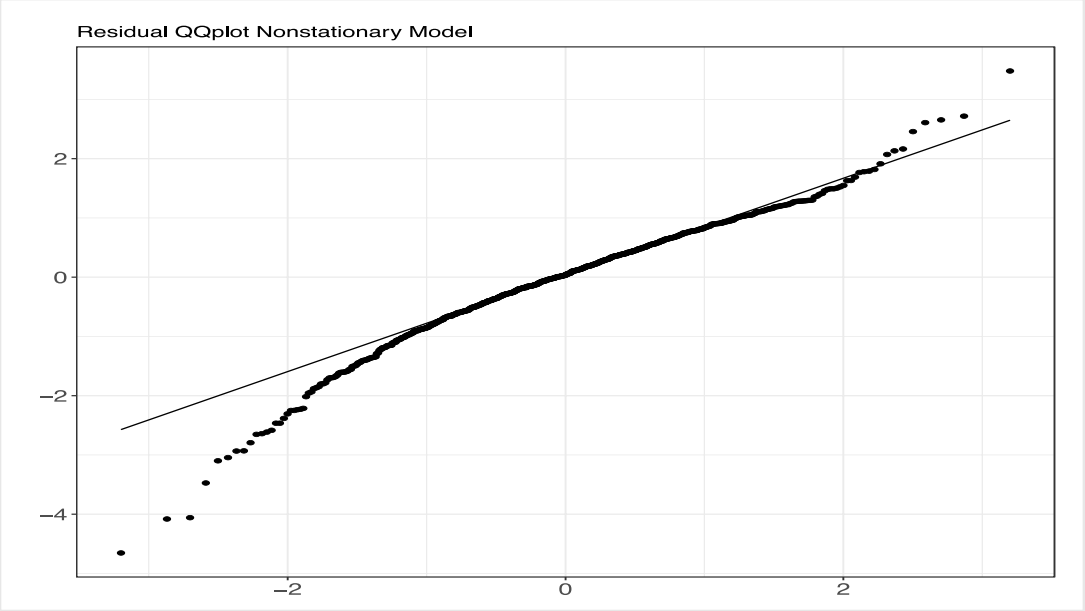

(b) QQplots of the model residual including covariates.

3.5.2 COPENHAGEN

Table 2 summarizes the estimates for both the location and scale parameters of the best selected model for Copenhagen. Similar to the case of New York, the location parameter exhibits a high degree of seasonality. In contrast, the scale parameter appears not to follow any deterministic seasonality and to be impacted only by the long-term trend. The coefficient for SCAND is negative both for location and scale parameters, which is consistent with the findings of previous studies (Lang and Mikolajewicz, 2019; Hieronymus and Kalén, 2020). This means that positive phases of SCAND are associated with above-normal atmospheric pressure in Northern Europe and lower magnitude of extreme sea level.

Table 2
COEFFICIENT ESTIMATES FOR COPENHAGEN

Covariate	Name	Unit	Location	Scale(log-scale)
Constant	Base Level	mm	341.68	5.46
t	Long Term Trend	mm/month	1.12**	-0.0005
$\cos(2\pi t/12)$	Seasonal Component	mm/month	9.83	-
$\sin(2\pi t/12)$	Seasonal Component	mm/month	-24.94**	-
$\sin(4\pi t/12)$	Seasonal Component	mm/month	19.18	-
$\cos(2\pi t/12 \times 18.6)$	Nodal Component	mm/month	4.25	-
$Clim_{SCAND,t}$	SCAND	mm/millibar	-101.15***	-0.08***

This table shows coefficient estimates for location parameter $a(t)$ and scale parameter $b(t)$ for the model obtained using the procedure in Menéndez and Woodworth (2010). Significance levels are reported following the standard convention, i.e., $*$ corresponds to 10%, $**$ corresponds to 5%, and $***$ corresponds to 1%

Figure 14 shows the fitted values of location and scale parameters and the corresponding distributional mean. As can be seen, the location parameter exhibits seasonality and an increasing trend, which is mirrored in the distributional mean. The scale variability of the scale parameter is only affected by the stochasticity of the SCAND.

Figure 14

FITTED VALUES FOR THE LOCATION, AND SCALE PARAMETER AND THE CORRESPONDING DISTRIBUTIONAL MEAN VALUE, FOR THE GEV MODEL IN COPENHAGEN

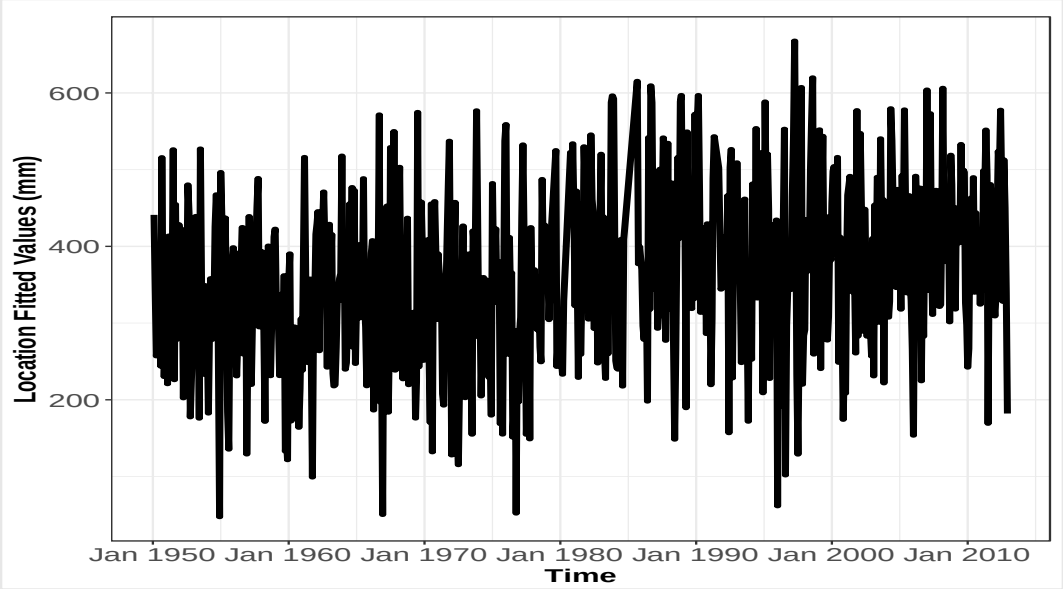

(a) Fitted location values for Copenhagen

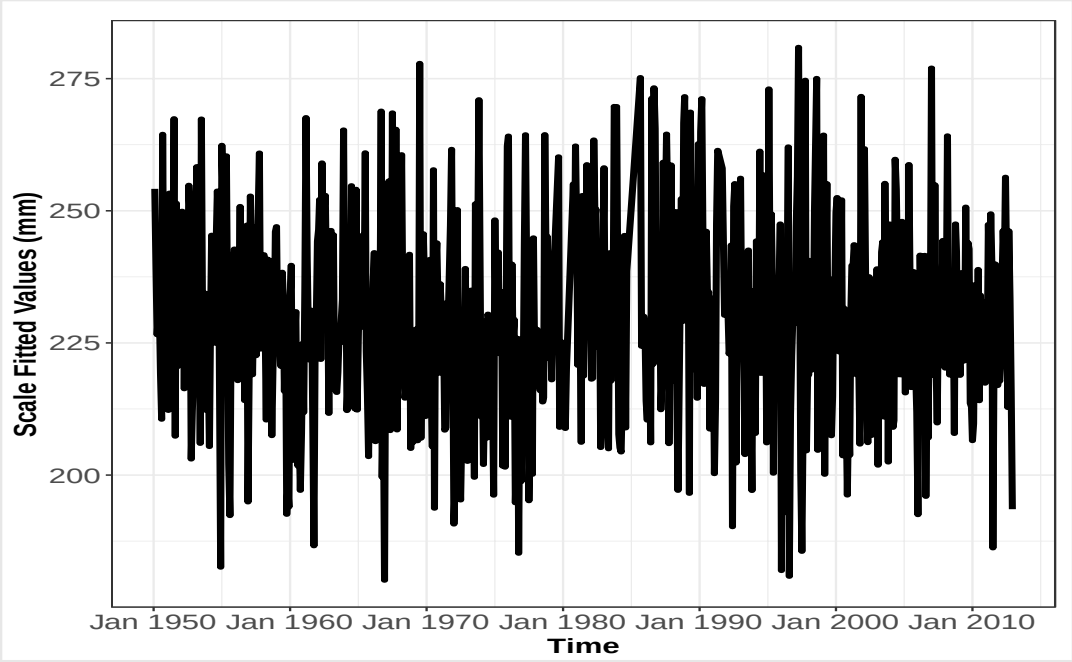

(b) Fitted scale values for Copenhagen

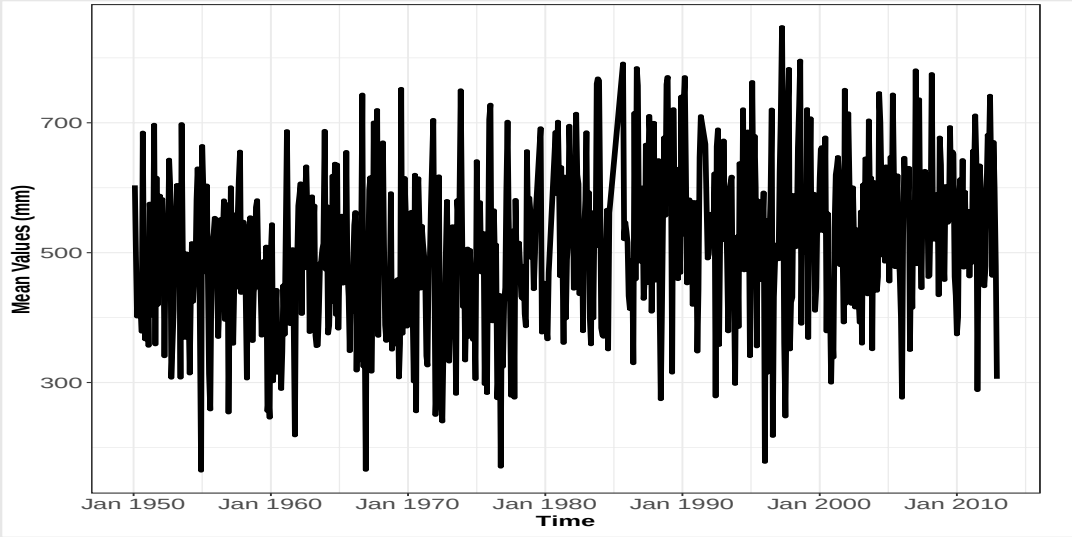

(c) Mean values for Copenhagen

Similar to the case of New York City, we present the impact of the SCAND index on the distribution of non-tidal water level in Figure 15. The effect of the atmospheric phenomena, represented by the climate index, is clearly visible from the graph and follows a reverse pattern. Since the SCAND negatively affects the location parameter, a lower value of the index corresponds to a shift of the

probability distribution to the right and leads to an increase in the magnitude of extreme sea level events.

Figure 15

EFFECT OF SCAND ON PROBABILITY DENSITY FUNCTION

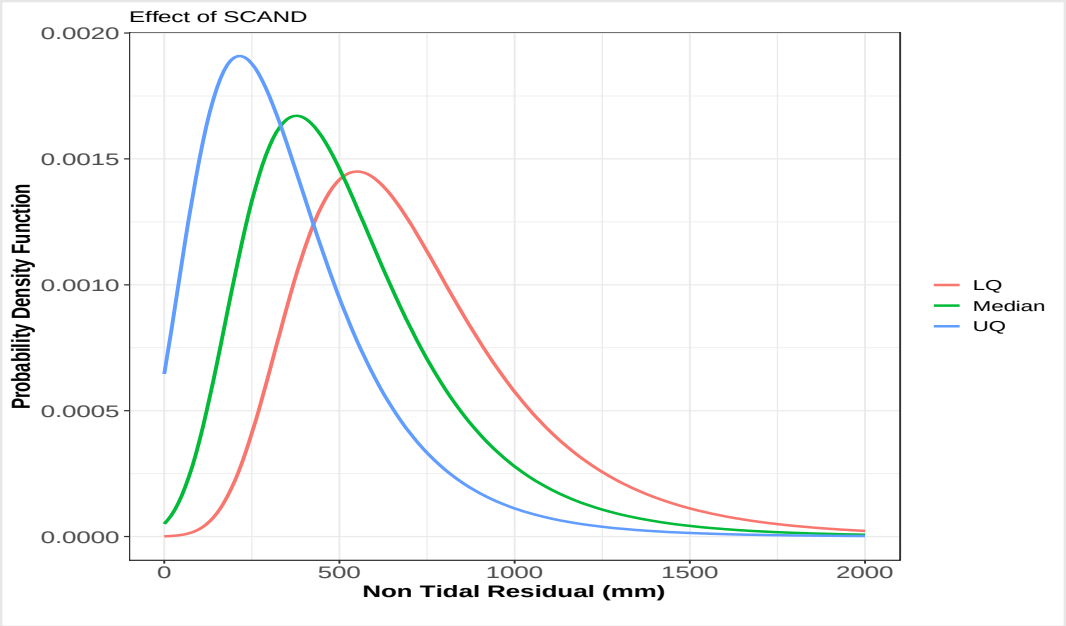

Finally, Figure 16 compares the QQ plots of residual of stationary model with those from the model in Table 2. Also in this case, including covariates improves the quality of the fitting.

Figure 16

QQ PLOTS OF STATIONARY AND NONSTATIONARY MODELS IN COPENHAGEN

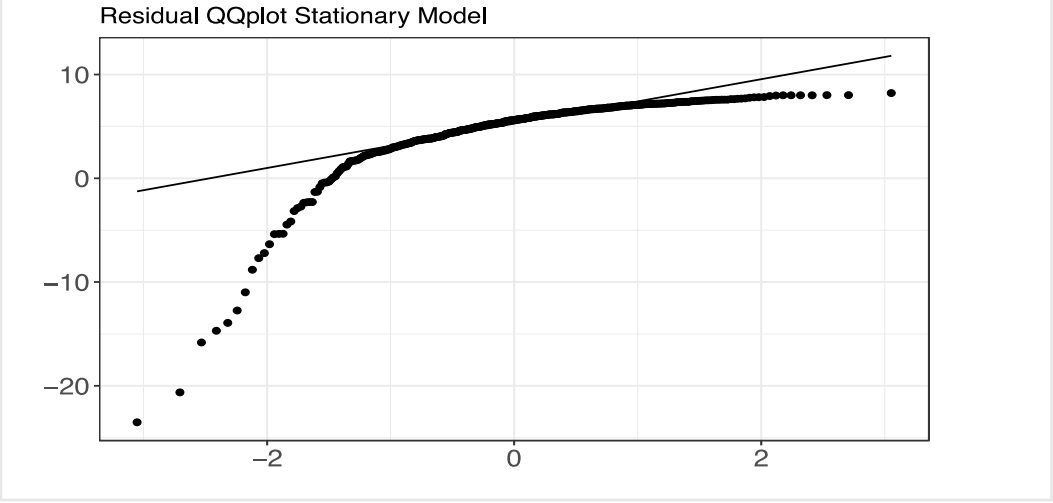

(a) QQ plots of the model residual without covariates.

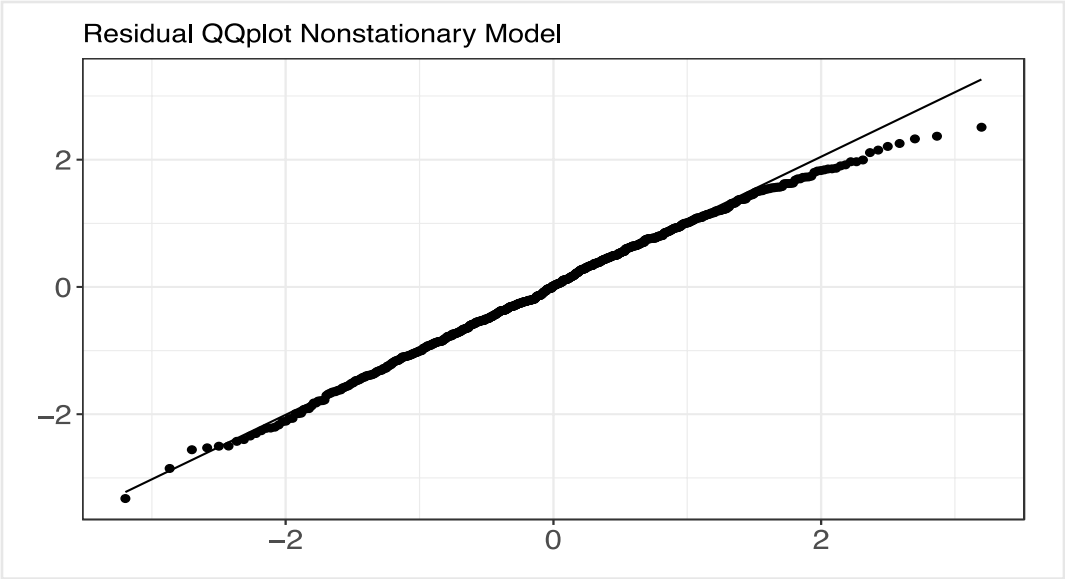

(b) QQ plots of the model residual including covariates.

3.5.3 SOUTH EAST QUEENSLAND

Estimation results for South-East Queensland are reported in Table 3. The location parameter exhibits seasonality and follows an increasing trend, but it does not seem to be impacted by neither nodal nor perigean cycles, while the scale parameter is not affected by seasonality. The long-term trend in the scale parameter has a negative coefficient, but it is still in-significant. Atmospheric phenomena linked with positive phases of the AAO and the SOI have positive impact on the location parameter, increasing the magnitude of extreme sea level event. This is consistent with the findings by previous studies, see e.g., Muis et al. (2018). On the other hand, the scale parameter is negatively affected by any increase in the climate indices considered.

Table 3
COEFFICIENT ESTIMATES FOR SOUTH EAST QUEENSLAND

Covariate	Name	Unit	Location	Scale(log-scale)
Constant	Base Level	mm	61.75	4.47
t	Long Term Trend	mm/month	3.85***	-0.003
$\sin(2\pi t/12)$	mm/month	Seasonal Component	15.81***	-
$Clim_{IOD,t}$	IOD	mm/$^{\circ}C$	-10.63	-0.21*
$Clim_{AAO,t}$	AAO	mm/millibar	2.37	-0.04
$Clim_{SOI,t}$	SOI	mm/millibar	3.50	-0.03

This table shows coefficient estimates for location parameter $a(t)$ and scale parameter $b(t)$ for the model obtained using the procedure in Menéndez and Woodworth (2010). Significance levels are reported following the standard convention, i.e., $*$ corresponds to 10%, $**$ corresponds to 5%, and $***$ corresponds to 1%

Figure 17 depicts the fitted location and scale parameters for the model in Table 3. The fitted location parameter exhibits increasing trend and seasonality, while the scale parameter follows a decreasing trend with a variability depending entirely on IOD, AAO, and SOI. As expected, the corresponding distributional mean values exhibit an increasing trend, following more closely the evolution of the fitted location parameter rather than the fitted scale one.

Figure 17

FITTED VALUES FOR THE LOCATION, AND SCALE PARAMETER AND THE CORRESPONDING DISTRIBUTIONAL MEAN VALUE, FOR THE GEV MODEL IN BRISBANE

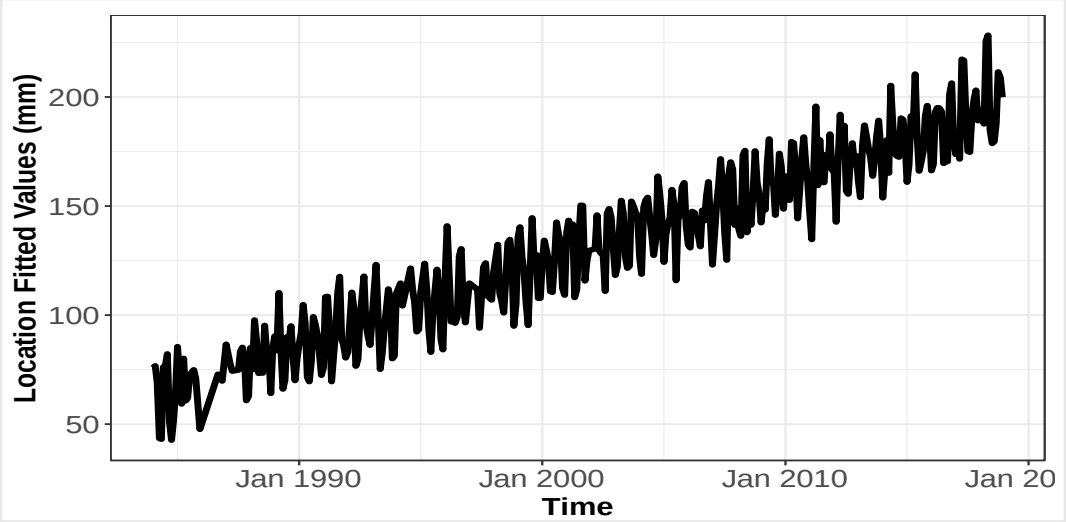

(a) Fitted location values for the Brisbane station

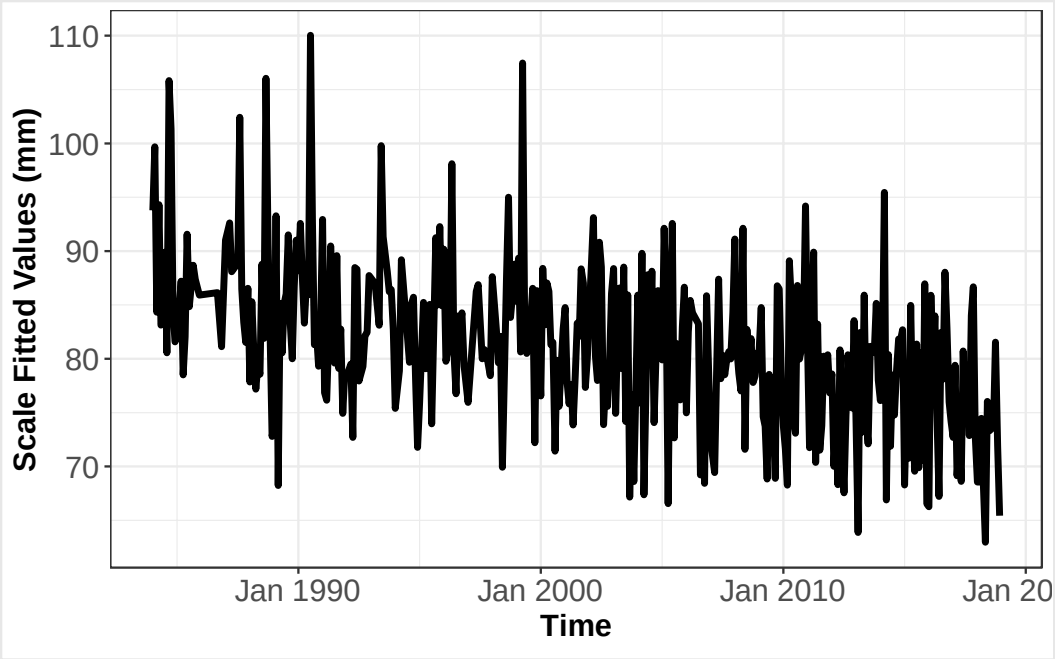

(b) Fitted scale values for the Brisbane station

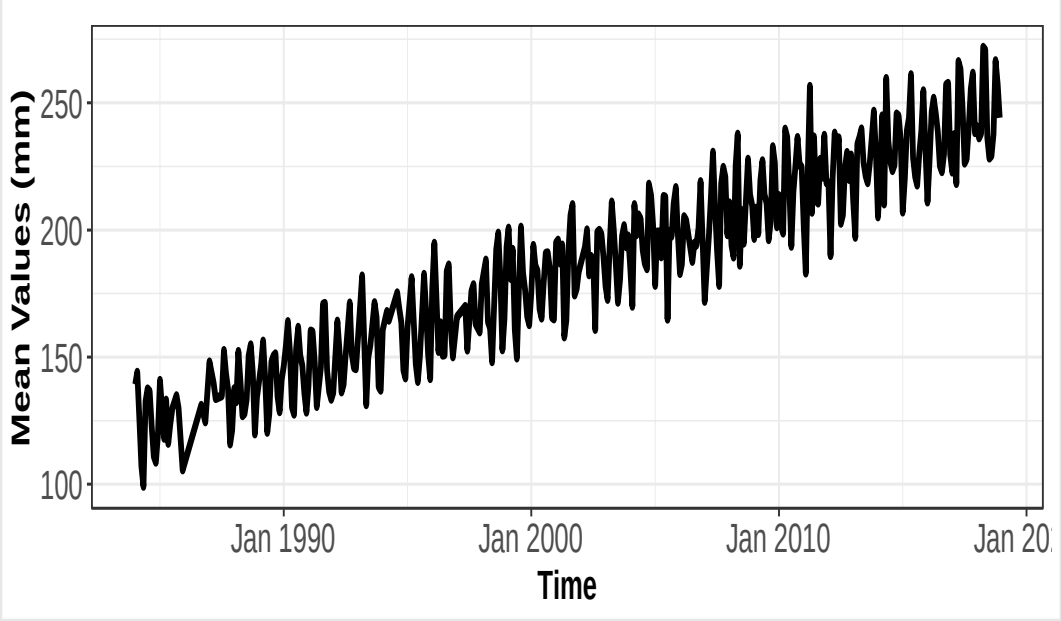

(c) Mean values for the Brisbane station

The effect of atmospheric phenomena on the probability density function of monthly maximum non-tidal residual is shown in Figure 18. Panel (a) illustrates the negative relationship between the

IOD and location parameter, showing how an increase in the IOD shifts the distribution to the left, reducing the average magnitude of the non-tidal residual. Panel (b) and (c) show the similar behavior of the impact of the AAO and SOI, where a positive phase in one of the indices generates and increases the magnitude of the non-tidal residual.

Figure 18

EFFECTS OF CLIMATE INDICES ON PROBABILITY DISTRIBUTION

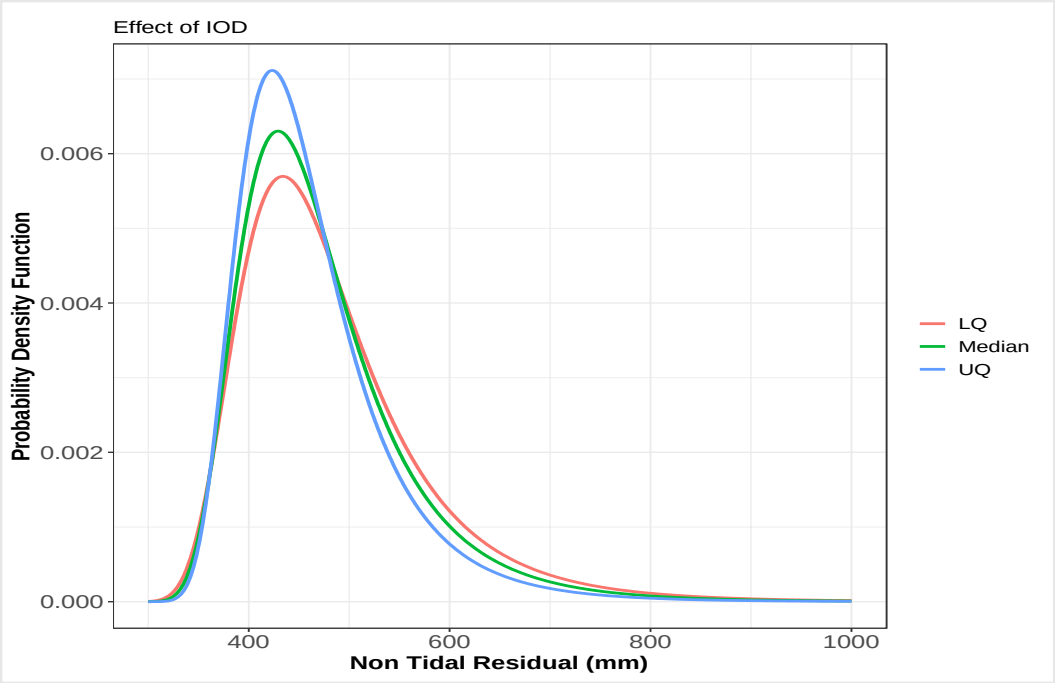

(a) Effects of variation in the IOD on the probability density function

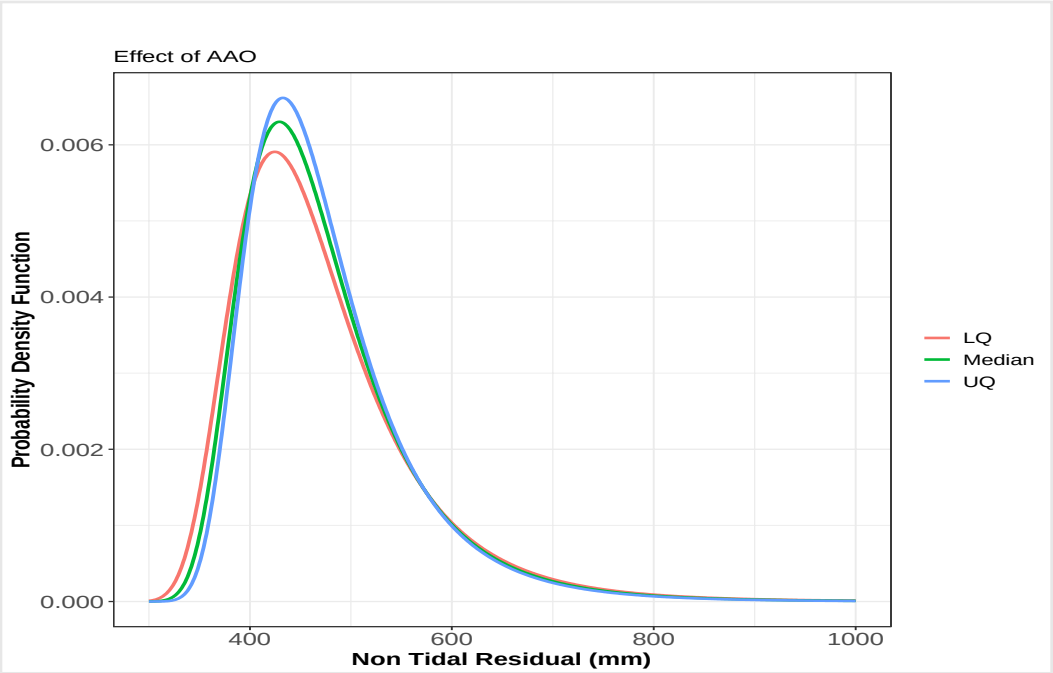

(b) Effects on variation in the AAO on the probability density function

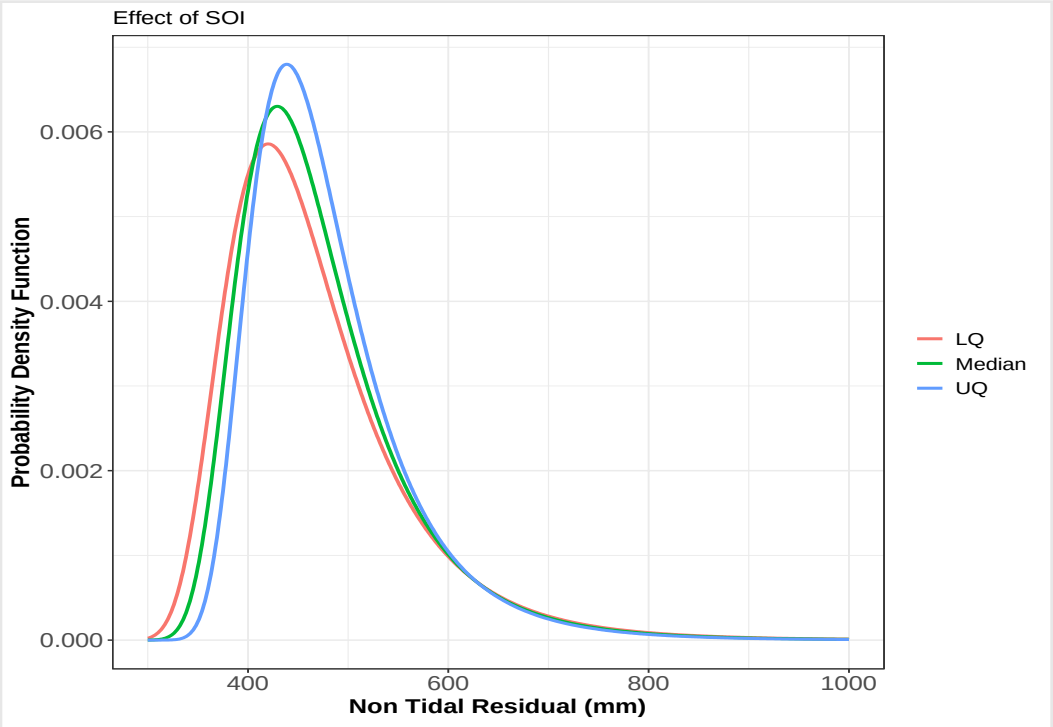

(c) Effects of variation in the SOI on the probability density function

Finally, Figure 19 compares the QQ plots of residual of a stationary model with the one from the model in Table 18. Also in this case, the nonstationary model provides a better fit than the stationary.

Figure 19

QQPLOTS OF STATIONARY AND NONSTATIONARY MODELS IN SOUTH EAST QUEENSLAND

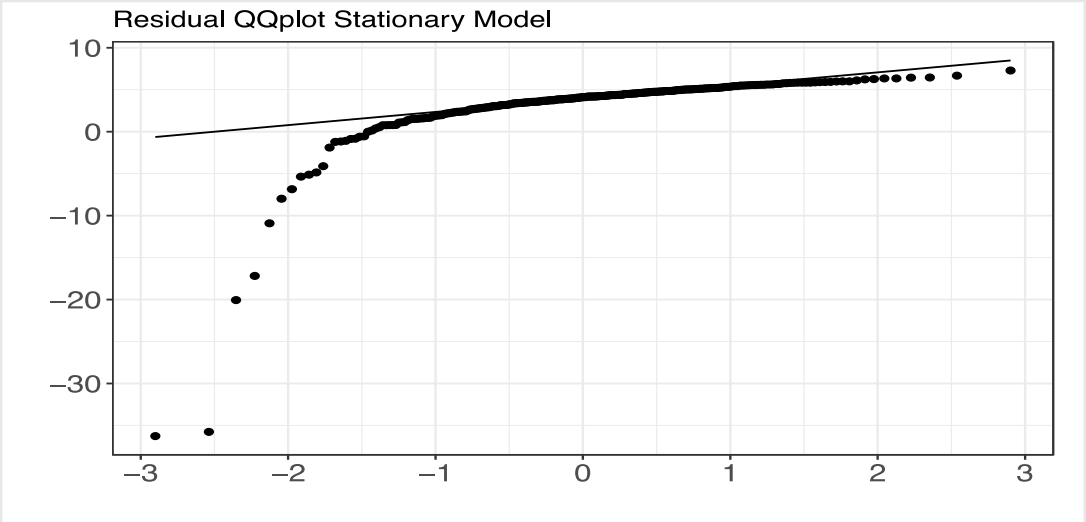

(a) QQ plots of the model residual without covariates.

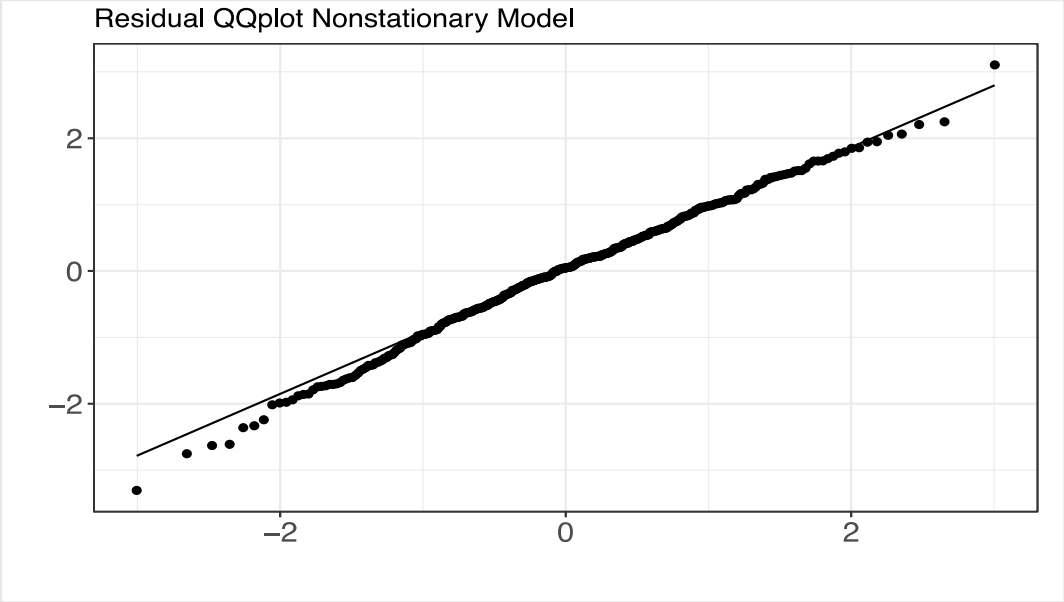

(b) QQ plots of the model residual including covariates.

3.6 SUMMARY

This section provides an econometric framework to estimate the distribution of extreme water levels in a nonstationary environment. Applying the framework to the three case studies, we find evidence for sea level rise in all the three areas. We also find significant impacts of intra-year seasonality as well as inter-year in the sea levels of the studied regions. Climate indices are also found to have impacts in one of the case studies, Copenhagen, and can be useful for predicting future storm surges. The results of these econometric exercises have important implications for investment analysis. The presence of a trend in extreme water levels suggests that sea level rise is real, and it is important to use real options models rather than the NPV rule to determine the optimal investment decision. In the presence of upward trends in the sea levels and hence the increasing flood risk, investment according to the NPV rule can lead to too early investment and inefficient use of capital. The next section will outline the real option models and how they can be used to analyze investment flexibility in the presence of sea level rises.

4: Investment analysis – Methodology

This section will describe the modeling framework developed for real option analysis. The framework has three main components: 1) a component for modeling the sea water level, 2) an insurance model, and 3) a component for conducting real options analysis (see Figure 20). The first component provides for each future time a distribution of high-water marks – the highest level to which sea water level rises in a particular year. The second component relates the high-water marks to flood damage via a loss curve. This model calculates the insurance premium without flood mitigation as well as with flood mitigation measures in place at a given time. Finally, the third component uses the reduction in the insurance premium by a mitigation measure to calculate the value of implementing that measure. This approach allows us to determine the optimal time to implement a single measure, or multiple measures when several flood mitigation investment options are available.

It is important to note that in this project, we follow real options analysis studies and determine the optimal investment decisions based on the market values of the projects. This involves treating investment projects as assets in financial markets and use the asset pricing tools to determine the values of these projects if they were traded in the markets (Dixit and Pindyck, 1994). This approach is suitable to the evaluation of public infrastructure that may involve co-benefits or social externalities as long as these additional benefits/impacts can be determined and added to the cash flows of the projects. In addition, the proposed framework separates risk from the discount rate and allows the evaluation of projects that involve complex optionality and therefore changing risks (Brealey et al. 2020). This is in contrast to the traditional risk adjusted approach or the social discounting approach that uses the discount rate to account for the impact of risk or co-benefits of the projects.

Figure 20
MODELING FRAMEWORK

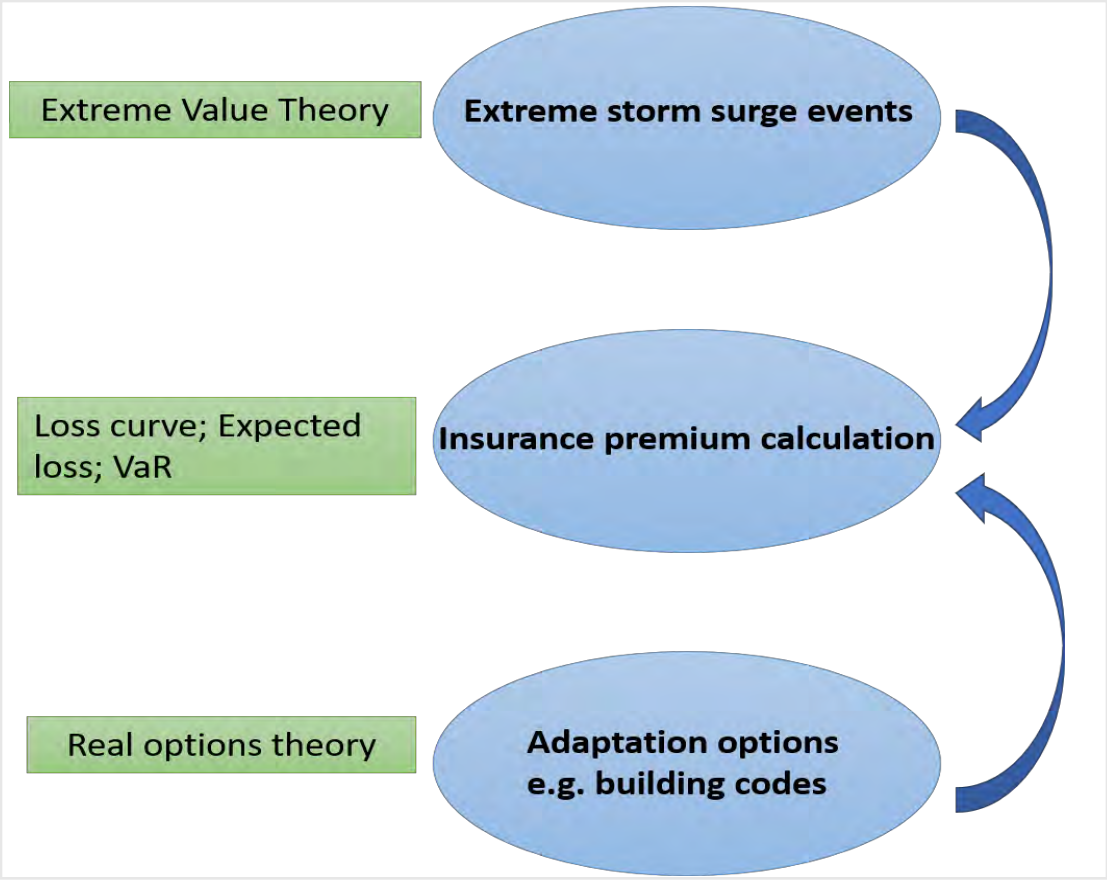

4.1 SEA WATER LEVEL MODELING

The maximum S_t of the storm surge height observed in period t is assumed to follow a GEV distribution:

$$H(S_t; m, s, \xi) = \exp\left\{-\left[1 + \xi\left(\frac{S_t - m}{s}\right)\right]^{-1/\xi}\right\}, \quad 1 + \xi\left(\frac{S_t - m}{s}\right) > 0, \tag{2}$$

where m, s, ξ are called the location, scale and shape parameters. We define the high-water mark M_t as the sum of mean sea level $W(t)$, $Tide(t)$ and the block maximum surge S_t. Since S_t follows a GEV distribution $H(S_t; m, s, \xi)$, conditional on the mean sea level $W(t)$ and tide $Tide(t)$ at time t, the high water mark M_t also follows a GEV $H(M_t; \alpha, s, \xi)$ with the same scale and shape parameters as S_t, but the location parameter is given by $\alpha = W(t) + Tide_t + m$. In the investment model, we adopt the deseasonalization approach often used in the real options literature, see e.g. Abadie and Chamorro (2008); Boomsma et al. (2012); Ernstsen and Boomsma (2018) and in flood

risk adaptation, see e.g. Aerts et al. (2013, 2014); Wang et al. (2015); Hallegatte et al. (2011) and replace $Tide_t$ by its average level $\overline{Tide}$.

4.2 INSURANCE MODEL

The insurance model helps to determine catastrophic losses corresponding to each high-water mark M. We adopt loss curves estimated by previous studies (see, e.g., Prettenthaler et al., 2010; Hallegatte et al., 2011; Wang et al., 2015; Aerts et al., 2014; Han et al., 2020) to associate sea level with economic damages. Typically, a loss curve $L(M)$ provides the loss estimate for each water level M when loss exposure is as currently observed. When loss exposure grows at a rate γ, a water level M_t will cause a loss $e^{\gamma t}L(M_t)$. The insurance premium for a full loss coverage at time t, when the mean sea level is α, can be obtained as

$$\pi(u,t,\alpha;L) = (1+\delta)e^{\gamma t}\int_u^{\infty} L\,(M)dH(M), \tag{3}$$

where δ is the premium loading and u is the flood threshold such that when the water level is lower than u, no damage is caused.

Figure 21

IMPACT OF FLOOD-PROOFING MEASURES ON FLOOD LOSS DISTRIBUTION

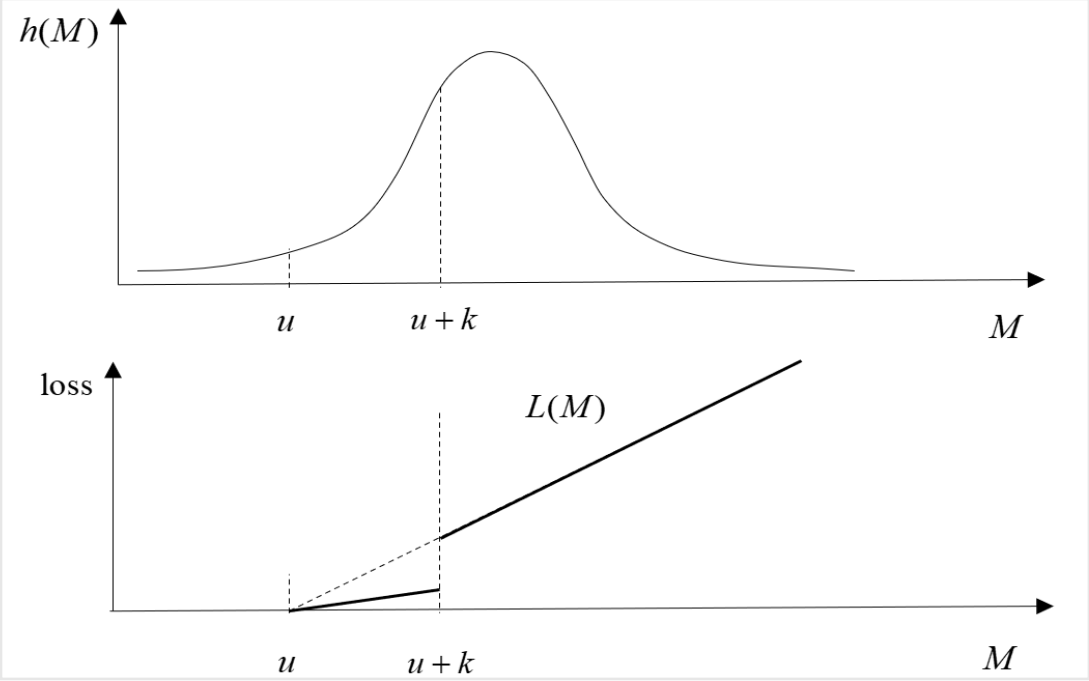

Building code requirements such as dry-proofing or wet-proofing can help to reduce damages by a proportion κ as long as the water level is lower than a certain height, say $u + k$. As illustrated in Figure 21, these measures rotate downwards a lower portion of the damage curve. By alleviating the impact of smaller floods, flood-proofing measures reduce the insurance premium by an amount

$$R(k,t,\alpha;L) = \kappa[\pi(u,t,\alpha;L) - \pi(u+k,t,\alpha;L)]. \quad (4)$$

Building a dike or seawall that raises the flood threshold from u to $u+k$ will help avoid damages from flood with heights up to $u+k$. The impact is similar to that of flood-proofing where $\kappa = 1$. The dike helps to reduce the insurance premium at time t from $\pi(u,t,\alpha;L)$ to $\pi(u+k,t,\alpha;L)$, and so the benefit flow of this adaptation measure is

$$R(k,t,\alpha;L) = \pi(u,t,\alpha;L) - \pi(u+k,t,\alpha;L). \quad (5)$$

Converting houses in the most vulnerable areas to parkland, or elevating houses in the region by a height k, can be modeled by shifting the loss curve horizontally (Figure 22). The insurance premium reduction by house elevation is

$$R(k,t,\alpha;L) = \pi(u,t,\alpha;L) - \pi(u,t,\alpha;L_1), \quad (6)$$

where $L_1(M) = L(M-k)$ for all M.

Figure 22

IMPACT OF ELEVATING HOUSES IN THE REGION

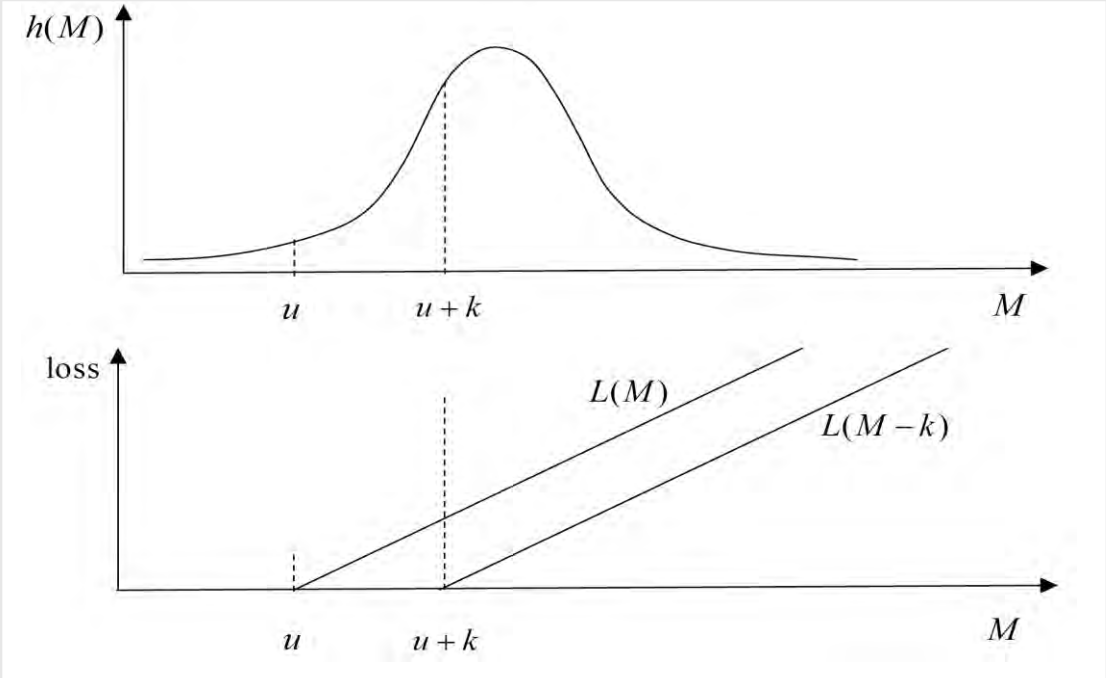

4.3 PARAMETRIC LOSS CURVE

Polynomial curves can be used to fit losses for different water levels. We use a quadratic form for the loss function $L(M)$:

$$L(M) = aM^2 + bM + c = X\beta \quad (7)$$

where $X = [M^2 \quad M \quad 1]$ and $\beta = [a \quad b \quad c]'$. With this loss function, the original flood threshold u satisfies $au^2 + bu + c = 0$. The water level u is the flood threshold in the absence of any flood mitigation. The flood threshold x that is effective when flood mitigation measures such as dams are in presence can be higher than u. With the flood threshold x, the insurance premium $\pi(x, t, \alpha; L)$ can be expressed as

$$\pi(x, t, \alpha; L) = (1 + \delta)e^{\gamma t} D(x, \alpha; \beta), \tag{8}$$

where $D(x, \alpha; \beta)$ is the expected damage given by

$$D(x, \alpha; \beta) = \int_x^{\infty} (aM^2 + bM + c) dH(M). \tag{9}$$

When GEV is used to model the maximum water level, the expected damage function $D(x, \alpha; ; \beta)$ in the above equation takes the following form (El Sherpieny et al., 2013; Embrechts et al., 2013):

$$D(x, \alpha; \beta) = \begin{cases} D_1(x, \alpha; \beta) & \text{if } \xi > 0 \text{ and } x > \alpha - \frac{s}{\xi} \\ D_2(x, \alpha; \beta) & \text{if } \xi > 0 \text{ and } x \leq \alpha - \frac{s}{\xi} \\ 0 & \text{if } \xi < 0 \text{ and } x > \alpha - \frac{s}{\xi} \\ D_1(x, \alpha; \beta) & \text{if } \xi < 0 \text{ and } x \leq \alpha - \frac{s}{\xi} \end{cases} \tag{10}$$

where $D_1(x, \alpha; \beta)$ and $D_2(x, \alpha; \beta)$ are given by:

$$\begin{aligned} D_1(x, \alpha; \beta) \quad &= a\left(\frac{s}{\xi}\right)^2 \Gamma(1 - 2\xi, [1 + \xi(\tfrac{x-\alpha}{s})]^{-\frac{1}{\xi}}) \\ &+ 2\frac{s}{\xi}(a\alpha - a\frac{s}{\xi} + b/2)\Gamma(1 - \xi, [1 + \xi(\tfrac{x-\alpha}{s})]^{-\frac{1}{\xi}}) \\ &+ [a(\alpha - \tfrac{s}{\xi})^2 + b(\alpha - \tfrac{s}{\xi}) + c][1 - H(x)], \end{aligned} \tag{11}$$

$$\begin{aligned} D_2(x, \alpha; \beta) \quad &= a(\alpha - \tfrac{s}{\xi})^2 + \tfrac{sa}{\xi}(\tfrac{s}{\xi}\Gamma(1 - 2\xi) - 2(\tfrac{s}{\xi} - \alpha)\Gamma(1 - \xi)) \\ &+ b\alpha + \tfrac{sb}{\xi}[\Gamma(1 - \xi) - 1]. \end{aligned} \tag{12}$$

4.4 SINGLE INVESTMENT REAL OPTIONS MODEL

Recall that M_t follows a GEV distribution $H(M_t; \alpha(t), s(t), \xi)$, where $\alpha(t) = W(t) + \overline{Tide} + m$. Due to the impact of climate change, we assume that the mean sea level W_t follows an arithmetic Brownian motion process:

$$dW_t = \mu dt + \sigma dB_t, \tag{13}$$

where B_t is a standard Brownian motion, μ is the expected change in the mean sea level and σ represents the uncertainty in the estimates of sea-level changes. Then, the location parameter α_t follows the same process and the location parameter for the high-water mark at time T is $\alpha_T \sim N(\alpha_0 + \mu T, \sigma^2 T)$. The simple relation between the location parameter α_t and the mean water level provides a way to estimate the time varying location parameter α_t by observing the mean water level. We estimate the mean water level by the average hourly water level for each year and use the annual mean water level to estimate the stochastic process in Equation 13.

It should be noted that some city may experience land subsidence that further exacerbates the impact of sea level rise. Land subsidence can be incorporated into the model by increasing the level of sea rise. It is, however, often difficult to obtain data on land subsidence and a deterministic rate of subsidence is usually assumed. In that case, parameter μ is increased to allow for land subsidence.

We examine a project that lasts infinitely and costs I to invest. The project provides a benefit flow $R(t, k, \alpha)$, which is a product of a time invariant component $R(k, \alpha)$ and a growth component $e^{\gamma t}$, i.e. $R(t, k, \alpha) = e^{\gamma t} R(k, \alpha)$.[3]

To facilitate the evaluation of the project and option values, we formulate a risk-neutral measure under which derivative prices can be obtained as the present value of the expected cash flows. Based on the capital asset pricing model (CAPM), the expected return μ_X on an asset X that has a return standard deviation σ_X is given by:

$$\mu_X = r + \phi \rho_{xm} \sigma_X, \tag{14}$$

where ρ_{xm} is the correlation between the asset return and market return, $\phi = \frac{r_m - r}{\sigma_m}$ is the market price of risk and r_m and σ_m are the expected value and standard deviation of the market return.

A risk-neutral measure $\mathbb{P}^*$ is a probability measure under which all non-dividend paying assets have an expected rate of return equal to the risk-free rate r. If $B(t)$ is a Brownian motion under the physical measure $\mathbb{P}$, then $B^*(t)$ that satisfies $dB^*(t) = dB(t) + \phi \rho_{xm} \sigma dt$ is a Brownian motion under the risk-neutral measure $\mathbb{P}^*$. As a result, the process for $W(t)$ under the risk-neutral measure is given by:

$$dW(t) \quad = (\mu - \theta) dt + \sigma dB^*(t) \tag{15}$$

where $\theta = \phi \sigma \rho_{wm}$ and ρ_{wm} is the correlation between the changes in the mean sea level and the market return.

Using the risk-neutral measure, the project value can be calculated as

$$V(\alpha) = \int_t^\infty e^{-(r-\gamma)(u-t)} E^*[R(k, \alpha(u)) | \alpha(t) = \alpha] du, \tag{16}$$

where $R(k, \alpha(u))$ (for the case of flood-proofing) is given by

[3] Note that the benefit flow also depends on the loss curve L. We have dropped L to simplify notations.

$$R(k, \alpha(u)) = (1 + \delta)\kappa(D(u, \alpha; \beta) - D(u + k, \alpha; \beta)). \quad (17)$$

The value of the option to invest, $\Phi(\alpha)$, can be shown to follow the stochastic differential equation, see, e.g., Dixit and Pindyck (1994):

$$\frac{1}{2}\sigma^2\Phi_{\alpha\alpha} + (\mu - \theta)\Phi_\alpha - r\Phi = 0. \quad (18)$$

Furthermore, at the option exercise threshold α^*, the value matching and smooth pasting conditions need to be satisfied, providing two boundary conditions:

$$\Phi(\alpha^*) \quad = V(\alpha^*) - I, \quad (19)$$

$$\Phi_\alpha(\alpha^*) \quad = V_\alpha(\alpha^*). \quad (20)$$

We use the binomial lattice to solve for the project value, the optimal investment boundary and the option value, since it is simple to find the investment boundary with this method.

4.5 MULTIPLE INVESTMENTS

When several adaptation projects can be invested, identifying the optimal investment sequence can help to improve the investment value. We define the optimal investment sequence as the one that gives the highest investment value. For an example of two mutually non-exclusive investment projects, Project 1 and Project 2, two investment sequences are possible: i) Project 1 is invested first, and then Project 2 is invested thereafter and ii) Project 2 is invested first and then Project 1 is invested. It is necessary to compute the investment value for each sequence and identify the optimal sequence that gives the highest value. The same procedure applies when more than two projects are considered.

To evaluate the investment value of one investment sequence, for example, the first sequence in the above example, suppose the investment costs of the two projects are I_1 and I_2. In addition, suppose $R_1(k_1, t, \alpha; L_1)$ is the benefit flow that is obtained when Project 1 is invested. The benefit flow $R_1(k_1, t, \alpha; L_1)$ is the same as that obtained when in the case of single investment. In contrast, the benefit flow $R_{12}(k_2, t, \alpha; L_2)$ obtained when we further invest in Project 2 after Project 1 has been invested is the marginal benefit obtained due to the additional protection offered by Project 2. For example, for the case of upgrading the height of the same dike, the loss curve does not change ($L_2 = L_1 = L$) and $R_{12}(k_2, t, \alpha; L_2)$ can be obtained as

$$R_{12}(k_2, t, \alpha; L) = \pi(u + k_1, t, \alpha; L) - \pi(u + k_1 + k_2, t, \alpha; L). \quad (21)$$

Once we have defined the benefit flow provided by each investment, we need to determine the optimal time τ_1 to invest in Project 1, and the optimal time τ_2 to invest in Project 2 thereafter:

$$\Phi_1(\alpha_t) + \Phi_{12}(\alpha_t) = \max_{\tau_1,\tau_2} E_t^Q \left[\int_{\tau_1}^{\infty} e^{-rs} R_1(k_1, t, \alpha_s; L_1) ds - e^{-r\tau_1} I_1 + \int_{\tau_2}^{\infty} e^{-rs} R_{12}(k_2, t, \alpha_s; L_2) ds - e^{-r\tau_2} I_2 | \alpha_t \right], \quad (22)$$

where $\Phi_1(\alpha_t)$ is the value of the option to invest in Project 1 and $\Phi_{12}(\alpha_t)$ is the value of the option to invest in Project 2, after Project 1 has already been invested. Similarly, if Project 2 is invested first, then $\Phi_2(\alpha_t) + \Phi_{21}(\alpha_t)$ is obtained. In considering which project to be invested first, the decision maker needs to select a sequence that maximizes the option to invest, $\Phi_s(\alpha_t)$, i.e.

$$\Phi_s(\alpha_t) = \max\{\Phi_1(\alpha_t) + \Phi_{12}(\alpha_t), \Phi_2(\alpha_t) + \Phi_{21}(\alpha_t)\}. \quad (23)$$

5: Investment analysis – Case studies

In this section we present the results of the numerical analysis for three case studies. In the case study of New York City, we consider single investments of i) a barrier and dike project and ii) a water proofing project, as well as a multiple investment when the two projects are considered together. Consideration of multiple investments is necessary for the formulation of dynamic investment pathways. In South-East Queensland, we investigate the optimal time to invest in a house elevation project. In the Copenhagen, we consider the problem of investing in a dike system where the ultimate height of the dike is achieved in one go (a single investment) or achieved in two stages (a multistage investment).

5.1 CASE STUDY OF NEW YORK CITY

We examine the optimal investment strategies for two projects for New York City based on Aerts et al. (2014): a) a barrier project that uses barriers and dikes to protect the region and b) a wet flood-proofing project that adjusts the interior and material of buildings in the one-in-100-year flood area (i.e. the area in which the probability of having a flood in any single year is at least 0.01) to limit flood damage.

The barrier project is referred to as project S2c in Aerts et al. (2014), which aims to reduce the length of the coastline of the New York City area as much as possible. It involves the construction of two storm surge barriers. One barrier will connect Sandy Hook in New Jersey and the tip of the Rockaways in Queens, New York and the other barrier will close the East River. The investment cost is estimated to range from $11 billion to $15 billion and the maintenance cost is $118 million per year. We use a mid-range value of the investment cost, which is $13 billion. The project is assumed to raise the flood threshold by 1000mm for houses and infrastructure.

The flood-proofing project is a measure that helps to keep the options open. Building codes can be further enhanced in the future or storm surge barriers can be developed. It involves wet flood-proofing of existing buildings in the one-in-100-year flood area. We consider the most cost-effective measure found by Aerts et al. (2014), which involves wet-proofing 2 feet (610mm) of buildings with 30% effectiveness. The cost of this measure is $246 million.

Table 4

INFORMATION ON ESTIMATED AND ASSUMED PARAMETER VALUES FOR NEW YORK CITY

Parameters	Values
Location parameter (α)	1642
Scale parameter (s)	131
Shape parameter (ξ)	0.27
Current flood threshold (u)	2506mm
Quadratic coefficient of damage curve (a)	0
Linear coefficient of damage curve (b)	0.0393
Mean sea level rise per year (μ)	6mm
Standard deviation of sea level rise per year (σ)	25mm

Safety loading of flood risk (δ)	3%
Risk-free rate (r)	4%
Growth rate of loss exposure (γ)	1%
Market risk premium (θ)	0.15
Dike construction	
Investment cost (I)	$15.95 billion
Flood mitigation (k)	1000mm
Flood-proofing	
Investment cost	$246 million
Flood mitigation	610mm
Effectiveness	30%

5.1.1 PARAMETER ESTIMATION FOR NEW YORK CITY

We start by estimating flood risk in the area based on the surge height at the Battery in lower Manhattan, NYC. We obtain the surge height by excluding the tide and the mean sea level from the hourly water level. We then obtain the annual maximum of storm surge height for each year to estimate the GEV distribution. The average tide and the mean sea level are then added back to the estimated location parameter to obtain the distribution of the high-water mark. The estimated parameters of the high-water mark distribution are: $\alpha = 1642, s = 131, \xi = 0.27$.

Figure 23

OBSERVED ANNUAL MEAN AND ANNUAL MAXIMUM SEA LEVELS AT THE BATTERY IN LOWER MANHATTAN, NYC

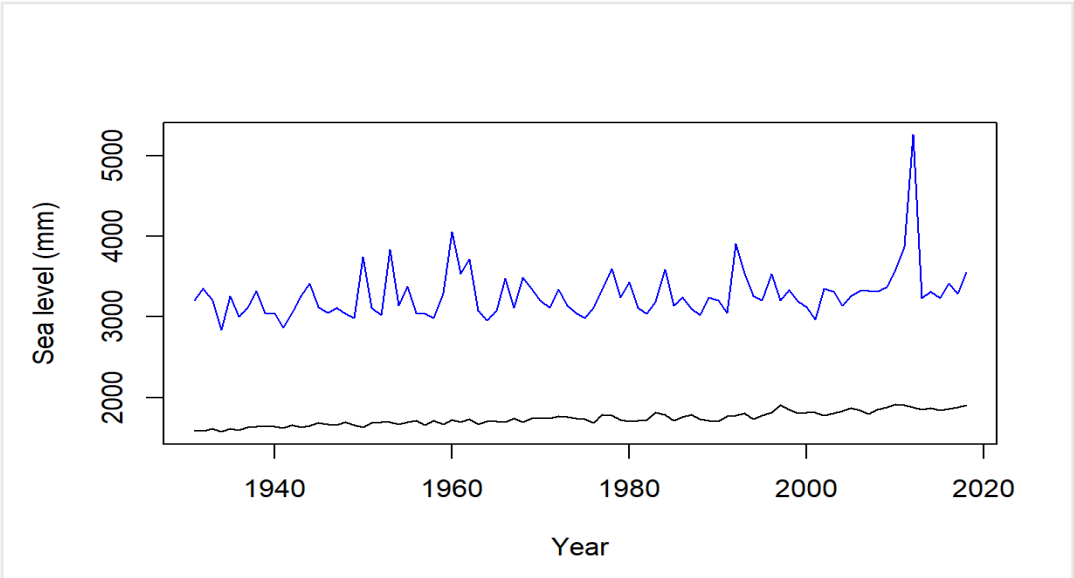

We assume a 1.31% growth in loss exposure for the area in this study, based GDP and population growth in the region (see Weinkle et al. [2018] for details). In addition, we assume a real risk-free rate of 4% based on the study by Newell and Pizer (2003), who estimate the real risk-free rate using 10-year treasury bond yields observed since 1800.[4]

We use an estimate of the market risk premium θ of 0.15, based on the correlation between the annual change in the mean sea level and the rate of return on the stock market index (S&P 500) (corr= 0.0283), the market price of risk $\phi = 0.1382$, and the historical standard deviation of 38.48.

A safety loading of $\delta = 3\%$ is assumed, following the estimation results reported by Shao et al. (2015) based on CAT bond prices. We use results from climate change studies to calibrate the mean sea level rise process. We follow Aerts et al. (2014) to assume a mean sea level rise of 6.5 mm per year for the area that takes into account land subsidence in the area and use σ =25mm to summarise the uncertainty in sea level change estimates, based on data provided by Johansson et al. (2014). The ratio of the standard deviation and the mean of the sea level rise is quite high, which indicates significant uncertainty related to the estimate of future sea level changes.

We use the damage curve estimated by Aerts et al. (2014) (Figure 25). Without adaptation, flood loss occurs whenever the sea level exceeds 2.506m. This flood threshold occurs at the extreme right tail of the distribution where $1 - H(u) = 0.023$. Using the estimated damage curve and the high-water mark distribution, the expected annual damage without adaptation is $498M, which is slightly lower than the expected annual damage of $508M estimated by Aerts et al. (2014). The discrepancy is likely due to the difference in the approach to high water mark estimation: Aerts et al. (2014) use a model-based approach that estimates the high-water mark distribution based on simulated storm surge events, while we use historical data.

[4] This is also the discount rate used by Aerts et al. (2014).

Figure 24

LOSS CURVE FOR THE STUDIED AREA IN NEW YORK CITY

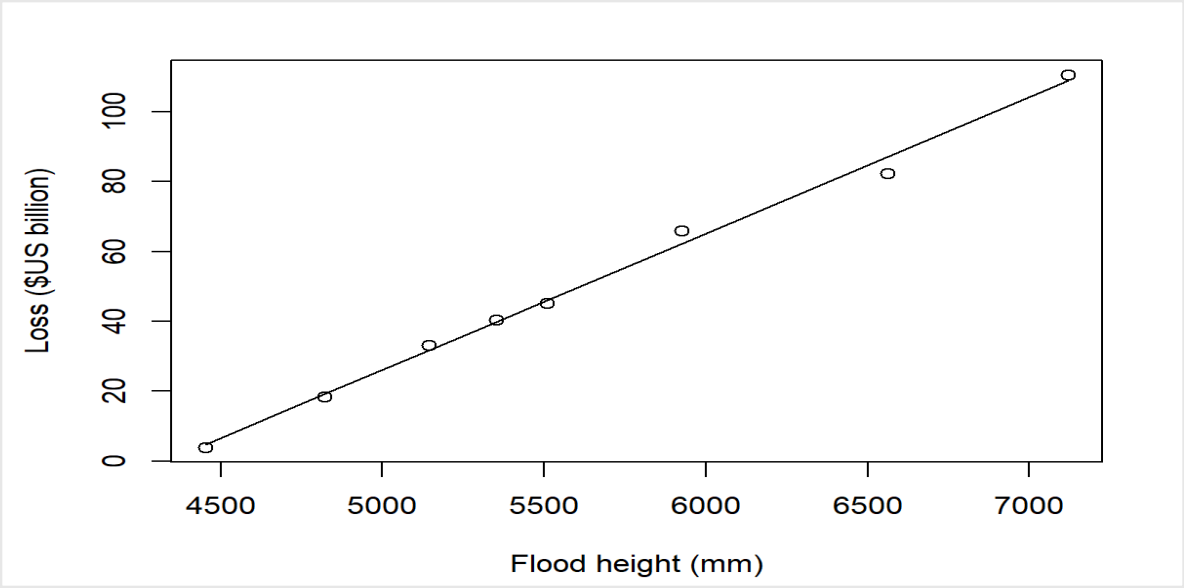

The flood-proofing project will reduce flood damages to buildings, leaving flood losses to business interruption, infrastructure and vehicles unchanged. Aerts et al. (2014) consider flood-proofing for buildings in the one-in-100-year flood area, leaving buildings in other areas unchanged. To recognize the impact of this measure in our model, we scale down the total damage curve in Figure 26 so that the annual benefit of flood-proofing under no loss exposure growth and no climate change is the same as that estimated by Aerts et al. (2014).

Figure 25 shows the damage curves for the two projects. The barrier and dike project helps to prevent water from coming into the city and provides a large risk reduction. In contrast, the flood-proofing project focuses on only protecting buildings and leaving business interruptions and damages to infrastructure unchanged. These two projects may provide a good example of supplementary projects in the dynamic dimension. It appears that the barrier project is costly and optimal to invest only when climate change is sufficiently serious. The flood-proofing project has a low investment cost and may be worthwhile to invest in the absence of the barrier project. Actual investment timing, however, will depend on the benefit of each project relative to the cost.

Figure 25
DAMAGE CURVES FOR NYC

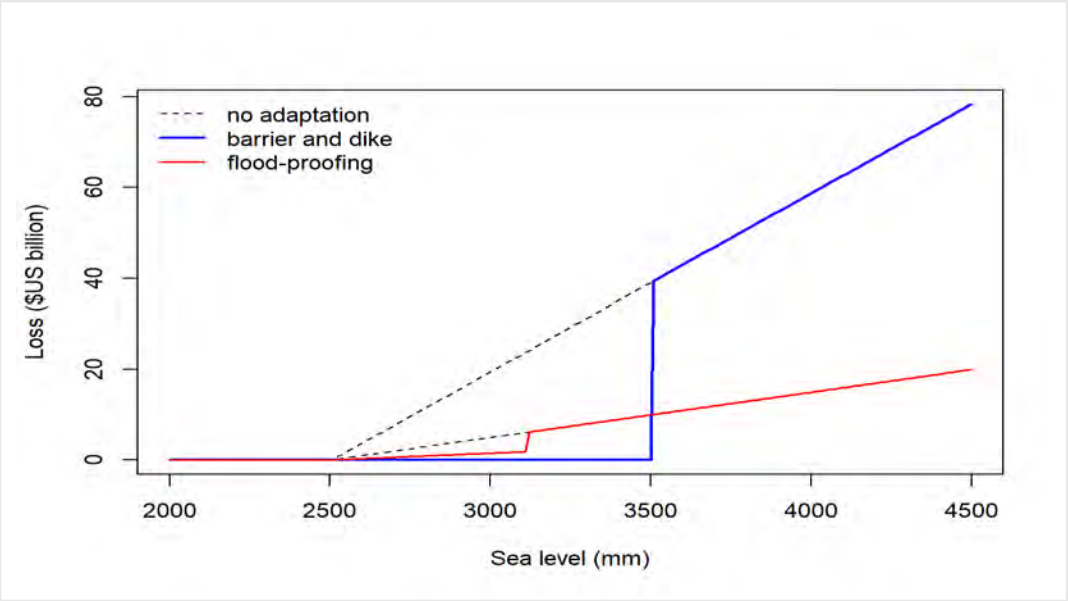

Damage curves estimated for the studied area in New York City for the case of no adaptation, adaptation with barriers and dikes and adaptation with flood-proofing buildings.

5.1.2 PROTECTING NYC USING STORM SURGE BARRIERS

The NPVs and option values of the investment project for different scenarios are reported in Table 5. The project has negative NPVs when the climate does not change, which indicates that the current risk infrastructure is quite adequate. In presence of climate change and positive growth in loss exposure, the NPV of the project is positive and the project is worth investing. However, due to the uncertainty that is related to the future sea level changes, deferring the investment to a future time would result in a higher investment value. This is illustrated by the difference between the total value with optionality and the NPV of the project in the table. The project would be invested when the location parameter reaches 1770mm.

Table 5
INVESTMENT ANALYSIS FOR BARRIER AND DIKE PROJECT IN NYC

	$\mu = 0, \gamma = 1.31\%$	$\mu = 6.5, \gamma = 1.31\%$	$\mu = 13, \gamma = 1.31\%\%$	$\mu = 6.5, \gamma = 2.6\%$
NPV	-7.07	9.90	58.35	59.01
Total value with optionality	0.19	11.25	58.35	59.01
Difference	7.25	1.35	0.00	0.00

Investment analysis for barrier and dike project using NPV rule and real options methods. We report (in billion USD) the NPV, the total value with optionality and the difference of the two values. Results are reported for four cases: i) no climatic change and zero exposure growth, ii) climatic change and exposure growth, iii) doubled expected sea level rise and exposure growth, iv) climatic change and doubled exposure growth. All cases assume σ = 25mm.

Sensitivity analysis results in Tables 6, 7 and 8 show that the value of the project is higher when the discount rate is lower, when the expected sea level rise is higher, and when the uncertainty on the sea level rise is higher. For low discount rates or high levels of sea rise, the project has high NPVs, and it is optimal to invest in the project immediately. No difference would exist between the value of optionality and the value given by the NPV rule in these cases. As the sea level rise uncertainty increases the difference between NPV and optionality decreases.

Table 6

INVESTMENT ANALYSIS FOR BARRIER AND DIKE PROJECT IN NYC UNDER DIFFERENT DISCOUNT RATES

	r=2%	r=3%	r=4%	r=5%	r=6%
NPV	349.18	58.02	9.90	-2.30	-6.62
Total value with optionality	349.18	58.02	11.24	2.88	0.90
Difference	0.00	0.00	1.35	5.18	7.52

Investment analysis for barrier and dike project using NPV rule and real options methods under different discount rates. We report (in billion USD) the NPV, the total value with optionality and the difference between the two values.

Table 7

INVESTMENT ANALYSIS FOR BARRIER AND DIKE IN NYC UNDER DIFFERENT SEA LEVEL RISE

	μ=0	μ=3	μ=6	μ=9	μ=12
NPV	-7.20	-2.60	9.90	32.43	59.73
Total value with optionality	0.17	2.05	11.24	32.43	59.73
Difference	7.37	4.65	1.35	0.00	0.00

Investment analysis for barrier and dike project using NPV rule and real options methods under different levels of sea rise. We report (in billion USD) the NPV, the total value with optionality and the difference between the two values.

Table 8

INVESTMENT ANALYSIS FOR BARRIER AND DIKE IN NYC UNDER DIFFERENT SEA LEVEL RISE UNCERTAINTY

	σ=7	σ=15	σ=25	σ=30	σ=45
NPV	5.25	6.71	9.90	11.99	19.72
Total value with optionality	6.83	8.22	11.24	13.22	20.57

Difference	1.57	1.51	1.35	1.23	0.85

Investment analysis for barrier and dike project using NPV rule and real options methods under different sea level rise uncertainty. We report (in billion USD) the NPV, the total value with optionality and the difference between the two values.5.1.3 Wet flood-proofing buildings in vulnerable areas.

Flood-proofing buildings in the most vulnerable area may provide a low-cost adaptation option that is relevant when the mean sea level remains low. The results in Table 9 suggest that this adaptation measure has a positive NPV even in the case of zero expected sea level rise, in contrast with the dike and barrier cases. As expected, the NPV increases in both sea level change and loss exposure growth. In addition, this adaptation measure provides a high value relative to its cost and there is no value in waiting to invest.

Table 9

INVESTMENT ANALYSIS FOR FLOOD PROOFING PROJECT IN NYC

	$\mu = 0, \gamma = 1.31\%$	$\mu = 6.5, \gamma = 1.31\%$	$\mu = 13, \gamma = 1.31\%\%$	$\mu = 6.5, \gamma = 2.6\%$
NPV	0.10	0.81	2.43	2.63
Total value with optionality	0.10	0.81	2.43	2.63
Difference	0.00	0.00	0.00	0.00

Investment analysis for wet flood-proofing project using NPV rule and real options methods. We report (in billion USD) the NPV, the total value with optionality and the difference of the two values. Results are reported for four cases: i) no climatic change and zero exposure growth, ii) climatic change and exposure growth, iii) doubled expected sea level rise and exposure growth, iv) climatic change and doubled exposure growth. All cases assume σ = 25mm.

Sensitivity analysis results in Tables 10, 11, and 12 show that the NPV of the project remains positive for different discount rates and different levels of sea rise. Only for a discount rate of 6%, it is optimal to defer the project investment.

Table 10

INVESTMENT ANALYSIS FOR FLOOD PROOFING PROJECT IN NYC UNDER DIFFERENT DISCOUNT RATES

	r=2%	r=3%	r=4%	r=5%	r=6%
NPV	11.42	2.63	0.81	0.29	0.09
Total value with optionality	11.42	2.63	0.81	0.29	0.11
Difference	0.00	0.00	0.00	0.00	0.02

Investment analysis for wet flood-proofing project using NPV rule and real options methods under different discount rates. We report (in billion USD) the NPV, the total value with optionality and the difference between the two values.

Table 11

INVESTMENT ANALYSIS FOR FLOOD PROOFING PROJECT IN NYC UNDER DIFFERENT SEA LEVEL RISE

	μ=0	μ=3	μ=6	μ=9	μ=12
NPV	0.09	0.29	0.81	1.62	2.47
Total value with optionality	0.09	0.29	0.81	1.62	2.47
Difference	0.00	0.00	0.00	0.00	0.00

Investment analysis for wet flood-proofing project using NPV rule and real options methods under different levels of sea rise. We report (in billion USD) the NPV, the total value with optionality and the difference between the two values.

Table 12

INVESTMENT ANALYSIS FOR FLOOD PROOFING PROJECT IN NYC UNDER DIFFERENT SEA LEVEL RISE UNCERTAINTY

	σ=7	σ=15	σ=25	σ=30	σ=45
NPV	0.63	0.69	0.81	0.89	1.16
Total value with optionality	0.63	0.69	0.81	0.89	1.16
Difference	0.00	0.00	0.00	0.00	0.00

Investment analysis for wet flood-proofing project using NPV rule and real options methods under different levels of sea rise. We report (in billion USD) the NPV, the total value with optionality and the difference between the two values.

5.1.4 DYNAMIC ADAPTATION PATHWAYS FOR NYC

Although the optimal investment time can be determined for single projects, separate consideration of each project does not allow to take into account the flexibility offered by project combinations. It is possible that low-cost projects can be invested first to lower flood risk and provide more time to observe the development of the mean sea levels before high-cost projects are committed. It is also possible that high-cost projects are much more cost effective than low-cost projects and it is optimal to invest in high-cost projects first to avoid having to invest in low-cost projects. Considering multiple projects simultaneously allows to determine the optimal pathway for adaptation.

Table 13 provides the results for two alternative pathways: i) invest in the flood-proofing measure first and in the barrier and dike measure later; ii) invest in the barrier and dike measure first and consider the flood-proofing measure later. The results suggest that it is not optimal to invest in the flood-proofing measure now and wait to invest in the barrier and dike project later, although single investment analysis suggests that immediate investment in the flood-proofing measure is optimal. Wait and invest in the barrier and dike project, ignoring the flood-proofing project would provide a higher investment value.

Table 13

DYNAMIC ADAPTATION PATHWAYS FOR NYC

	Flood-proofing then dike			Dike then flood-proofing		
	Flood-proofing	Barrier and Dike	Total	Barrier and Dike	Flood-proofing	Total
NPV	0.81	8.34	9.15	9.90	-0.74	9.15
Total value with optionality	0.81	10.10	10.91	11.24	0.00	11.24
Difference	0.00	1.76	1.76	1.35	0.74	2.09

Investment analysis for investment sequences using NPV rule and real options methods. We report (in billion euro) the NPV, the total value with optionality and the difference of the two values.

Sensitivity analysis results in Table 14 show that investment results depend significantly on the discount rate. The strategy to invest in barrier and dike first remains optimal as the discount rate changes. Results in Table 15 suggest that this strategy of investing in barrier and dike first is optimal for high sea level rise. When the level of sea rise is low, it is optimal to invest in the flood-proofing first and wait for the sea level to rise to a high level before investing in barrier and dike. Table 16 shows the results of the sensitivity analysis with respect to the sea level rise uncertainty. As it can be seen from the table, investing in the dike and barrier project first, and in the flood proofing project then returns higher project values for every scenario.

Table 14

DYNAMIC ADAPTATION PATHWAYS FOR NYC UNDER DIFFERENT DISCOUNT RATES

	Flood-proofing then dike					Dike then flood-proofing				
	r=2%	r=3%	r=4%	r=5%	r=6%	r=2%	r=3%	r=4%	r=5%	r=6%
NPV	338.40	56.13	9.15	-2.79	-7.03	338.40	56.13	9.15	-2.79	-7.03
Total value with optionality	338.40	56.13	10.91	2.86	0.90	349.18	58.02	11.24	2.88	0.90
Difference	0.00	0.00	1.76	5.65	7.93	10.78	1.90	2.09	5.68	7.93

Investment sequences under different discount rates. We report (in billion euro) the NPV, the total value with optionality and the difference between the two values.

Table 15

DYNAMIC ADAPTATION PATHWAYS FOR NYC UNDER DIFFERENT SEA LEVEL RISE

	Flood-proofing then dike					Dike then flood-proofing				
	μ=0	μ=3	μ=6	μ=9	μ=12	μ=0	μ=3	μ=6	μ=9	μ=12
NPV	-7.64	-3.11	9.15	31.13	57.64	-7.64	-3.11	9.15	31.13	57.64
Total value with optionality	0.22	2.08	10.91	31.14	57.64	0.17	2.05	11.24	32.43	59.73
Difference	7.86	5.19	1.76	0.00	0.00	7.81	5.16	2.09	1.29	2.09

Investment sequences under different discount rates. We report (in billion euro) the NPV, the total value with optionality and the difference between the two values.

Table 16

DYNAMIC ADAPTATION PATHWAYS FOR NYC UNDER DIFFERENT SEA LEVEL RISE

	Flood-proofing then dike					Dike then flood-proofing				
	σ=7	σ=15	σ=25	σ=30	σ=45	σ=7	σ=15	σ=25	σ=30	σ=45
NPV	4.61	6.04	9.15	11.20	18.72	4.61	6.04	9.15	11.20	18.72
Total value with optionality	6.65	8.00	10.91	12.82	19.90	6.83	8.22	11.24	13.22	20.57
Difference	2.04	1.96	1.76	1.63	1.18	2.22	2.19	2.09	2.03	1.84

Investment sequences under different sea level rise uncertainty. We report (in billion euro) the NPV, the total value with optionality and the difference between the two values.

5.2 CASE STUDY OF SOUTH EAST QUEENSLAND

South East Queensland is the most populated area in the state of Queensland, Australia. It accounts for 70% of the state population while covers only 1.3% of the state's total area. The area suffers from extreme climate events including floods, droughts, heatwaves and bushfires. It is expected that climate change will increase losses from these catastrophes.

This case study is based on previous research carried out by Wang et al. (2015). The study area has 983,000 residential and 21,000 commercial buildings, 2.94% of which are exposed in 1-in-100 storm events. Similar to Wang et al. (2015), we consider the adaptation strategy of lifting all buildings in the 1-in-100-year flood area[5] by 1m. Since the total number of buildings in the area is 29,518 and the average cost of lifting a building is $43,000, the cost of adapting existing buildings is $1.27 billion.

[5] This is the area that would be flooded when a 1-in-100 event occurs

The cost of adapting new buildings depends on the number of buildings added to the area, the unit elevation cost and the discount rate. As in Wang et al. (2015), we assume a unit lifting cost of 0.2% per-square-meter cost of a dwelling for every 10cm elevation. We also follow Wang et al. (2015) to assume that the number of future residential and commercial buildings will grow at the same rate of population, which is estimated to be 1%. We assume a median size of 150 square meters per house and a median building cost of $1,285 per squared meters. The total cost of adapting new buildings is then $0.36 million.

Using water level data collected at Brisbane tide gauge station, we plot the mean and the annual maximum water levels in Figure 26. The mean sea levels show a slight upward trend. As for other regions, we use the estimates from climate change for the estimates of the mean sea level process parameters, i.e., $\mu = 8.7$ and $\sigma = 25$. No previous studies and data are available on the land subsidence for the region, so we assume zero land subsidence in this study. We de-tide and detrend the data before fitting the GEV distribution. The estimated parameters of the GEV distribution are $\alpha = 1666, s = 53.23, \xi = 0.45$.[6]

Figure 26

OBSERVED ANNUAL MEAN AND ANNUAL MAXIMUM SEA LEVELS AT BRISBANE TIDE GAUGE STATION, AUSTRALIA

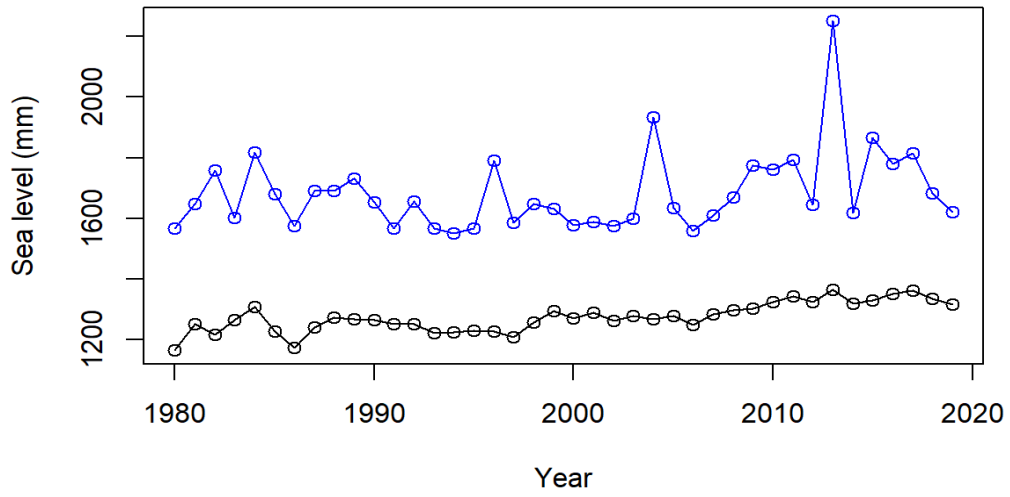

[6] The estimates by Wang et al. (2015) are $\alpha = 1.372, s = 0.012, \xi = 0.463$. The shape parameter is very close to our estimate. Their scale and location parameters are different, which may be because they use different treatments for tide and different data set.

Wang et al. (2015) provide the damage cost for the area that covers the damage to residential and commercial buildings. The total losses in the 1 in 10, 100, 1000, 10000-year floods are estimated to be 0.012, 0.120, 0.450 and 1.925 billion AUD, respectively (Figure 27).

Figure 27

DAMAGE CURVE ESTIMATED FOR THE 1-IN-100 YEAR FLOOD AREA IN THE SOUTH EAST QUEENSLAND

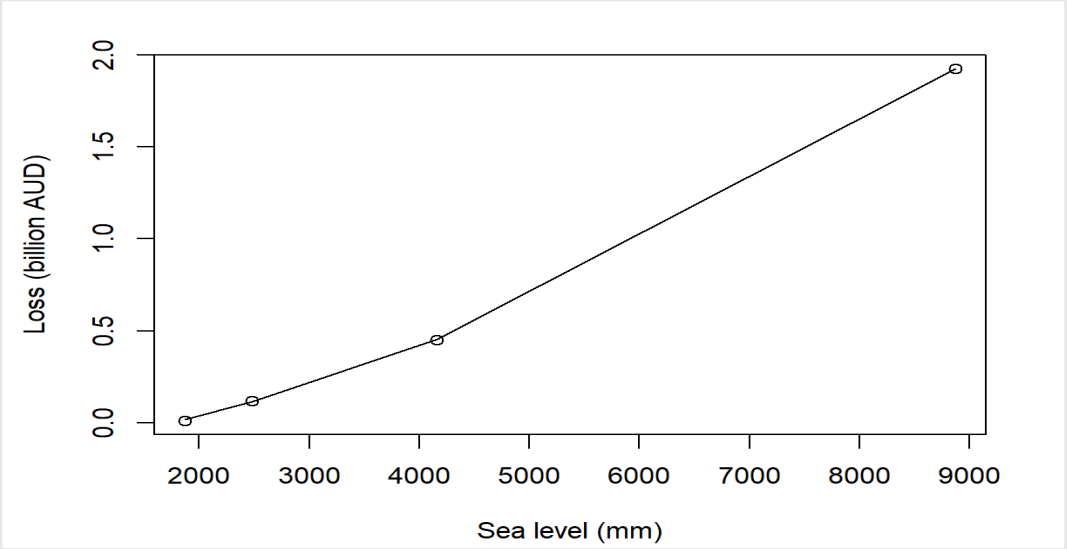

Based on the estimates of Wang et al. (2015).

We assume a real risk-free rate of 4% and a 1% growth in loss exposure based on population growth data as estimated by Wang et al. (2015). The estimate for the risk premium θ is -0.38 based on a market price of risk $\phi = 0.1274$, and a correlation of-0.09 between the annual sea level change and the market return on All Ordinary Index. The assumed parameters are summarized in Table 17.

Table 17

INFORMATION ON ESTIMATED AND ASSUMED PARAMETER VALUES FOR SOUTH EAST QUEENSLAND

Parameters	Values
Location parameter (α)	1666
Scale parameter (s)	53.23
Shape parameter (ξ)	0.45
Current flood threshold (u)	1765mm
Quadratic coefficient of damage curve (a)	1.744×10^{-8}
Linear coefficient of damage curve (b)	8.535×10^{-5}
Mean sea level rise per year (μ)	8.7mm
Standard deviation of sea level rise per year (σ)	25mm

Safety loading of flood risk (δ)	3%
Risk-free rate (r)	4%
Growth rate of loss exposure (γ)	1%
Market risk premium (θ)	-0.38
Adaptation by elevation	
Investment cost (I)	AUD 1.276 billion
Flood mitigation (k)	1000mm

5.2.1 BASELINE ANALYSIS

The results of investment analysis are provided in Table 18. In the absence of sea level rise and with a positive loss exposure growth, the NPV is positive, but lower than the total value with optionality, indicating that while it's beneficial to invest right away, deferring the investment is a more valuable strategy. The NPV of the project is highest when both the sea level rise and the loss exposure increase over time. There is also an interaction between sea level change and loss exposure growth, since the NPV of adaptation is much larger when both factors are present. In this case, deferring investment does not provide additional values and it is optimal to invest in the project immediately.

Table 18

INVESTMENT ANALYSIS FOR ELEVATION PROJECT IN SOUTH EAST QUEENSLAND

	$\mu = 0, \gamma = 1\%$	$\mu = 8.7, \gamma = 1\%$	$\mu = 17.4, \gamma = 1\%$	$\mu = 8.7, \gamma = 2\%$
NPV	0.33	2.61	2.80	4.80
Total value with optionality	0.52	2.61	2.80	4.80
Difference	0.19	0.00	0.00	0.00

Investment analysis for elevation of 100-year inundation area using NPV rule and real options methods. All cases assume σ = 25mm.

5.2.2 SENSITIVITY ANALYSIS

Sensitivity analysis results in Tables 19, 20, and 21 suggest that it is only optimal to defer investment into the project when the discount rate is higher than 4% or when there is no sea level rise.

Table 19

INVESTMENT ANALYSIS FOR ELEVATION PROJECT IN SOUTH EAST QUEENSLAND UNDER DIFFERENT DISCOUNT RATES

	r=2%	r=3%	r=4%	r=5%	r=6%
NPV	9.41	4.80	2.61	1.42	0.72
Total value with optionality	9.41	4.80	2.61	1.45	0.84

Difference	0.00	0.00	0.00	0.03	0.12

Sensitivity analysis for South East Queensland adaptation with respect to discount rate. We report (in billion AUD) the NPV, the total value with optionality and the difference between the two values.

Table 20

INVESTMENT ANALYSIS FOR ELEVATION PROJECT IN SOUTH EAST QUEENSLAND UNDER DIFFERENT SEA LEVEL RISE

	μ=0	μ=4.35	μ=8.7	μ=13.05	μ=17.4
NPV	0.45	1.80	2.61	2.85	2.81
Total value with optionality	0.60	1.80	2.61	2.85	2.81
Difference	0.16	0.00	0.00	0.00	0.00

Sensitivity analysis for SEQ adaptation with respect to the expected sea level rise. We report (in billion AUD) the NPV, the total value with optionality and the difference between the two values.

Table 21

INVESTMENT ANALYSIS FOR ELEVATION PROJECT IN SOUTH EAST QUEENSLAND UNDER DIFFERENT SEA LEVEL RISE UNCERTAINTY

	σ=7	σ=15	σ=25	σ=30	σ=45
NPV	2.79	2.73	2.61	2.54	2.32
Total value with optionality	2.79	2.73	2.61	2.54	2.32
Difference	0.16	0.00	0.00	0.00	0.00

Sensitivity analysis for SEQ adaptation with respect to the sea level rise uncertainty. We report (in billion AUD) the NPV, the total value with optionality and the difference between the two values.

5.3 CASE STUDY OF COPENHAGEN.

Copenhagen is the capital of Denmark, and one of the major cities in the Swedish-Danish Oresund region. As a low-lying city with a population of over 600 thousand people living in proximity to water, Copenhagen is particularly vulnerable to extreme sea level rise, making it a perfect candidate to showcase the contribution of real option methodology. This case study builds on previous analysis in Hallegatte et al. (2011); Lenk et al. (2017); Tsvetanov and Shah (2013), jointly with our estimation results based on monthly data.

We consider the construction of a dike and barrier up to 2000mm to protect the city of Copenhagen from flood damages. We first consider a single investment in which the 2000mm height of the dike system is developed in one go. We then consider a multiple investment project in which the 2000mm height is achieved in two stages with Stage 1 building a 1000mm height dike system and Stage 2 increasing the height from 1000mm to 2000mm. The difference between the single

investment project and the multiple investment project shows the value of flexibility obtained via real option analysis.

Location, scale, and shape parameters for the GEV distribution for the high-water mark are taken as follows: $\alpha = 402$, $s = 254$, and $\xi = -0.0554$. The negative value of ξ implies the existence of a short tail flood risk in the case of Copenhagen, which is consistent with previous studies such as Hallegatte et al. (2011). Regarding the sea level, we consider a mean sea level rise per year (μ) of 6.5mm (0.541mm monthly), which represents a median value between a high sea level rise scenario (8.4mm per year) and low sea level rise scenario (4.8mm per year), based on the level of carbon emission provided by Pörtner et al. (2019). Consistently with other studies we assume a standard deviation of sea level rise per year of 25mm (7.21mm monthly). We further follow Hallegatte (2011) to assume zero land subsidence due to the lack of data.

Figure 28 depicts the damage curve for Copenhagen, based on the results in Hallegatte (2009, 2011). The shape of the curve seems to suggest a quadratic relationship between the sea level and the loss, expressed in billions of euros. The effective threshold u is estimated to be 330.92mm and the fitted loss function is:

$$L(M_t) = 7.453 \times 10^{-7}(M_t - u)^2 + 1.562 \times 10^{-3}(M_t - u).$$

Following Haer et al. (2020) and Aerts et al. (2014), we assume a yearly real risk-free rate of 4%. The growth exposure rate γ is set at 1.31%, based on a population growth estimate of 0.1% and a yearly GDP increase of 1.30% (see Hallegatte et al., 2011). The estimate for market risk premium θ is -0.79 (monthly -0.065), based on a market price of risk $\phi = 0.0846$, and a correlation of $\rho_{m,s} = -0.17$ between the annual sea level change and the Dow Jones stock market return. Similarly, to the previous case studies, the safety loading parameter δ is set at 3%.

Figure 28
LOSS CURVE IN COPENHAGEN

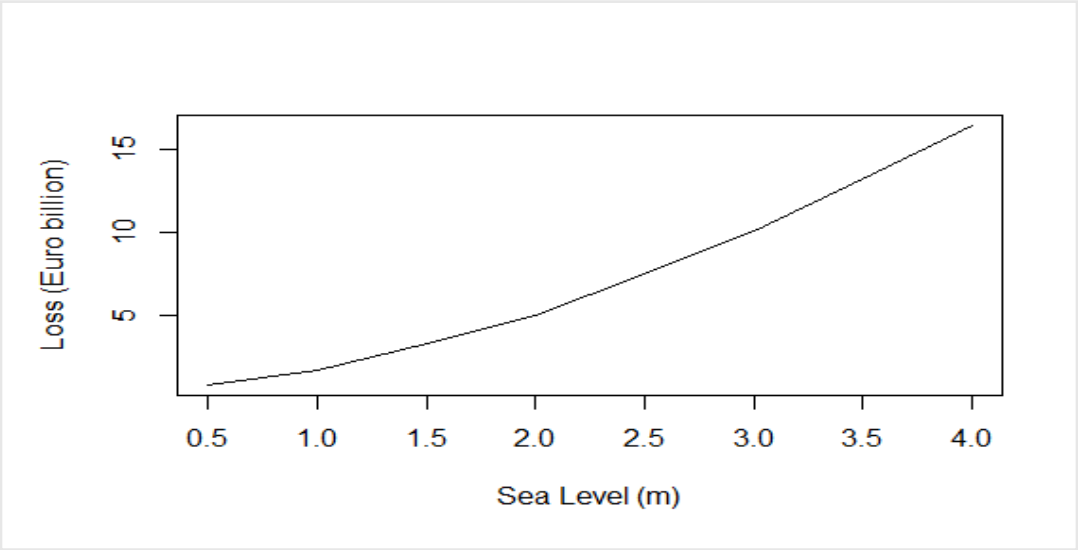

Damage Curve in Copenhagen based on the estimates by Hallegatte et al. (2011).

We consider the following quadratic cost function (see, for example Ng and Mendelsohn, 2005; Lenk et al. (2017); Tsvetanov and Shah, 2013):

$$I(k) = c_0 + c_1 k^2$$

where k is the dike height, c_0 the fixed cost, c_1 the variable cost. For Copenhagen we follow Lenk et al. (2017) and Tsvetanov and Shah (2013) and assume $c_0 =$ €160,000 and $c_1 =$ €1,371/mm.

Figure 29

TOTAL PROJECT VALUE FOR THE SINGLE INVESTMENT OF THE DIKE IN COPENHAGEN

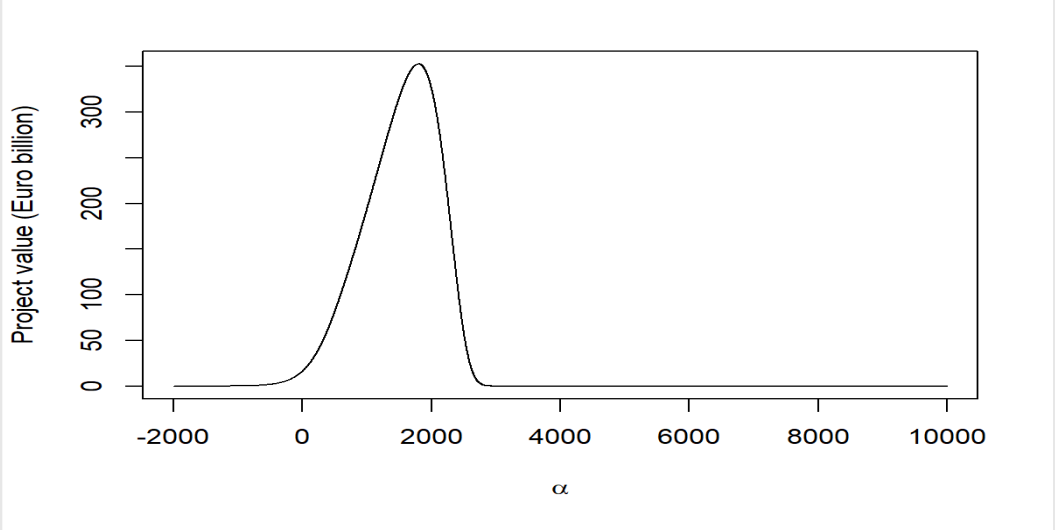

Figure 29 shows the project value, for different level of the location parameter α. The values of other parameters for the case study are summarized in Table 22.

Table 22

INFORMATION ON ESTIMATED AND ASSUMED PARAMETER VALUES FOR COPENHAGEN

Parameters	Values
Location parameter (α)	402
Scale parameter (s)	254.56
Shape parameter (ξ)	-0.0554
Current flood threshold (u)	330.92mm
Quadratic coefficient of damage curve (a)	7.434×10^{-7}
Linear coefficient of damage curve (b)	0.001562
Mean sea level rise per month (μ)	0.79mm
Standard deviation of sea level rise per month (σ)	7.21mm
Safety loading of flood risk (δ)	3%
Risk-free rate (r)	3.9%
Growth rate of loss exposure (γ)	1.3%

Market risk premium (θ)	- 0.79
Adaptation by barrier and dike	
Investment cost Stage 1 ($I1$)	€1.37116 billion
Investment cost Stage 2 ($I2$)	€4.11316 billion
Investment cost Single Investment ($I12$)	€5.48416 billion
Fixed cost (c_0)	€160,000
Flood mitigation ($k1$)	1000mm
Flood mitigation ($k2$)	1000mm

5.3.1 BASELINE ANALYSIS

The numerical analysis is conducted based on monthly data, but reported at a yearly frequency, to be consistent with previous case studies. Table 23 reports the results of the numerical analysis. In Stage 1 of the multistage approach, the NPV and the option value are equivalent. As expected, the project value increases with both the growth exposure parameter and the mean sea level rise. The positive NPV in Stage 1, suggests that the project is invested immediately. Interestingly, the project value in Stage 1 is much higher than the project value in Stage 2, suggesting that it is beneficial to defer the investment to see how the climate uncertainty unfolds, as it provides a much lower benefit. Finally, except the fourth case, where Stage 1 and Stage 2 are invested immediately, the multistage approach returns a higher aggregate project value than the single investment project, even if the multistage has higher fixed cost, due to the added value of flexibility captured by the real option framework.

Table 23

INVESTMENT ANALYSIS FOR BARRIER AND DIKE PROJECT IN COPENHAGEN

	$\mu = 0, \gamma = 1.31\%$	$\mu = 6.5, \gamma = 1.31\%$	$\mu = 13, \gamma = 1.31\%$	$\mu = 6.5, \gamma = 2.6\%$
Stage 1 ($k1 = 1000$mm)				
NPV	24.02	25.64	27.30	55.49
Total value with optionality	24.02	25.64	27.30	55.49
Difference	0.00	0.00	0.00	0.00
Stage 2 ($k2 = 1000$mm)				
NPV	-1.50	-1.17	-0.75	2.69
Total value with optionality	0.004	0.03	0.13	2.69
Difference	1.50	1.20	0.89	0.00
Total value with optionality (Stage 1 + Stage 2)	24.025	25.67	27.43	58.19

Single Investment ($k = 2000$mm)				
NPV	22.51	24.46	26.54	58.19
Total value with optionality	22.51	24.46	26.54	58.19
Difference	0.00	0.00	0.00	0.00

Investment analysis for barrier and dike project using NPV rule and real options methods. The multistage approach and the single investment approach are compared. We report (in billion euro) the NPV, the total value with optionality and the difference of the two values. Results are reported for four cases: i) no climatic change and zero exposure growth, ii) climatic change and exposure growth, iii) doubled expected sea level rise and exposure growth, iv) climatic change and doubled exposure growth. All cases assume σ = 25mm (7.21mm monthly). Despite the higher fixed cost, the multistage approach returns a higher value of investment due to the added value of flexibility captured by the real option framework.

5.3.2 SENSITIVITY ANALYSIS

Finally, we conclude this section presenting a sensitivity analysis along the line of those in NYC and South East Queensland. Table 24 shows the numerical results of the sensitivity analysis. For low values of the real interest rate, the project value for the single investment project is greater than the aggregate project value for the multistage investment, both according to NPV and real option. However, as the interest rate rises, the benefit of the multistage project with respect to the single investment increases.

Table 24

INVESTMENT ANALYSIS FOR BARRIER AND DIKE PROJECT IN COPENHAGEN UNDER DIFFERENT DISCOUNT RATES

	r=2%	r=3%	r=4%	r=5%	r=6%
Stage 1 ($k1 = 1000$mm)					
NPV	117.05	41.84	25.64	17.46	13.30
Total value with optionality	117.05	41.84	25.64	17.46	13.30
Difference	0.00	0.00	0.00	0.00	0.00
Stage 2 ($k2 = 1000$mm)					
NPV	13.66	0.83	-1.17	-2.11	-2.57
Total value with optionality	13.66	0.84	0.03	0.001	0.00006
Difference	0.00	0.009	1.20	2.11	2.57
Total value with optionality (Stage 1 + Stage 2)	130.71	42.68	25.67	17.46	13.30006

Single Investment ($k = 2000$mm)					
NPV	130.72	42.68	24.46	15.35	10.73
Total value with optionality	130.723	42.68	24.46	15.35	10.73
Difference	0.00	0.00	0.00	0.00	0.00

Investment analysis for the dike project, using NPV rule and real options methods under different discount rates. We report (in billion euros) the NPV, total value with optionality and the difference between the two values.

Table 25 shows the numerical results for a sensitivity analysis in the sea level rise, for the multistage and single investment project. As the sea level rise increases, the project value increases in both the multistage and the single investment projects.

Consistently with the expectations, as the rate of mean sea level rise increases, the difference between the NPV and the option value in the second stage decreases. As climate change impact increases the sea level rises severity, the value of waiting reduces, therefore investing right away becomes more valuable. Similarly, Table 26 shows the numerical results for a sensitivity analysis in the sea level rise uncertainty: as the sea level rise uncertainty increases the project values increases, both in the multistage and the single investment projects.

Table 25

INVESTMENT ANALYSIS FOR BARRIER AND DIKE IN COPENHAGEN UNDER DIFFERENT SEA LEVEL RISE

	μ=0	μ=4.5	μ=6.5	μ=13.05	μ=17.4
Stage 1 ($k1 = 1000$mm)					
NPV	24.19	25.15	25.64	27.13	28.12
Total value with optionality	24.19	25.15	25.64	27.13	28.12
Difference	0.00	0.00	0.00	0.00	0.00
Stage 2 ($k2 = 1000$mm)					
NPV	-1.46	-1.27	-1.05	-0.80	-0.51
Total value with optionality	0.005	0.02	0.03	0.12	0.23
Difference	1.47	1.29	1.39	0.92	0.74
Total value with optionality (Stage 1 + Stage 2)	24.195	25.17	25.67	27.25	28.35
Single Investment ($k = 2000$mm)					
NPV	22.72	23.88	24.46	26.32	27.61

Total value with optionality	22.72	23.88	24.46	26.32	27.61
Difference	0.00	0.00	0.00	0.00	0.00

Sensitivity analysis for barrier and dike project using NPV rule and real options methods with respect to sea level rise. We report (in billion euros) the NPV, the total value with optionality and the difference between the two values.

Table 26

INVESTMENT ANALYSIS FOR BARRIER AND DIKE IN COPENHAGEN UNDER DIFFERENT SEA LEVEL RISE UNCERTAINTY

	σ=7	σ=15	σ=25	σ=30	σ=45
Stage 1 ($k1 = 1000$mm)					
NPV	25.58	25.60	25.64	25.66	25.75
Total value with optionality	25.58	25.60	25.64	25.66	25.75
Difference	0.00	0.00	0.00	0.00	0.00
Stage 2 ($k2 = 1000$mm)					
NPV	-1.23	-1.21	-1.05	-1.03	-1.01
Total value with optionality	0.002	0.009	0.03	0.05	0.14
Difference	1.232	1.219	1.08	1.08	1.15
Total value with optionality (Stage 1 + Stage 2)	25.582	25.609	25.67	25.71	25.89
Single Investment ($k = 2000$mm)					
NPV	24.35	24.39	24.46	24.52	24.74
Total value with optionality	24.35	24.39	24.46	24.52	24.74
Difference	0.00	0.00	0.00	0.00	0.00

Sensitivity analysis for barrier and dike project using NPV rule and real options methods with respect to sea level rise uncertainty. We report (in billion euros) the NPV, the total value with optionality and the difference between the two values.

6: Insurance premium distributions

This section presents the results of a simulation study on the effect of climate adaptation policies on insurance premium distribution, and optimal investment timing in the three cities. Firstly, we consider insurance premium from the point of view of city councils willing to insure the losses due to extreme sea level rise for the entire city for 12 months. Secondly, we introduce the presence of a top cover limit, where only losses up to 1 billion dollars can be insured, to more closely resemble real world applications. Finally, we perform a sensitivity analysis on the insurance premium distribution, with respect to three possible scenarios of mean sea level rise.

6.1 NEW YORK CITY

Figure 30 shows how the distribution of insurance premium changes over time when: i) the dike and barrier project is optimally invested and ii) the flood-proofing project is optimally invested. It also compares these distributions with those obtained when there is no adaptation. Recall from the previous section that when the dike and barrier project is considered together with the flood-proofing project, the flood-proofing project becomes redundant and therefore, the insurance premium distributions under the optimal investment pathway would be the same as the ones obtained under the single investment of the dike and barrier project. Here, insurance premium distributions are obtained by simulations conducted for the following years: year 10, year 20, ..., year 100 into the future. The simulation is done assuming a mean sea level rise of 65cm in 100 years and a loss exposure growth as in the baseline case in the previous section. The decision to invest into the adaptation project depends on whether the sea level is higher than the exercise boundaries. When the mean sea level increases and reaches the exercise boundary, the considered adaptation project is invested. In the flood-proofing case, this happens right away, as the current sea level is already higher than the boundary. As a result, the premium distributions in the case of flood-proofing immediately deviates from the no adaptation one for every year reported (Figure 30b).

In the case of the dike and barrier project, the optimal decision is to defer investment to a future period, and as a result, the premium distribution with adaptation only deviates from the no adaptation distribution in years 30-40 onwards (Figure 30a). The increase in the skewness and standard deviation in year 40, compared to year 30, indicates that a great number of simulated trajectories hit the investment boundary in or before year 40. However, for some trajectories, the investment occurs even earlier, as it can be seen from the small differences in the distribution at years 20 and 30. This shows that investment is adaptive, depending on the development of the mean sea level, and investment time is stochastic and uncertain. It is also apparent that with adaptation, insurance premiums are less uncertain, having lower standard deviation compared to the case of no adaptation. Once the dike and barrier project is invested, it greatly reduces the impact of climate change, which is then reflected into downward shifted insurance premium trajectories. After the year 40, insurance premium distributions have a much lower mean, median, standard deviation, and kurtosis.

Figure 30

DEVELOPMENT OF INSURANCE PREMIUM DISTRIBUTION IN NYC WITH AND WITHOUT ADAPTATION

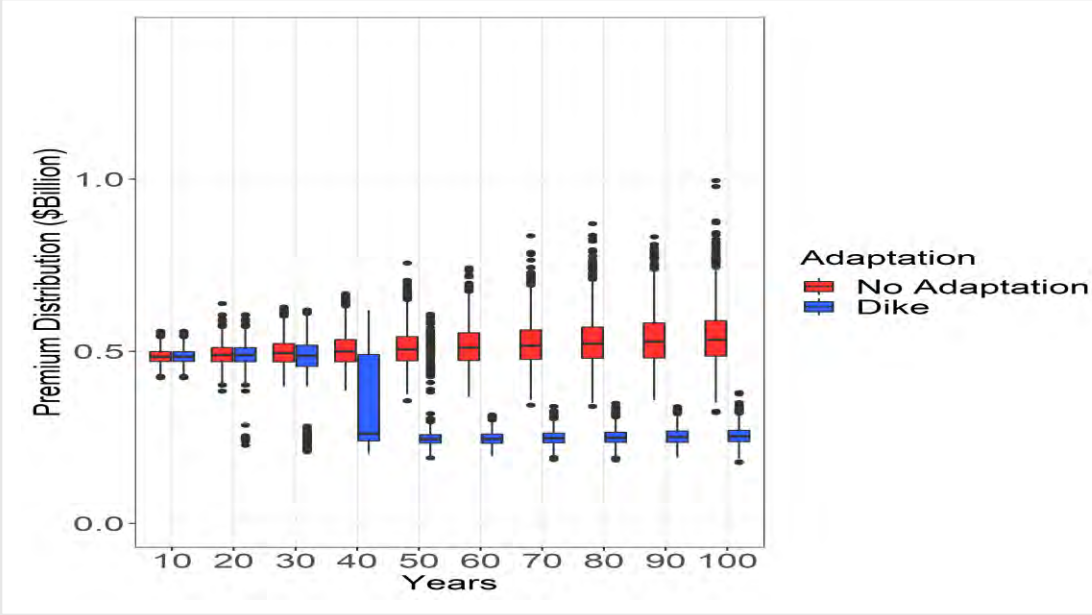

(a) Time evolution of insurance premium distribution with dike project in NYC

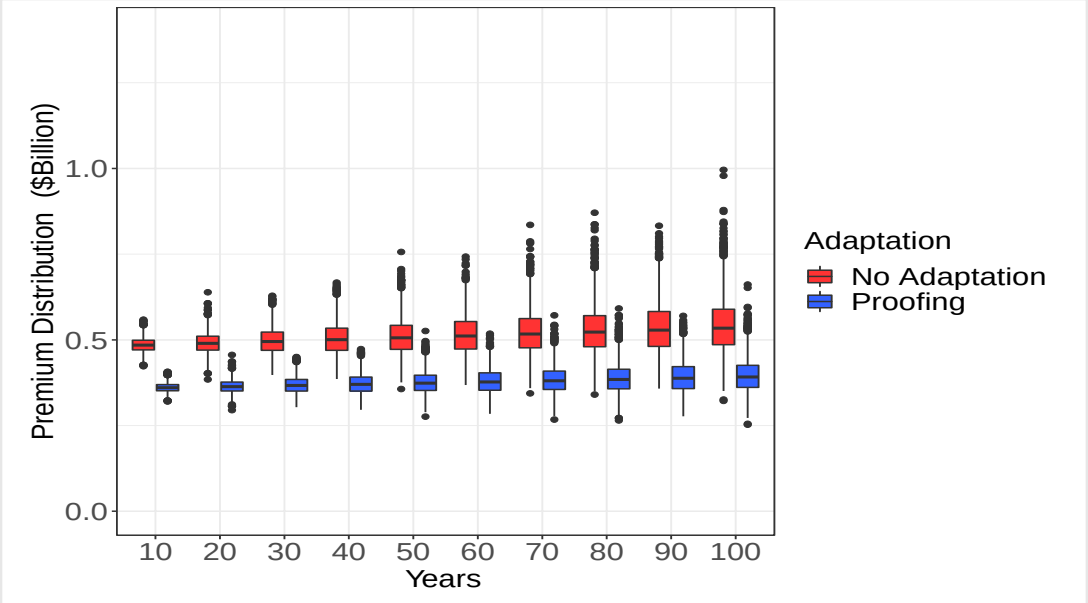

(b) Time evolution of insurance premium distribution with flood proofing project in NYC

This figure compares the time evolution of insurance premiums in three cases: no adaptation policy (red), dike and barrier project (blue panel a), flood proofing (blue panel b). Insurance premium distributions are depicted at 10, 20, 30, 40, 50, 60, 70, 80, 90, and 100 years.

Flood-proofing has lower impact on insurance premium compared to the dike and barrier project, since the protection provided by flood-proofing accounts for only a small proportion of the flood damage. Different from the dike and barrier project, the condition triggering the investment in the flood-proofing project is already met, and the project is invested in year zero.

Figure 31 shows the histogram for the time at which the dike project is invested. Consistent with Figure 30a, the average investing time is around 400 months.

Figure 31

SIMULATE DISTRIBUTION FOR OPTIMAL INVESTMENT TIME

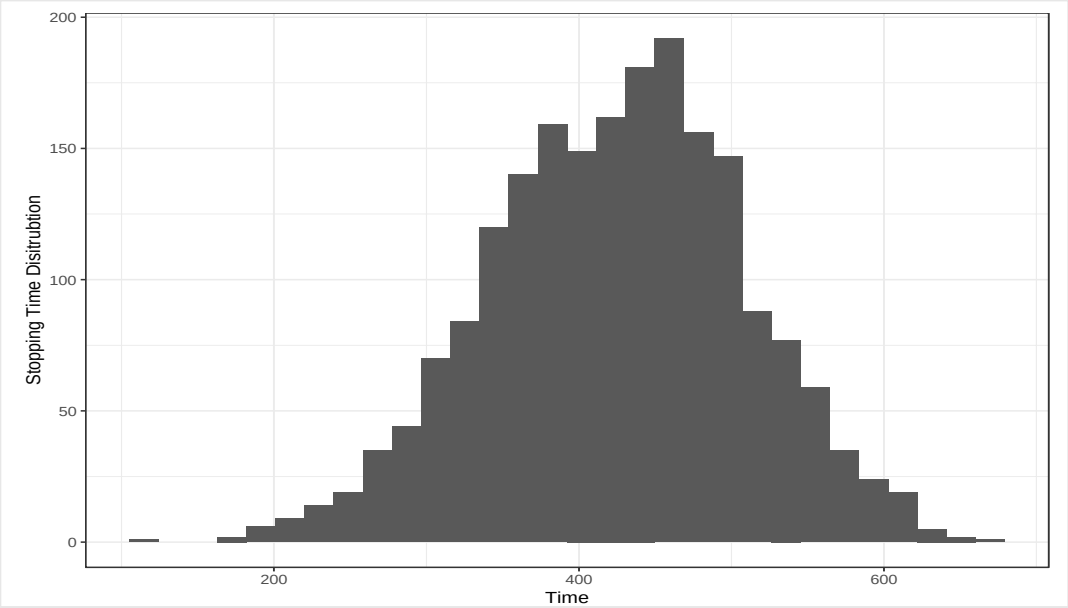

This figure shows the distribution of the optimal investment time (in months) for the dike project in NYC. The average waiting period is around 400 months.

Table 27 compares the quantiles of the premium distributions at year 100, in the case of no adaptation, dike and barrier project, flood-proofing. Confirming the results depicted in Figure 30, the dike project provides the highest reduction in premiums among the alternative considered.

Table 27

INSURANCE PREMIUM QUANTILES UNDER DIFFERENT ADAPTATION POLICIES.

Adaptation	0%	25%	50%	75%	100%
No Adaptation	0.32	0.48	0.53	0.59	0.99
Proofing	0.25	0.36	0.39	0.42	0.66
Dike	0.17	0.23	0.25	0.27	0.38

This table reports the quantiles (in billion USD) of insurance premium in Year 100 in NYC for three cases: no adaptation, proofing, and dike.

6.2 SOUTH EAST QUEENSLAND

The project considered in the case of South East Queensland is the elevation of all the houses in the 1 in 100-year flood area. Figure 32 shows the development of the insurance premium distribution over time, with and without adaptation. Recall that the project is invested right away as the current sea level is higher than the exercise boundary. Elevating houses has the potential to greatly balance the impact of climate change, shifting the insurance premium distribution downward and reduce the mean, median, kurtosis, and standard deviation of the insurance premium.

Figure 32

DEVELOPMENT OF INSURANCE PREMIUM DISTRIBUTION IN SOUTH EAST QUEENSLAND WITH AND WITHOUT ADAPTATION

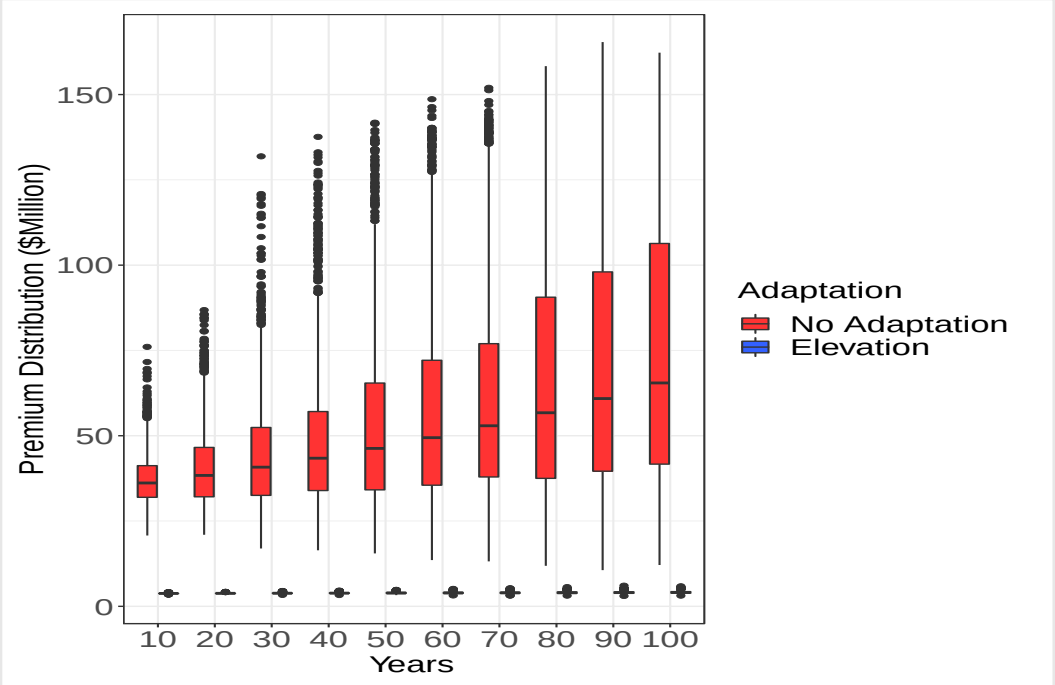

This figure compares the time evolution of insurance premiums in South East Queensland in two cases: no adaptation policy (red), and elevating houses (blue). Insurance premium distributions are depicted at 10, 20, 30, 40, 50, 60, 70, 80, 90, and 100 years.

Table 28 compares the quantiles of insurance premium in the case of no adaptation with the ones resulting from the case where houses are elevated. It is apparent that elevating houses reduces climate change impact on the insurance premiums, consistent with Figure 32.

Table 28

INSURANCE PREMIUM QUANTILES UNDER DIFFERENT ADAPTATION POLICIES.

Adaptation	0%	25%	50%	75%	100%
No Adaptation	12.08	41.64	65.44	106.34	162.28
Elevation	3.11	3.82	4.05	4.30	5.84

This table reports the quantiles (in billion AUD) of insurance premium distribution in Year 100 in South East Queensland for two cases: no adaptation, and house elevation.

6.3 COPENHAGEN

The project analyzed for Copenhagen is the construction of a dike system in two stages, each involves elevating the height of the dike by 1000mm. Figure 33 shows the development of insurance premium distribution over time for two cases: i) no adaptation and ii) adaptation with the multistage dike project. Recall that the current mean sea level is already higher than the exercise boundary of Stage 1 of the project, and therefore the first stage of the project is invested right away, shifting the premium distribution downwards. The investment into the first stage of the project provides sufficient protection for many years. The exercise boundary for the second stage is reached much later, in years 70, 80, 90 and 100. Once the second stage exercise boundary is reached, the premium distribution is further pushed downwards.

It is interesting to observe that the insurance premium distribution obtained under the optimal investment of the project has a higher standard deviation in year 100 than the previous years. This is due to the fact that for a considerable number of simulated trajectories, the investment boundary is hit after year 90 but before year 100. Note also that we plot only insurance premium distributions every 10 years, which creates an impression of a sudden change in the distribution when we move from year 90 to year 100.

Figure 33

DEVELOPMENT OF INSURANCE PREMIUM DISTRIBUTION IN COPENHAGEN WITH AND WITHOUT ADAPTATION.

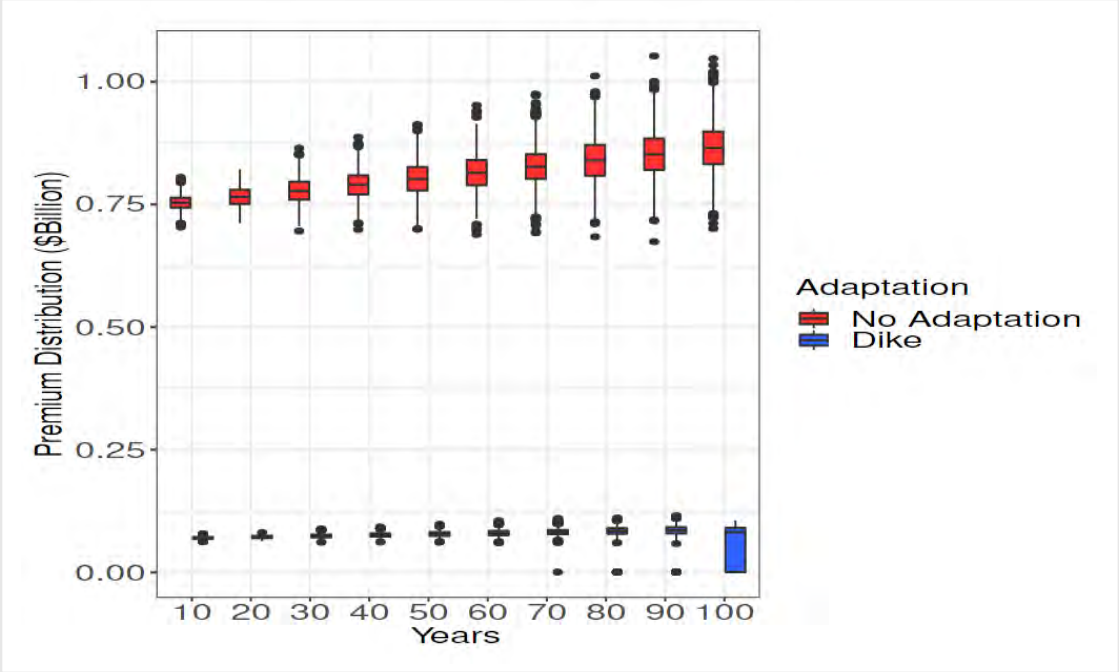

This figure compares the time evolution of insurance premiums in Copenhagen in two cases: no adaptation policy (red), and multistage dike (blue). Insurance premium distributions are depicted at 10, 20, 30, 40, 50, 60, 70, 80, 90, and 100 years.

Figure 34 shows the distribution of the optimal investment timing in the first 100 years. It's worth to note that trajectories that do not reach the second stage exercise boundary in 100 years are not plotted in Figure 34. It is also probable that some trajectories never hit the boundary.

Figure 34

SIMULATED DISTRIBUTION FOR OPTIMAL INVESTMENT TIME.

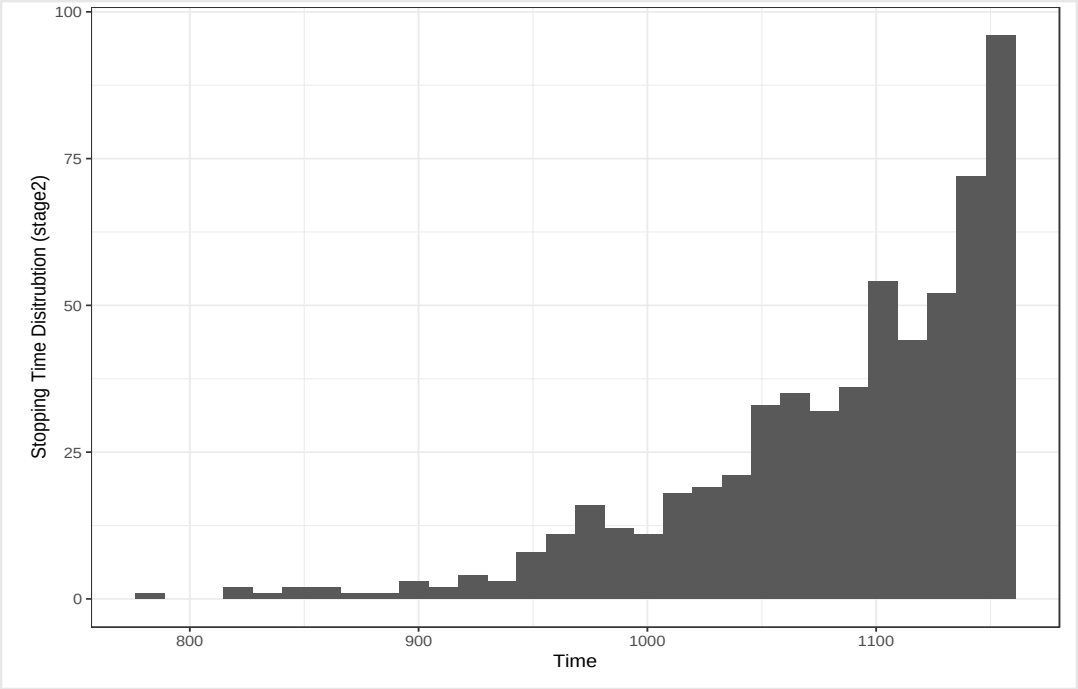

This figure shows the distribution of the optimal investment time (in months) for the multistage investment in Dike in Copenhagen.

Table 29 shows the quantiles of insurance premium in year 100 for the case of no adaptation and the case of adaptation with the multistage dike project. The results confirm the previous findings in Figure 33 that investing in the dike reduces the impact of climate change across the entire premium distribution.

Table 29

INSURANCE PREMIUM QUANTILES UNDER DIFFERENT ADAPTATION POLICIES.

Adaptation	0%	25%	50%	75%	100%
No Adaptation	0.70	0.83	0.86	0.898	1.04
Dike	0.0005	0.0009	0.08	0.09	0.11

This table reports the quantiles (in billion euro) of insurance premium distribution in Year 100 in Copenhagen for two cases: no adaptation and dike.

6.4 PREMIUM DISTRIBUTION IN PRESENCE OF A TOP COVER LIMIT

In this section, we introduce the presence of a top cover limit in the insurance policy. Although the insurance premium exercise is carried out with the intent to assign a monetary value to the benefit derived from investing into a climate adaptation policy, considering a city council willing to insure the entirety of a city or district might be too far-fetched. The introduction of a top cover limit, where

losses due to floods are insured only up to a pre-specified amount, might provide a more accurate representation of the real-world insurance perspective. In the three cities, we then consider an insurance policy, which covers the losses due to floods, for 1 year, up to 1 billion dollars. The corresponding insurance premium is then computed as follows:

$$\begin{aligned}\pi(u, u^*, t, \alpha; L) &= (1+\delta)e^{\gamma t}\left[\int_u^{\infty} L\,(M)dH(M) - \int_{u^*}^{\infty} L\,(M)dH(M)\right], \\ &= \pi(u, t, \alpha; L) - \pi(u^*, t, \alpha; L),\end{aligned}$$

where $L(u^*) =$1 billion USD dollars.

Figures 35, 36, and 37 show the result of the simulation study for the dike and proofing project in New York City, the house elevation project in South East Queensland, and the two-stage dike project in Copenhagen. The numerical results follow the one presented in the previous section, but with lower insurance premiums. In the New York City case, the average reduced premiums in the case of dike and flood-proofing are very similar. However, the dike project generates a premium distribution with lower standard deviation and kurtosis than the flood-proofing one. Notice how the investment timing remains unchanged, since the top cover limit does not affect the exercise boundary, nor the mean sea level. In the case of South East Queensland, the impact of imposing the top cover limit of $1 billion is visible, but small: the change in the insurance premium distribution for the case of no adaptation is minor. Similar to the case without the top cover limit, elevating the houses provides sufficient protection, and the impact of climate change is greatly reduced. Similarly, in the case of Copenhagen, the no adaptation premiums are left-skewed, and the two-stage dike project diminishes the impact of climate change. Also in this case, the investment timing remains unchanged.

Figure 35

DEVELOPMENT OF INSURANCE PREMIUM DISTRIBUTION IN PRESENCE OF TOP COVER LIMIT.

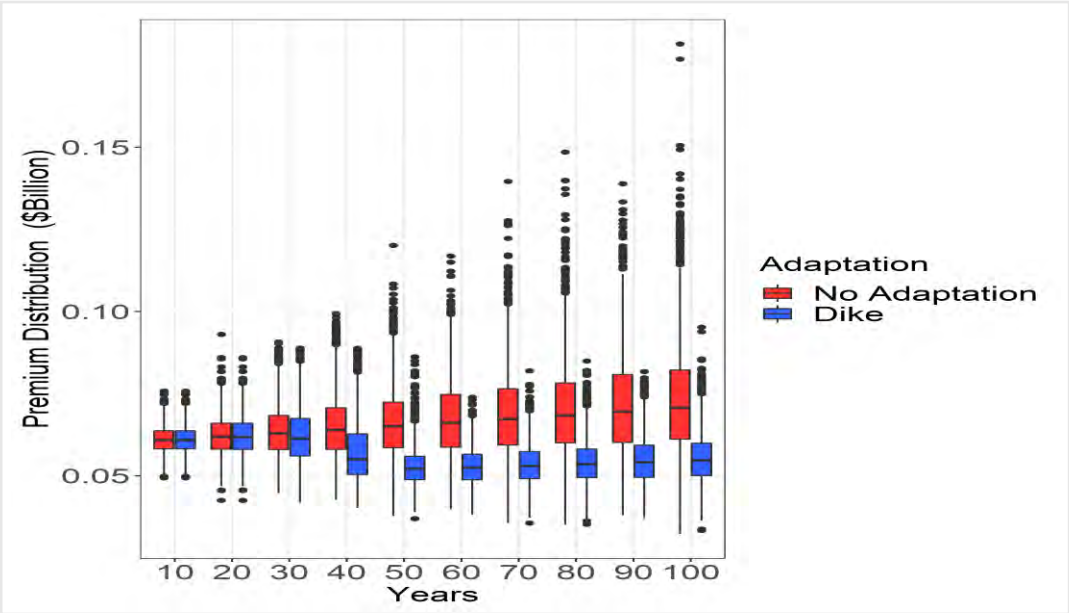

(a) Time evolution of insurance premium distribution for a top cover limit policy with the dike project in NYC.

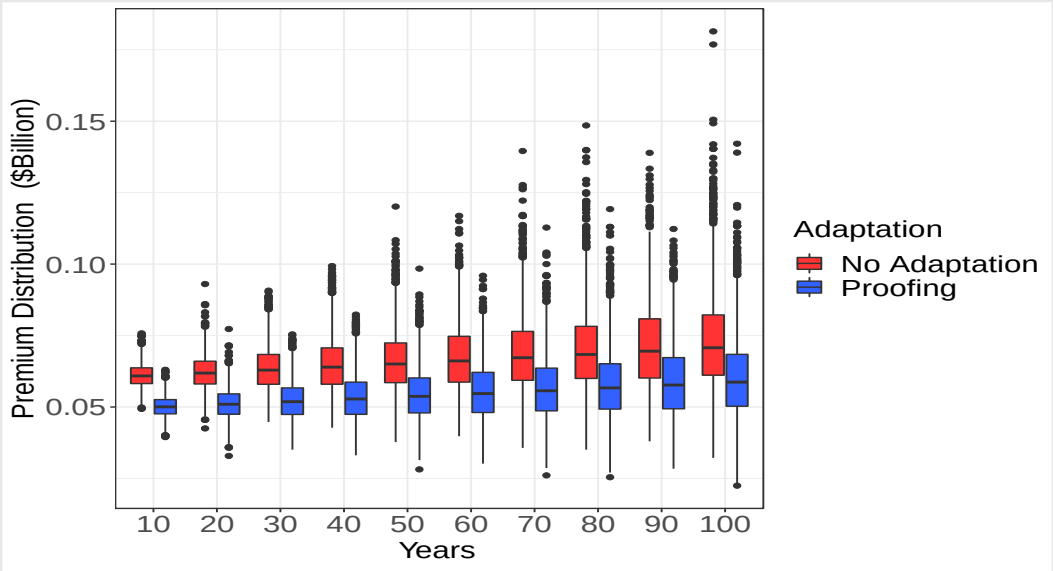

(b) Time evolution of insurance premium distribution for a top cover limit policy with flood proofing project in NYC

This figure compares the time evolution of insurance premiums for a policy with a top cover limit of 1 billion dollars, in three cases: no adaptation policy (red), dike and barrier project (blue panel a), flood proofing (blue panel b). Insurance premium distributions are depicted at 10, 20, 30, 40, 50, 60, 70, 80, 90, and 100 years.

Figure 36

DEVELOPMENT OF INSURANCE PREMIUM DISTRIBUTION IN PRESENCE OF TOP COVER LIMIT.

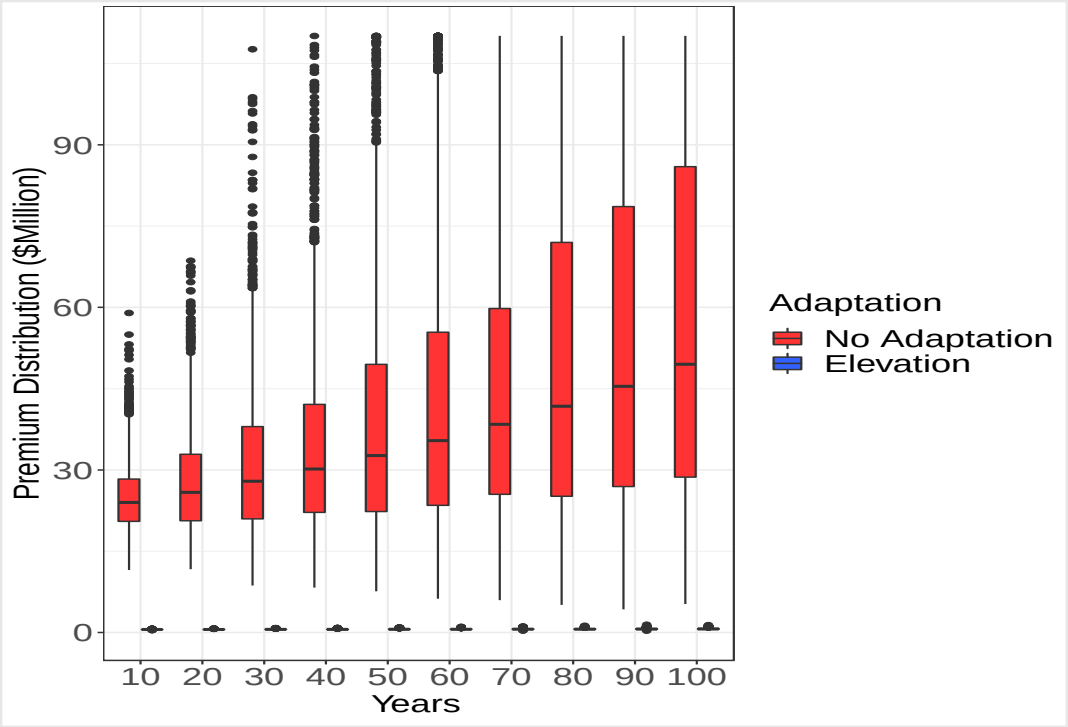

This figure compares the time evolution of insurance premiums of a policy with a top cover limit of 1 billion dollars in South East Queensland in two cases: no adaptation policy (red), and elevating houses (blue). Insurance premium distributions are depicted at 10, 20, 30, 40, 50, 60, 70, 80, 90, and 100 years.

Figure 37

DEVELOPMENT OF INSURANCE PREMIUM DISTRIBUTION IN PRESENCE OF TOP COVER LIMIT.

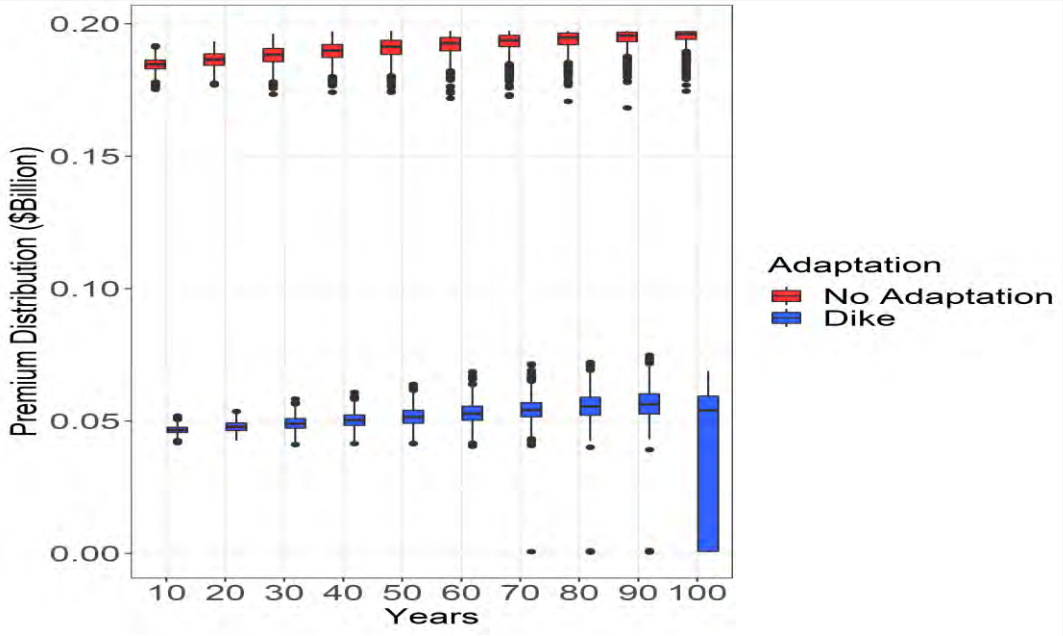

This figure compares the time evolution of insurance premiums of a policy with a top cover limit of 1 billion dollars in Copenhagen in two cases: no adaptation policy (red), and multistage dike (blue). Insurance premium distributions are depicted at 10, 20, 30, 40, 50, 60, 70, 80, 90, and 100 years.

6.5 PREMIUM DISTRIBUTION: SENSITIVITY ANALYSIS

This section presents the results of sensitivity analysis in the insurance premium distributions, with respect to the sea level rise. We consider three scenarios, an optimistic scenario, with a global sea level rise of 18cm by the year 2100, a neutral scenario, where the mean sea level corresponds to the estimated one in each city, and a pessimistic one, where the sea levels are expected to rise by 190cm by the year 2100. The optimistic and pessimistic scenarios are taken from Johansson et al. (2014).

Figures 38 and 39 show the numerical results for New York City. Panel (a) shows the optimistic scenario, (b) the neutral, and (c) the pessimistic one. As it can be seen the insurance premium distribution depends quite heavily on the sea level rise parameter. In the optimistic scenario, premiums increase on average by less than in the other scenarios, while still presenting a comparable level of standard deviation. Figure 38 clearly shows how the optimal investment timing varies with different sea level rise scenarios as well. In the optimistic scenario, the optimal investment is further deferred in comparison to the neutral one, while as expected, the investment in the dike project occurs earlier in the pessimistic one.

Figure 38

DEVELOPMENT OF INSURANCE PREMIUM DISTRIBUTION IN NYC WITH DIKE UNDER DIFFERENT SEA LEVEL RISE SCENARIOS.

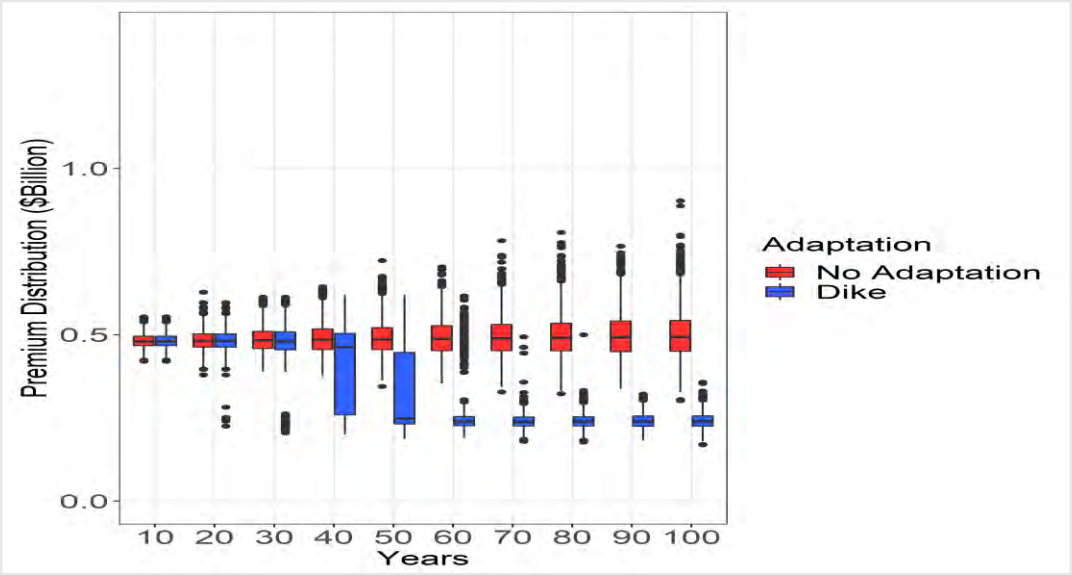

(a) Insurance premiums in the optimistic scenario.

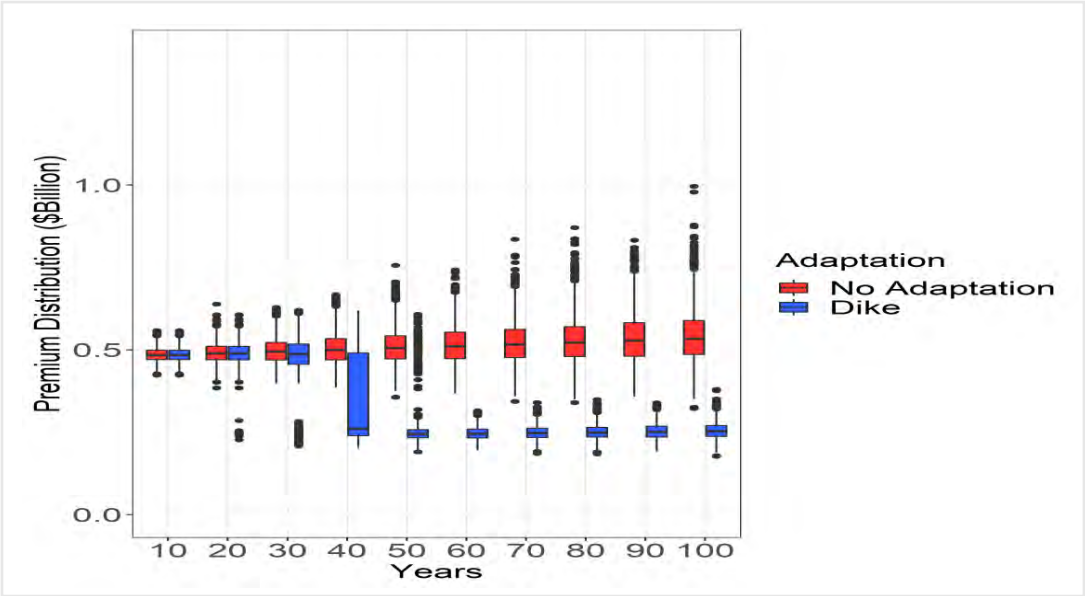

(b) Insurance premiums in the neutral scenario.

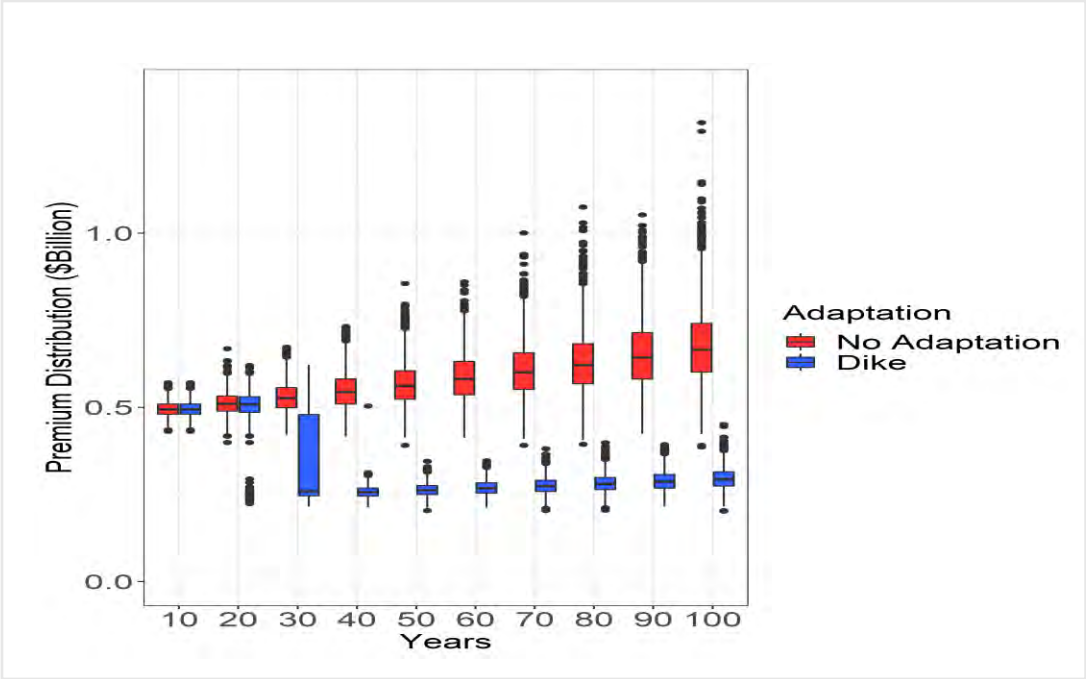

(c) Insurance premiums in the pessimistic scenario.

This figure shows the insurance premiums with three different scenarios in New York City with the dike project. The scenarios considered allows for a global average sea level rise by 2100 of: 19cm (optimistic); 65cm (neutral); 190cm (pessimistic). Insurance premium distributions are depicted at 10, 20, 30, 40, 50, 60, 70, 80, 90, and 74 100 years.

Figure 39

DEVELOPMENT OF INSURANCE PREMIUM DISTRIBUTION IN NYC WITH FLOOD PROOFING UNDER DIFFERENT SEA LEVEL RISE SCENARIOS.

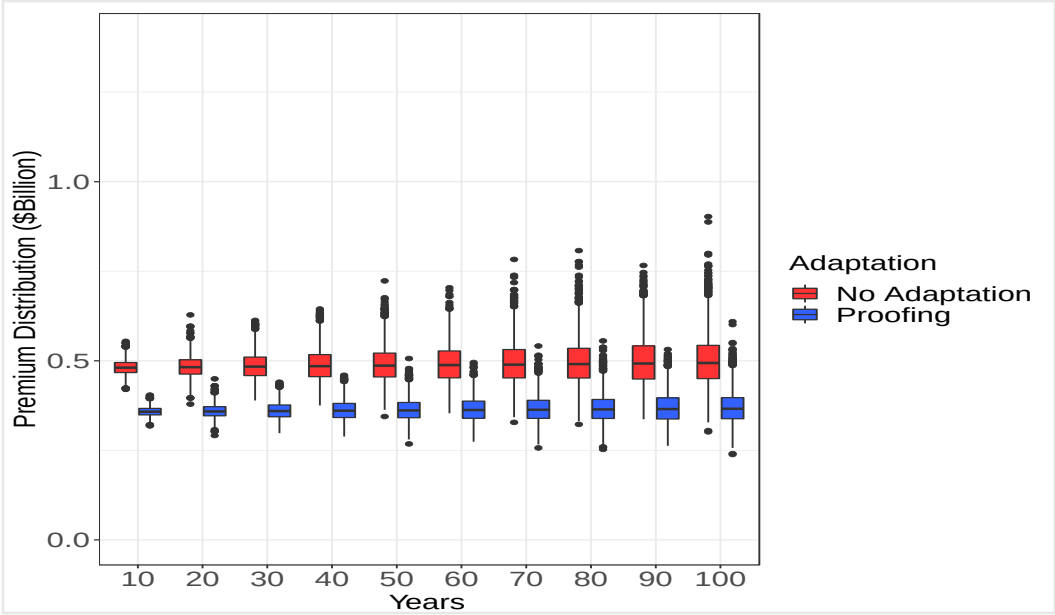

(a) Insurance premiums in the optimistic scenario.

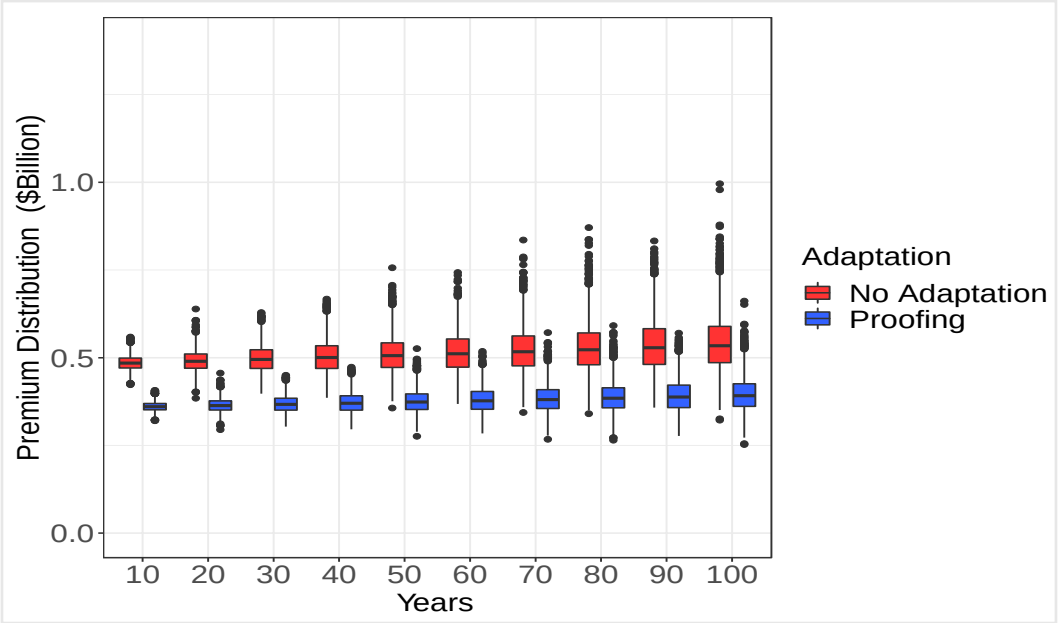

(b) Insurance premiums in the neutral scenario.

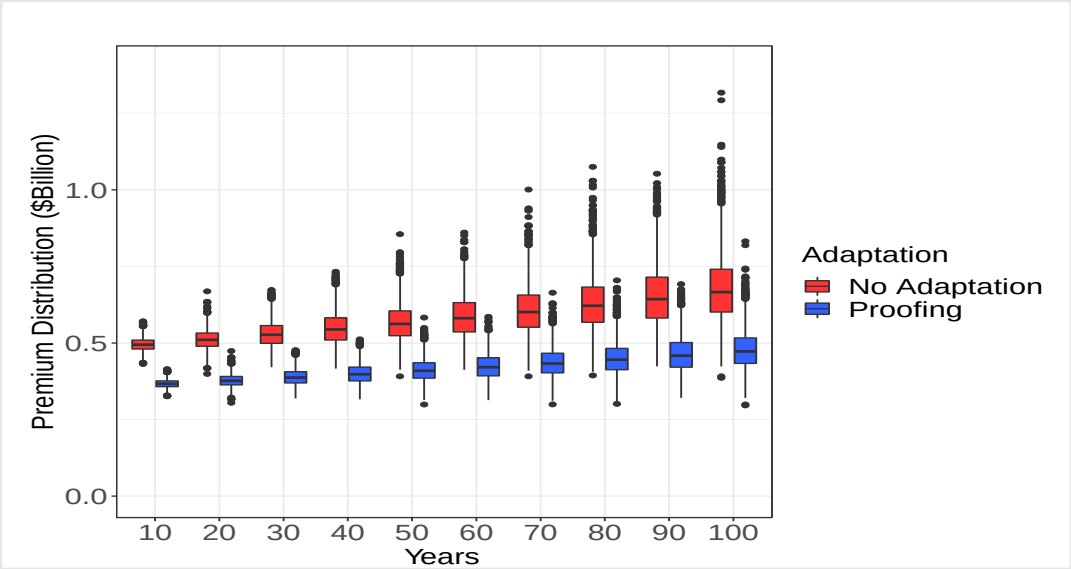

(c) Insurance premiums in the pessimistic scenario.

This figure shows the insurance premiums with three different scenarios in New York City with the flood proofing project. The scenarios considered allows for a global average sea level rise by 2100 of: 19cm (optimistic); 65cm (neutral); 190cm (pessimistic). Insurance premium distributions are depicted at 10, 20, 30, 40, 50, 60, 70, 75 80, 90, and 100 years.

Similar to the dike project, Figure 39 shows the numerical results of the sensitivity analysis for the flood-proofing project. Results are similar to the previous one: as the expected level of sea rise increases, the insurance premium distribution shifts upwards. Overall, flood-proofing seems to provide a more moderate protection from the effect of climate change in all three scenarios, compared to the construction of the dike.

Figure 40 shows the sensitivity analysis for the South East Queensland case. In all three scenarios, elevating houses provides enough protection, and reduces the impact of climate change.

Figure 40

DEVELOPMENT OF INSURANCE PREMIUM DISTRIBUTION IIN SOUTH EAST QUEENSLAND UNDER DIFFERENT SEA LEVEL RISE SCENARIO.

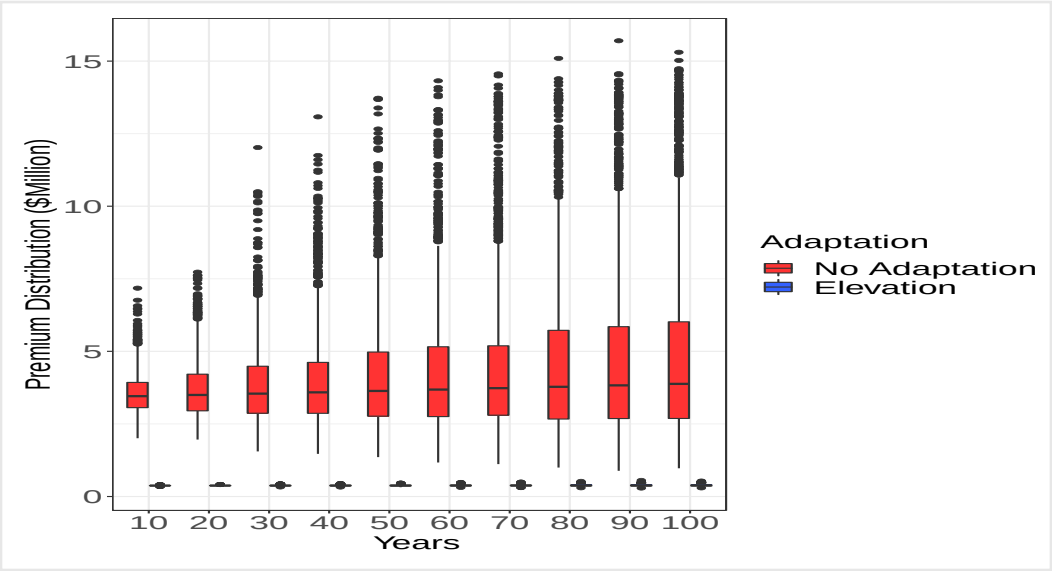

(a) Insurance premiums in the optimistic scenario.

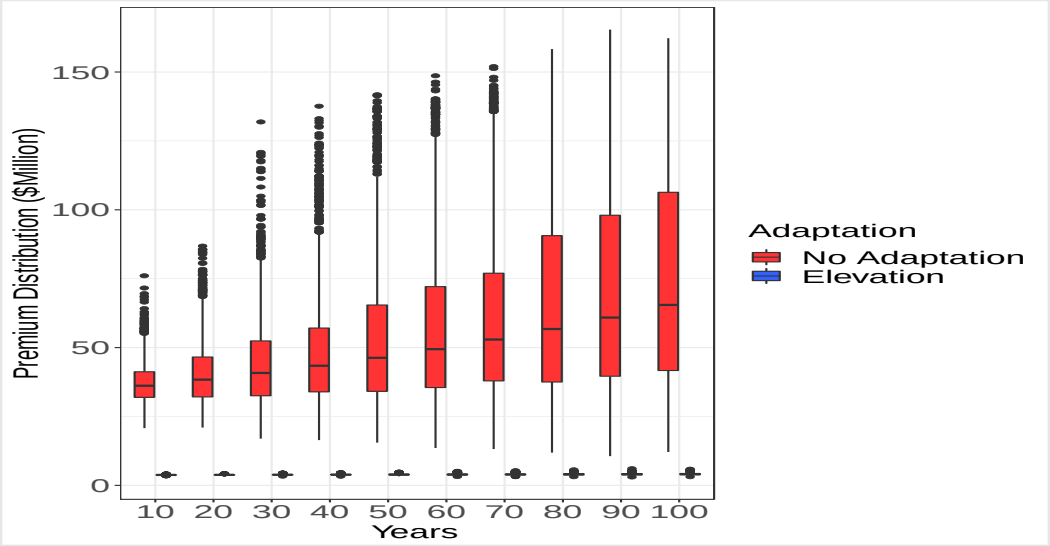

(b) Insurance premiums in the neutral scenario.

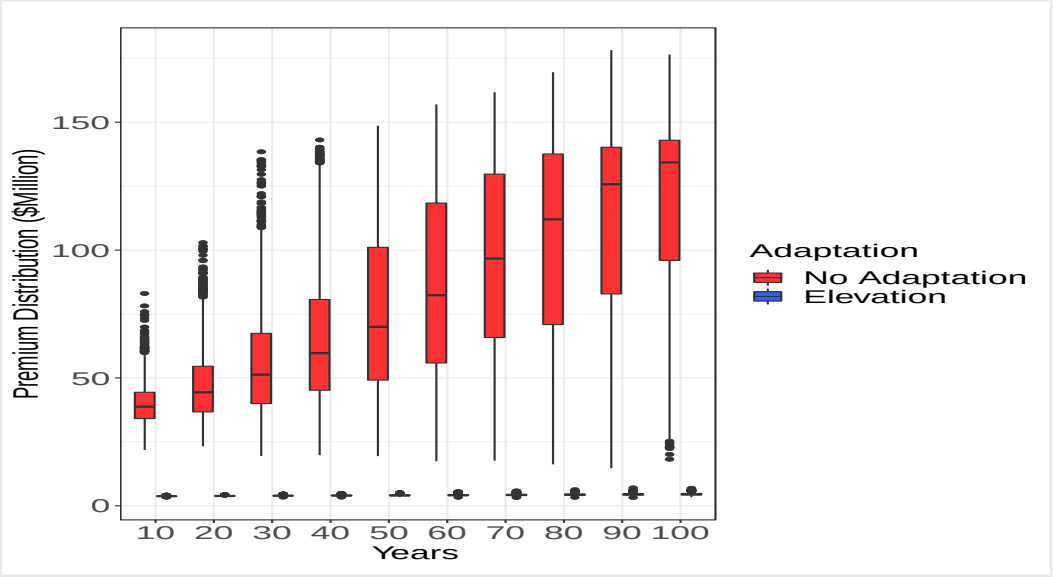

(c) Insurance premiums in the pessimistic scenario.

This figure shows the insurance premiums with three different scenarios in South East Queensland in the elevation project. The scenarios considered allows for a global average sea level rise by 2100 of: 19cm (optimistic); 87cm (neutral); 190cm (pessimistic). Insurance premium distributions are depicted at 10, 20, 30, 40, 50, 60, 70, 77 80, 90, and 100 years.

FIGURE 41 DEVELOPMENT OF INSURANCE PREMIUM DISTRIBUTION IN COPENHAGEN UNDER DIFFERENT SEA LEVEL RISE SCENARIOS.

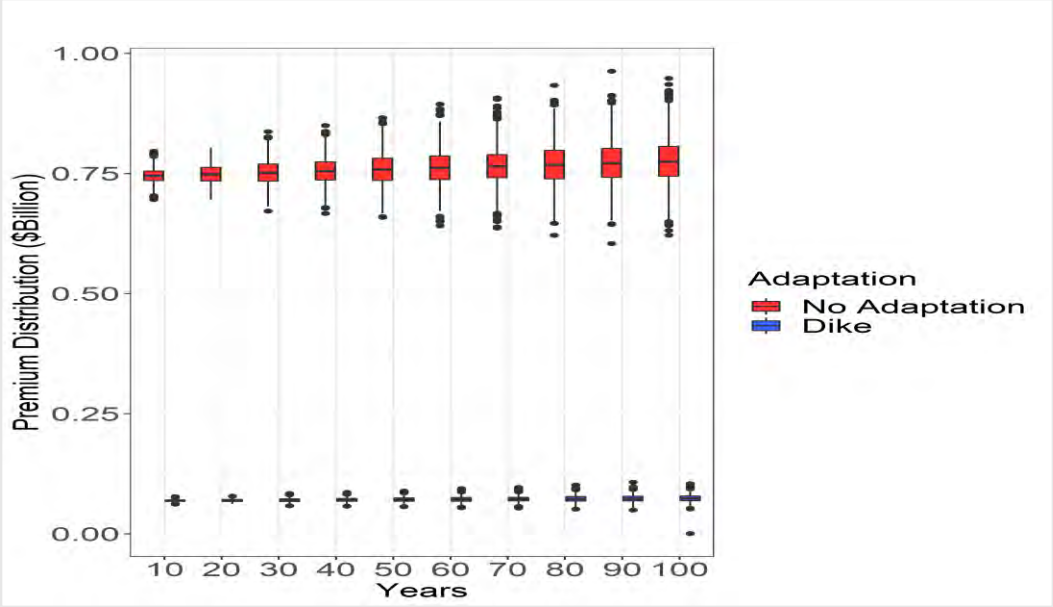

(a) Insurance premiums in the optimistic scenario.

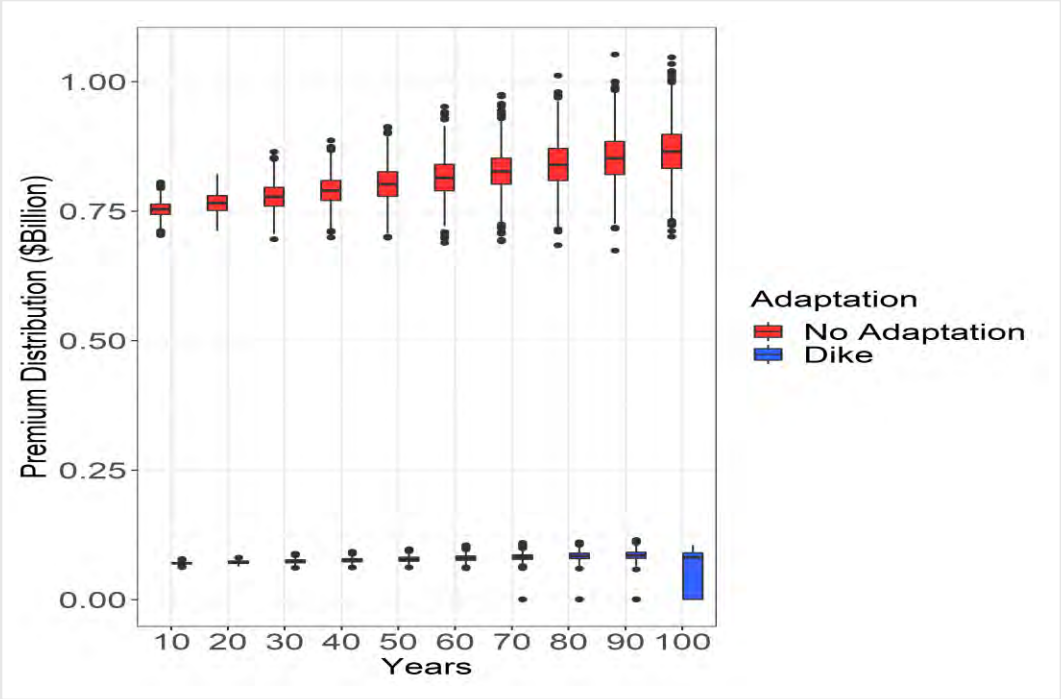

(b) Insurance premiums in the neutral scenario.

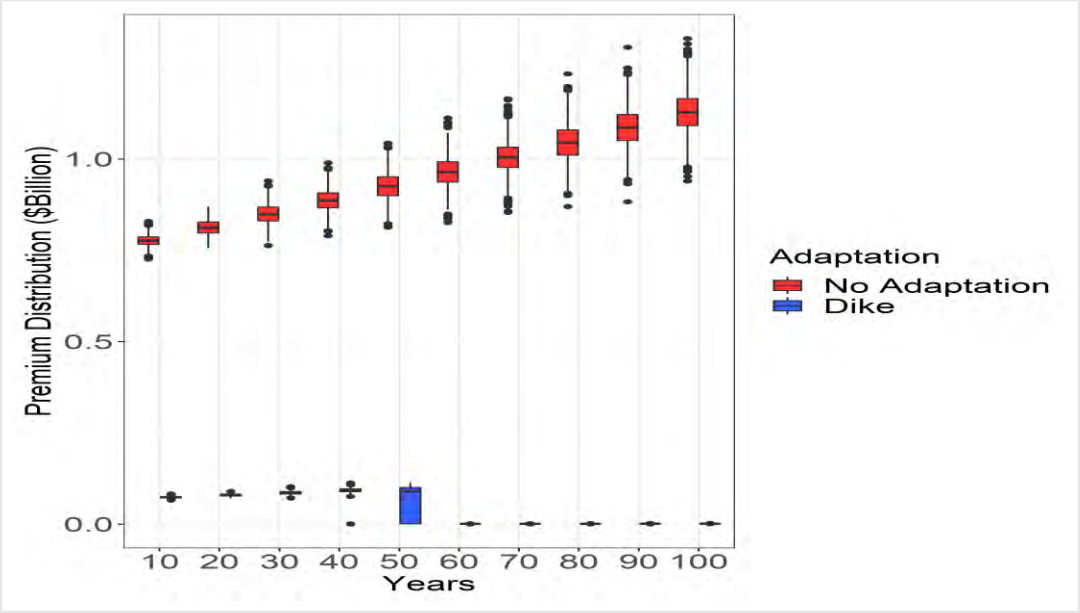

(c) Insurance premiums in the pessimistic scenario.

This figure shows the insurance premiums with three different scenarios in Copenhagen with dike project. The scenarios considered allows for a global average sea level rise by 2100 of: 19cm (optimistic); 65cm (neutral); 190cm (pessimistic). Insurance premium distributions are depicted at 10, 20, 30, 40, 50, 60, 70, 80, 90, and 78 100 years.

Finally, Figure 41 shows the numerical results for Copenhagen. Similar to the previous cases, the insurance premium distribution shifts upwards with the mean sea level expectation. While Stage 1 is always invested, the likelihood of Stage 2 being invested is close to zero in the optimistic scenario. In this case, the protection provided by the Stage 1 dike is more than enough to avoid extreme consequences in Copenhagen. In addition, while the Stage 2 is invested only close to the year 100 in the neutral scenario, in the pessimistic scenario the investment occurs much earlier, in around year 40 and 50.

7: Conclusion

In this report, we have proposed a new modeling framework for optimal climate adaptation pathways, based on real option analysis. Our methodology combines the block maxima approach from extreme value theory and the generalized additive model for location scale and shape framework, with real option analysis, allowing for pricing catastrophic risk in coastal regions, considering economic growth and uncertainty in the mean sea level rise. It also provides insights into the optimal investment timing, both for single investment projects and for optimal adaptation pathways, when multiple projects are feasible. We then showcased our proposed methodology with three cases studies based in New York City, Copenhagen, and in South East Queensland.

Sea-surface temperature and atmospheric pressure are two important predictors for the severity of extreme weather events. We have investigated the most commonly used climate indices and their statistical properties. Thanks to extreme value theory, we have used a block maxima approach combined with the generalized additive model for location scale and shape framework to model the behavior of extreme sea level events, using the climate indices as covariates. The estimation shows evidence of increasing sea level rise in all the three geographic areas investigated, and at the same time, a significant effect of the climate indices on the distribution of extreme water levels.

We then combined the estimation results with the proposed real option framework in three case studies, evaluating both hard and soft climate adaptation policies. For New York, we compared a hard and more expensive project, the construction of a barrier and dike, with a less invasive and less expensive flood-proofing project. On the one hand, numerical results suggest that while the barrier and dike project would provide the city of New York with a higher level of protection, it would be beneficial to defer the investment, as the current level of infrastructure appears to be adequate. On the other hand, the flood-proofing project is a low-cost adaptation option and according to the numerical experiment conducted, it would be beneficial for the city to invest right away in this technology. When analyzed jointly as a possible portfolio of climate adaptation policies, the applied real option approach suggests not to invest into the flood-proofing project, while it is optimal to wait and see how climate uncertainty unfolds and then invest in the barrier and dike project.

In the South East Queensland case study we analyzed house elevation as a climate adaptation policy to reduce the impact of climate risk. As it turns out, elevating houses reduces the impact of extreme weather events considerably, and while investing in it right away would be a valuable option, deferring the investment would provide an even higher benefit of the project. In the third case study we examine different climate adaptation measures in the Copenhagen region. Our study shows that according to the different scenarios, the real option framework can be flexible enough to adapt to and compare single investment options with multiple investments type of projects. In particular, we discussed under which conditions of expected sea level rise and growth exposure, it would be better to construct a barrier and dike project in two stages, raising the dike up to a certain height first, wait for the climate uncertainty to unfold, and then potentially further rising the dike, rather than elevating the dike to its total height right away.

Finally, we investigated how the adoption of the different projects in the three case studies impacts the distributions of future insurance premiums for an insurance policy covering the entire city from losses due to extreme sea level rise for 12 months. Then we considered the adoption of a top cover limit of 1 billion dollars.

Our study presents a comprehensive approach of real option analysis to climate adaptation policies aiming to mitigate flood risk. As shown in this report, real option analysis is a very flexible approach and could be applied to similar situations to those discussed in this report. Nevertheless, a few notes of caution need to be mentioned.

Firstly, real option analysis requires the estimation of several key parameters, such as the expected rate of sea level rise and the impact of climate indices, and therefore it must be based on high quality data, which is always a scarce commodity. While a lot of efforts have been made to collect appropriate data - also thanks to the vast networks of international scientific collaborations such as, e.g., the University of Hawaii Sea Level Center – information on sea level data is limited to locations, where it's possible to collect it. Secondly, focusing only on extreme events, one can then rely on extreme value theory as a sounded statistical methodology. However, data on extreme events is notoriously scarce and one should always bear that in mind. Thirdly, our approach requires reliable estimates of the loss function used to evaluate the insurance premiums, and reliable estimates of loss functions are typically very complicated to obtain, again due to the scarcity of data and a lack of complete scientific studies. Finally, real option analysis could be quite computationally intensive in complex investment problems.

Our analysis focused on the application of real option analysis to climate adaptation polices, mitigating the impact of flood risk and increasing resilience of coastal communities. In this report we presented a one factor model, where the impact of climate change is transmitted through the expected rate at which the mean sea level rises. For future research purposes, our framework can be extended to a two-factor analysis where stochasticity is also introduced in storm surge volatility. The stochasticity of storm surge volatility may be significant in some regions, as implied by the impact of climate indices on the scale parameter of storm surges. A two-factor model would help to capture the higher value for investment flexibility due to the stochasticity of the scale parameter and provide better investment decisions. In addition, this project has analyzed investment projects from the perspectives of governments. In practice, there is an interaction between the level of climate change adaptation and insurance uptake. Adaptation investments are costly, however, investing in adaptation projects will make insurance more affordable. Increases in insurance uptake help speed up disaster recovery, which may improve social welfare. This interaction between adaptation and insurance uptake decisions provides an interesting avenue for future research. Finally, although the project has examined adaptation at the building level (flood-proofing measures), it has not examined how the policy on building codes should be adapted. Future research on building codes policy would be of great interest to governments.

8: Acknowledgments

The researchers wish to extend their gratitude to those without whose efforts this project could not have come to fruition: POG members, and SOA members for their diligent work reviewing the report for accuracy and relevance and providing unfailing support to the project.

Project Oversight Group Members:

- Matthew Self
- Josh Rekula
- Remi Villeneuve
- Tamara Wilt
- Cindy Bruyere
- Priya Rohatgi
- Sam Gutterman
- Bronwyn Claire

At the Society of Actuaries:

- Rob Montgomery
- Erika Schulty
- Dale Hall

References

Abadie, L.M., Chamorro, J.M., 2008. European CO_2 prices and carbon capture investments. Energy Economics 30, 2992–3015.

Aerts, J.C., Botzen, W.W., Emanuel, K., Lin, N., De Moel, H., Michel-Kerjan, E.O., 2014. Evaluating flood resilience strategies for coastal megacities. Science 344, 473–475.

Aerts, J.C., Lin, N., Botzen, W., Emanuel, K., de Moel, H., 2013. Low-probability flood risk modeling for New York City. Risk Analysis 33, 772–788.

Ban, N., Rajczak, J., Schmidli, J., Schär, C., 2020. Analysis of alpine precipitation extremes using generalized extreme value theory in convection-resolving climate simulations. Climate Dynamics 55, 61–75.

Blackburn, M., Hoskins, B.J., 2001. The UK record-breaking wet autumn 2000. UGAMP newsletter 24, 38–40.

Boomsma, T.K., Meade, N., Fleten, S.E., 2012. Renewable energy investments under different support schemes: A real options approach. European Journal of Operational Research 220, 225–237. Brouwer, R., van Ek, R., 2004. Integrated ecological, economic and social impact assessment of alternative flood control policies in the Netherlands. Ecological Economics 50, 1–21.

Brealey, R.A., Myers, S.C., and Allen, F. 2020. *Principles of corporate finance*, 13e. McGraw-Hill Education.

Brown, J.M., Morrissey, K., Knight, P., Prime, T.D., Almeida, L.P., Masselink, G., Bird, C.O., Dodds, D., Plater, A.J., 2018. A coastal vulnerability assessment for planning climate resilient infrastructure. Ocean & Coastal Management 163, 101–112.

Bueh, C., Nakamura, H., 2007. Scandinavian pattern and its climatic impact. Quarterly Journal of the Royal Meteorological Society: A journal of the atmospheric sciences, applied meteorology and physical oceanography 133, 2117–2131.

Chan, R., Durango-Cohen, P.L., Schofer, J.L., 2016. Dynamic learning process for selecting storm protection investments. Transportation Research Record 2599, 1–8.

Cheng, L., AghaKouchak, A., Gilleland, E., Katz, R.W., 2014. Non-stationary extreme value analysis in a changing climate. Climatic Change 127, 353–369.

Codiga, D.L., 2011. Unified tidal analysis and prediction using the utide matlab functions.

Dahlman, L., 2009. Climate variability: North Atlantic oscillation. Climate. gov. Last modified August 30, 2009.

Dixit, A.K., Pindyck, R.S., 1994. Investment under uncertainty. Princeton University Press, Princeton, New Jersey.

Dobes, L., 2010. Notes on applying 'real options' to climate change adaptation measures, with examples from Vietnam. Crawford School Research Paper, Crawford School of Economics and Government Centre for Climate Economics & Policy (CCEP) Working Paper 7.

Downing, T.E., 2012. Views of the frontiers in climate change adaptation economics. Wiley Interdisciplinary Reviews: Climate Change 3, 161–170.

Eijgenraam, C., Brekelmans, R., den Hertog, D., Roos, K., 2016. Optimal strategies for flood prevention. Management Science 63, 1644–1656.

El Sherpieny, E., Assar, S., Amer, N., 2013. Parameters estimation of generalized extreme value distribution under progressive type ii censored. Asian Journal of Applied Sciences, Vol.2, Issue 2.

Embrechts, P., Klüppelberg, C., Mikosch, T., 2013. Modelling extremal events: for insurance and finance. volume 33. Springer Science & Business Media.

Embrechts, P., Resnick, S.I., Samorodnitsky, G., 1999. Extreme value theory as a risk management tool. North American Actuarial Journal 3, 30–41.

Ernstsen, R.R., Boomsma, T.K., 2018. Valuation of power plants. European Journal of Operational Research 266, 1153–1174.

Fazey, I., Wise, R.M., Lyon, C., Câmpeanu, C., Moug, P., Davies, T.E., 2016. Past and future adaptation pathways. Climate and Development 8, 26–44.

Froot, K.A., 2001. The market for catastrophe risk: a clinical examination. Journal of Financial Economics 60, 529–571.

Garmaise, M.J., Moskowitz, T.J., 2009. Catastrophic risk and credit markets. The Journal of Finance 64, 657–707.

Gersonius, B., Ashley, R., Pathirana, A., Zevenbergen, C., 2013. Climate change uncertainty: building flexibility into water and flood risk infrastructure. Climatic Change 116, 411–423.

Gersonius, B., Morselt, T., Van Nieuwenhuijzen, L., Ashley, R., Zevenbergen, C., 2011. How the failure to account for flexibility in the economic analysis of flood risk and coastal management strategies can result in maladaptive decisions. Journal of Waterway, Port, Coastal, and Ocean Engineering 138, 386–393.

Ginbo, T., Di Corato, L., Hoffmann, R., 2021. Investing in climate change adaptation and mitigation: A methodological review of real-options studies. Ambio 50, 229–241.

Haasnoot, M., Kwakkel, J.H., Walker, W.E., Ter Maat, J., 2013. Dynamic adaptive policy pathways: A method for crafting robust decisions for a deeply uncertain world. Global Environmental Change 23, 485–498.

Haasnoot, M., Middelkoop, H., Offermans, A., Van Beek, E., Van Deursen, W.P., 2012. Exploring pathways for sustainable water management in river deltas in a changing environment. Climatic Change 115, 795–819.

Haer, T., Husby, T.G., Botzen, W.W., Aerts, J.C., 2020. The safe development paradox: An agent-based model for flood risk under climate change in the European Union. Global Environmental Change 60, 102009.

Hallegatte, S., 2009. Strategies to adapt to an uncertain climate change. Global Environmental Change 19, 240–247.

Hallegatte, S., Ranger, N., Mestre, O., Dumas, P., Corfee-Morlot, J., Herweijer, C., Wood, R.M., 2011. Assessing climate change impacts, sea level rise and storm surge risk in port cities: a case study on Copenhagen. Climatic Change 104, 113–137.

Han, Y., Ash, K., Mao, L., Peng, Z.R., 2020. An agent-based model for community flood adaptation under uncertain sea-level rise. Climatic Change 162, 2257–2276.

Hieronymus, M., Kalén, O., 2020. Sea-level rise projections for Sweden based on the new IPCC special report: The ocean and cryosphere in a changing climate. Ambio 49, 1587–1600.

IPCC, 2007. Impacts, adaptation and vulnerability. Contribution of working group II to the fourth assessment report of the Intergovernmental Panel on Climate Change. 2007. Cambridge University Press.

Johansson, M.M., Pellikka, H., Kahma, K.K., Ruosteenoja, K., 2014. Global sea level rise scenarios adapted to the Finnish coast. Journal of Marine Systems 129, 35–46.

Jongman, B., Winsemius, H.C., Aerts, J.C., De Perez, E.C., Van Aalst, M.K., Kron, W., Ward, P.J., 2015. Declining vulnerability to river floods and the global benefits of adaptation. Proceedings of the National Academy of Sciences 112, E2271–E2280.

Kiem, A.S., Franks, S.W., Kuczera, G., 2003. Multi-decadal variability of flood risk. Geophysical Research Letters 30.

Kim, K., Ha, S., Kim, H., 2017. Using real options for urban infrastructure adaptation under climate change. Journal of Cleaner Production 143, 40–50.

Kim, K., Kim, J.S., 2018. Economic assessment of flood control facilities under climate uncertainty: A case of Nakdong River, South Korea. Sustainability 10, 308.

Kim, M.J., Nicholls, R.J., Preston, J.M., de Almeida, G.A., 2019. An assessment of the optimum timing of coastal flood adaptation given sea-level rise using real options analysis. Journal of Flood Risk Management 12, e12494.

Kind, J.M., Baayen, J.H., Botzen, W.W., 2018. Benefits and limitations of real options analysis for the practice of river flood risk management. Water Resources Research 54, 3018–3036.

Kirshen, P., Knee, K., Ruth, M., 2008. Climate change and coastal flooding in metro Boston: impacts and adaptation strategies. Climatic Change 90, 453–473.

Kontogianni, A., Tourkolias, C.H., Damigos, D., Skourtos, M., 2014. Assessing sea level rise costs and adaptation benefits under uncertainty in Greece. Environmental Science & Policy 37, 61–78.

Lang, A., Mikolajewicz, U., 2019. The long-term variability of extreme sea levels in the German Bight. Ocean Science 15, 651–668.

Lenk, S., Rybski, D., Heidrich, O., Dawson, R.J., Kropp, J.P., 2017. Costs of sea dikes–regressions and uncertainty estimates. Natural Hazards and Earth System Sciences 17, 765–779.

Letzing, J., Berkley, A., 2021. Flood risk is rising. Here's where – and what can be done. Technical Report. World Economic Forum.

Lobeto, H., Menendez, M., Losada, I., 2018. Toward a methodology for estimating coastal extreme sea levels from satellite altimetry. Journal of Geophysical Research: Oceans 123, 8284–8298.

Menéndez, M., Woodworth, P.L., 2010. Changes in extreme high-water levels based on a quasi-global tide-gauge data set. Journal of Geophysical Research: Oceans 115.

Michael, J.A., 2007. Episodic flooding and the cost of sea-level rise. Ecological Economics 63, 149–159. Muis, S., Haigh, I.D., Guimarães Nobre, G., Aerts, J.C., Ward, P.J., 2018. Influence of El Niño-southern oscillation on global coastal flooding. Earth's Future 6, 1311–1322.

Musulin, R., 2017. The reality of flood insurance repayment. Casualty Quarterly 1, 1–3.

Newell, R.G., Pizer, W.A., 2003. Discounting the distant future: how much do uncertain rates increase valuations? Journal of Environmental Economics and Management 46, 52–71.

Ng, W.S., Mendelsohn, R., 2005. The impact of sea level rise on Singapore. Environment and Development Economics 10, 201–215.

Nicholls, R.J., Hanson, S.E., Lowe, J.A., Warrick, R.A., Lu, X., Long, A.J., 2014. Sea-level scenarios for evaluating coastal impacts. Wiley Interdisciplinary Reviews: Climate Change 5, 129–150.

NOAA National Centers for Environmental Information (NCEI) U.S. Billion-Dollar Weather and Climate Disasters (2022). https://www.ncei.noaa.gov/access/billions/, DOI: 10.25921/stkw-7w73

Oh, S., Kim, K., Kim, H., 2018. Investment decision for coastal urban development projects considering the impact of climate change: Case study of the Great Garuda project in Indonesia. Journal of Cleaner Production 178, 507–514.

Park, J., Obeysekera, J., Irizarry, M., Barnes, J., Trimble, P., Park-Said, W., 2011. Storm surge projections and implications for water management in South Florida. Climatic Change 107, 109–128.

Park, T., Kim, C., Kim, H., 2014. Valuation of drainage infrastructure improvement under climate change using real options. Water Resources Management 28, 445–457.

Piecuch, C.G., Ponte, R.M., 2015. Inverted barometer contributions to recent sea level changes along the northeast coast of North America. Geophysical Research Letters 42, 5918–5925.

Pörtner, H.O., Roberts, D.C., Masson-Delmotte, V., Zhai, P., Tignor, M., Poloczanska, E., Weyer, N., 2019. The ocean and cryosphere in a changing climate. IPCC Special Report on the Ocean and Cryosphere in a Changing Climate.

Prettenthaler, F., Amrusch, P., Habsburg-Lothringen, C., 2010. Estimation of an absolute flood damage curve based on an Austrian case study under a dam breach scenario. Natural Hazards and Earth System Sciences 10, 881–894.

Prosdocimi, I., Kjeldsen, T., Miller, J., 2015. Detection and attribution of urbanization effect on flood extremes using nonstationary flood-frequency models. Water Resources Research 51, 4244–4262. Pugh, D.T., 1987. Tides, surges and mean sea level.

Ranger, N., Reeder, T., Lowe, J., 2013. Addressing 'deep' uncertainty over long-term climate in major infrastructure projects: four innovations of the Thames Estuary 2100 project. EURO Journal on Decision Processes 1, 233–262.

Razmi, A., Golian, S., Zahmatkesh, Z., 2017. Non-stationary frequency analysis of extreme water level: application of annual maximum series and peak-over threshold approaches. Water resources management 31, 2065.

Regan, C.M., Connor, J.D., Segaran, R.R., Meyer, W.S., Bryan, B.A., Ostendorf, B., 2017. Climate change and the economics of biomass energy feedstocks in semi-arid agricultural landscapes: A spatially explicit real options analysis. Journal of Environmental Management 192, 171–183.

Rigby, R.A., Stasinopoulos, D.M., 2001. The GAMLSS project: a flexible approach to statistical modelling, in: New trends in statistical modelling: Proceedings of the 16th international workshop on statistical modelling, University of Southern Denmark. p. 345.

Rigby, R.A., Stasinopoulos, D.M., 2005. Generalized additive models for location, scale and shape. Journal of the Royal Statistical Society: Series C (Applied Statistics) 54, 507–554.

Roth, M., Buishand, T., Jongbloed, G., Klein Tank, A., Van Zanten, J., 2012. A regional peaks-overthreshold model in a nonstationary climate. Water Resources Research 48.

Roth, M., Buishand, T., Jongbloed, G., Tank, A.K., Van Zanten, J., 2014. Projections of precipitation extremes based on a regional, non-stationary peaks-over-threshold approach: A case study for the Netherlands and north-western Germany. Weather and Climate Extremes 4, 1–10.

Ryu, Y., Kim, Y.O., Seo, S.B., Seo, I.W., 2018. Application of real option analysis for planning under climate change uncertainty: A case study for evaluation of flood mitigation plans in Korea. Mitigation and Adaptation Strategies for Global Change 23, 803–819.

Salas, J., Obeysekera, J., Vogel, R., 2018. Techniques for assessing water infrastructure for nonstationary extreme events: A review. Hydrological Sciences Journal 63, 325–352.

Schiel, C., Glöser-Chahoud, S., Schultmann, F., 2019. A real option application for emission control measures. Journal of Business Economics 89, 291–325.

Shao, J., Pantelous, A., Papaioannou, A.D., 2015. Catastrophe risk bonds with applications to earthquakes. European Actuarial Journal 5, 113–138.

Silva, A.T., Naghettini, M., Portela, M.M., 2016. On some aspects of peaks-over-threshold modeling of floods under nonstationarity using climate covariates. Stochastic environmental research and risk assessment 30, 207–224.

Silva, A.T., Portela, M.M., Naghettini, M., 2014. On peaks-over-threshold modeling of floods with zero-inflated Poisson arrivals under stationarity and nonstationarity. Stochastic environmental research and risk assessment 28, 1587–1599.

Smajgl, A., Toan, T.Q., Nhan, D.K., Ward, J., Trung, N.H., Tri, L., Tri, V., Vu, P., 2015. Responding to rising sea levels in the Mekong delta. Nature Climate Change 5, 167–174.

Symes, D., Akbar, D., Gillen, M., Smith, P., 2009. Land-use mitigation strategies for storm surge risk in South East Queensland. Australian Geographer 40, 121–136.

Tanoue, M., Hirabayashi, Y., Ikeuchi, H., 2016. Global-scale river flood vulnerability in the last 50 years. Scientific Reports 6, 1–9.

Tellman, B., Sullivan, J., Kuhn, C., Kettner, A., Doyle, C., Brakenridge, G., Erickson, T., Slayback, D., 2021. Satellite imaging reveals increased proportion of population exposed to floods. Nature 596, 80–86.

Thompson, D.W., Solomon, S., Kushner, P.J., England, M.H., Grise, K.M., Karoly, D.J., 2011. Signatures of the Antarctic ozone hole in southern hemisphere surface climate change. Nature Geoscience 4, 741–749.

Towler, E., Rajagopalan, B., Gilleland, E., Summers, R.S., Yates, D., Katz, R.W., 2010. Modeling hydrologic and water quality extremes in a changing climate: A statistical approach based on extreme value theory. Water Resources Research 46.

Trenberth, K.E., Stepaniak, D.P., 2001. Indices of El Niño evolution. Journal of climate 14, 1697–1701.

Truong, C., Trück, S., 2016. It's not now or never: Implications of investment timing and risk aversion on climate adaptation to extreme events. European Journal of Operational Research, – doi:http://dx.doi.org/10.1016/j.ejor.2016.01.044 .

Truong, C., Trück, S., Mathew, S., 2017. Managing risks from climate impacted hazards-the value of investment flexibility under uncertainty. European Journal of Operational Research.

Tsvetanov, T.G., Shah, F.A., 2013. The economic value of delaying adaptation to sea-level rise: An application to coastal properties in Connecticut. Climatic Change 121, 177–193.

Walter, K., Luksch, U., Fraedrich, K., 2001. A response climatology of idealized midlatitude thermal forcing experiments with and without a storm track. Journal of Climate 14, 467–484.

Wang, C.H., Khoo, Y.B., Wang, X., 2015. Adaptation benefits and costs of raising coastal buildings under storm-tide inundation in South East Queensland, Australia. Climatic Change 132, 545–558.

Wang, T., De Neufville, R., 2005. Real options "in" projects. Proceedings, 9th Real Options Annual International Conference, Paris, France.

Wang, T., Liu, B., Zhang, J., Li, G., 2019. A real options-based decision-making model for infrastructure investment to prevent rainstorm disasters. Production and Operations Management 28, 2699–2715.

Weinkle, J., Landsea, C., Collins, D., Musulin, R., Crompton, R.P., Klotzbach, P.J., Pielke, R., 2018. Normalized hurricane damage in the continental united states 1900–2017. Nature Sustainability 1, 808–813.

West, J.J., Small, M.J., Dowlatabadi, H., 2001. Storms, investor decisions, and the economic impacts of sea level rise. Climatic Change 48, 317–342.

Winsemius, H.C., Aerts, J.C., Van Beek, L.P., Bierkens, M.F., Bouwman, A., Jongman, B., Kwadijk, J.C., Ligtvoet, W., Lucas, P.L., Van Vuuren, D.P., et al., 2016. Global drivers of future river flood risk. Nature Climate Change 6, 381–385.

Wise, R.M., Fazey, I., Smith, M.S., Park, S.E., Eakin, H., Van Garderen, E.A., Campbell, B., 2014.

Reconceptualising adaptation to climate change as part of pathways of change and response. Global environmental change 28, 325–336.

Woodward, M., Gouldby, B., Kapelan, Z., Khu, S.T., Townend, I., 2011. Real options in flood risk management decision making. Journal of Flood Risk Management 4, 339–349.

Woodward, M., Kapelan, Z., Gouldby, B., 2014. Adaptive flood risk management under climate change uncertainty using real options and optimization. Risk Analysis 34, 75–92.

Wreford, A., Dittrich, R., van der Pol, T.D., 2020. The added value of real options analysis for climate change adaptation. Wiley Interdisciplinary Reviews: Climate Change 11, e642.

Zhu, T.J., Lund, J.R., Jenkins, M.W., Marques, G.F., Ritzema, R.S., 2007. Climate change, urbanization, and optimal long-term floodplain protection. Water Resources Research 43.

Feedback

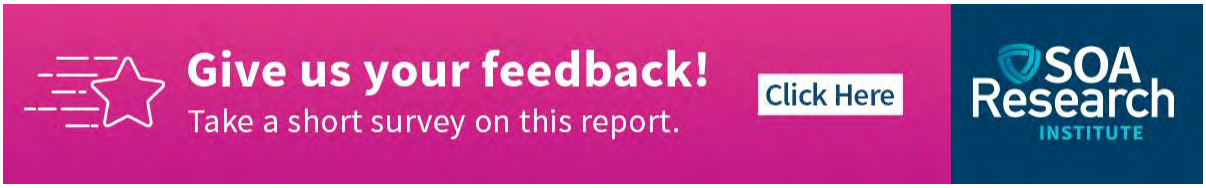
Give us your feedback!
Take a short survey on this report.
Click Here
SOA Research INSTITUTE

About The Society of Actuaries Research Institute

Serving as the research arm of the Society of Actuaries (SOA), the SOA Research Institute provides objective, data-driven research bringing together tried and true practices and future-focused approaches to address societal challenges and your business needs. The Institute provides trusted knowledge, extensive experience and new technologies to help effectively identify, predict and manage risks.

Representing the thousands of actuaries who help conduct critical research, the SOA Research Institute provides clarity and solutions on risks and societal challenges. The Institute connects actuaries, academics, employers, the insurance industry, regulators, research partners, foundations and research institutions, sponsors and non-governmental organizations, building an effective network which provides support, knowledge and expertise regarding the management of risk to benefit the industry and the public.

Managed by experienced actuaries and research experts from a broad range of industries, the SOA Research Institute creates, funds, develops and distributes research to elevate actuaries as leaders in measuring and managing risk. These efforts include studies, essay collections, webcasts, research papers, survey reports, and original research on topics impacting society.

Harnessing its peer-reviewed research, leading-edge technologies, new data tools and innovative practices, the Institute seeks to understand the underlying causes of risk and the possible outcomes. The Institute develops objective research spanning a variety of topics with its strategic research programs: aging and retirement; actuarial innovation and technology; mortality and longevity; diversity, equity and inclusion; health care cost trends; and catastrophe and climate risk. The Institute has a large volume of topical research available, including an expanding collection of international and market-specific research, experience studies, models and timely research.

Society of Actuaries Research Institute
475 N. Martingale Road, Suite 600
Schaumburg, Illinois 60173
www.SOA.org